AN ABSTRACT OF THE THESIS OF

Ruqi Li for the degree of Doctor of Philosophy in Electrical and Computer Engineering presented on May 2, 1991.

Title: **Dynamic Modeling, Simulation and Stability Analysis of Brushless Doubly-Fed Machines .**

Abstract Approved: _____.
Dr. Alan K. Wallace

A brushless doubly-fed machine (BDFM) is a single-frame, self-cascaded induction machine capable of operating in both the induction and the synchronous modes. This thesis presents some important advances concerning dynamic modeling, simulation and analysis of the BDFM.

Initially, a two-axis model and its associated parameters are developed and calculated. The development of the model is not subject to the commonly made assumption that the BDFM is electromagnetically equivalent to two wound rotor induction motors in cascade connection. Instead, the model is derived from a rigorous mathematical transformation of a detailed machine design model. This novel approach emphasizes not only the analysis of the machine performance in both dynamic and steady state conditions, but also the design aspects of the machine by correlating the machine performance with the actual machine parameters computed from machine geometry.

Using the two-axis model, simulation of the machine dynamic

performance in all conceivable modes of operation is carried out and the results are compared with test data available with good correlation.

Steady state models, under certain assumptions, are derived based on the two-axis model. For the synchronous mode, motoring operation, a solution technique is developed and utilized to perform steady state performance analysis of the BDFM.

Finally, stability analysis of the machine is examined using the linearized version of the two-axis model. Since the linearized two-axis model of the BDFM is time-varying, commonly used eigenvalue analysis techniques cannot be employed directly to investigate the stability characteristics of the machine. However, since the system matrix is a periodic function of time, the theory of Floquet is introduced so that the original linear time-varying system of equations are transformed into a set of equivalent system of equations with a constant system matrix. Eigenvalue analysis is then applied to analyze the stability of the BDFM system over a wide speed range. Predictions by the eigenvalue analysis are correlated with test data.

The study concludes that the proposed two-axis model is a good representation of the BDFM for dynamics, steady state, stability investigations of the machine and further development of control strategies for the proposed BDFM system for adjustable speed drive and variable speed generation applications.

Dynamic Modeling, Simulation and Stability Analysis of Brushless Doubly-Fed Machines

by

Ruqi Li

A THESIS

submitted to

Oregon State University

in partial fulfillment of
the requirement for the
degree of

Doctor of Philosophy

Completed May 2, 1991
Commencement June, 1991

APPROVED:

Redacted for Privacy

Professor of Electrical and Computer Engineering in charge of major

Redacted for Privacy

Head of Department of Electrical and Computer Engineering

Redacted for Privacy

Dean of Graduate School

Date thesis is presented May 2, 1991.

Typed by Ruqi Li for Ruqi Li.

ACKNOWLEDGEMENTS

I am grateful to Dr. A. K. Wallace, my major professor and thesis advisor, Dr. R. Spee my thesis co-advisor, for their overall guidance, many helpful suggestions and encouragement. Their generous advice, assistance and friendship are greatly appreciated.

I wish to thank Dr. D. Amort, Dr. R. Mohler and Dr. P. Cull for their serving on my graduate committee and providing me with a lot of valuable advice.

Special thanks go to the research sponsors, the Bonneville Power Administration, Electric Power Research Institute, Puget Sound Power and Light, Chevron U.S.A. and Southern California Edison, for their financial support.

Thanks are also extended to Dr. G. C. Alexander, Dr. H. K. Lauw, Dr. W. Kolodziej and many other professors who have taught me during my graduate study at Oregon State University.

Finally, I would like to express my sincere appreciation to my wife Lei Luo, my parents and Dr. W. Kraft and Mrs. R. Kraft for their love, assistance, self-sacrifice and encouragement.

TABLE OF CONTENTS

Page

LIST OF FIGURES

LIST OF TABLES

DYNAMIC MODELING, SIMULATION AND STABILITY ANALYSIS OF BRUSHLESS DOUBLY-FED MACHINES

INTRODUCTION

Background

The concept of using a self-cascaded induction machine in conjunction with a bi-directional power electronic converter as an adjustable speed drive (ASD) or variable speed generator (VSG) has recently been proposed at Oregon State University [1,2]. It is based on the research effects of several years related to ASD and VSG applications. By utilization of a self-cascaded induction machine, which is now referred to as a brushless doubly-fed machine or BDFM, operated in its doubly-fed version the slip rings of a commonly used doubly-fed wound rotor ASD or VSG system can be eliminated while a much lower rating power electronic converter can still be used.

Fig. a shows a conventional induction motor drive and a brushless doubly-fed machine drive. Compared with a commonly used ASD system, the newly proposed BDFM drive or VSG system has the following features:

(1) The stator of the experimental BDFM has two sets of terminals, a 6-pole system and a 2-pole system which are connected to the 60 Hz utility power supply and a power electronic converter, respectively [1,2];

(2) The rotor of the BDFM is a cage construction which is mechanically simple enough to be die-cast [3];

(3) The bi-directional, adjustable voltage and adjustable frequency power

converter used in the experimental drive is a series resonant converter capable of four quadrant operation. The immediate advantages of the BDFM system are:

(a) Lower cost of machine compared with that of a wound rotor induction machine;

(b) Lower cost of power converter compared with that of a conventional induction motor or synchronous motor ASD or VSG systems;

(c) Lower harmonic pollution to the power systems.

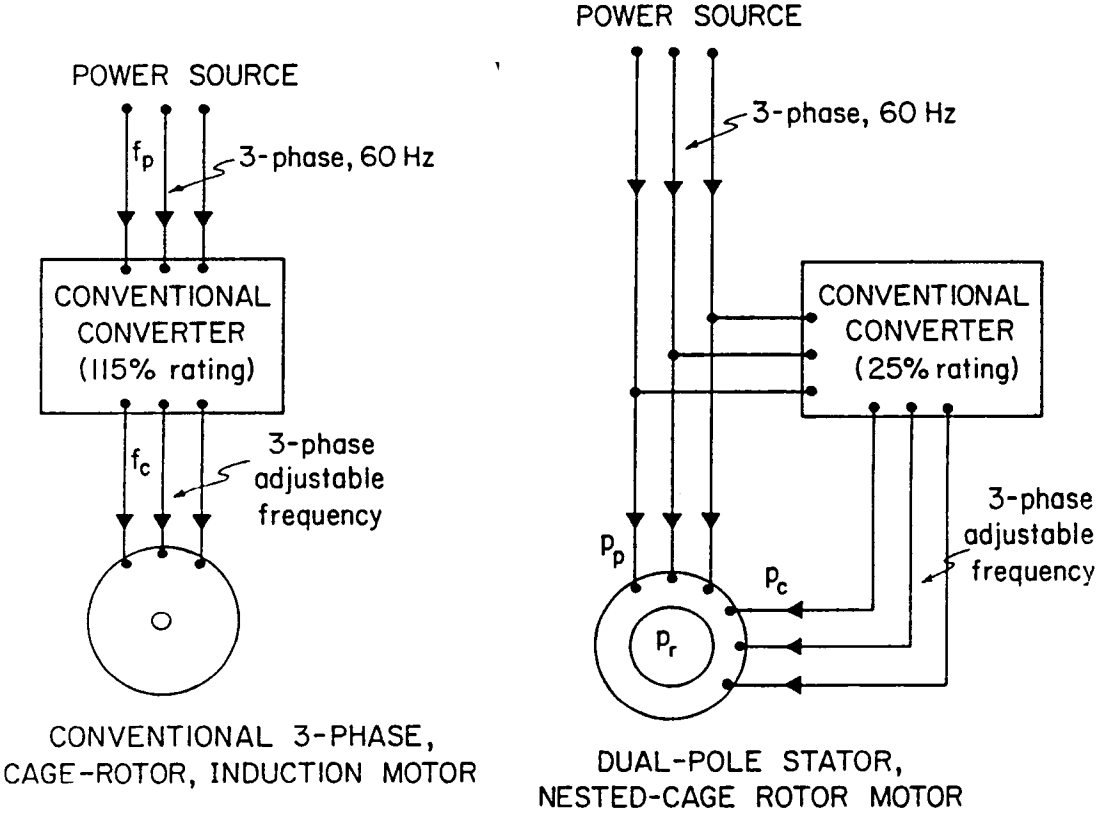

Fig. a(i) Conventional induction motor drive
(unidirectional converter at full rating)
(ii) Brushless doubly-fed drive
(bi-directional converter at fractional rating)

Based on the available information in the literature, prototype BDFM's have been designed and built with a 6-pole and 2-pole structure. However, laboratory tests showed that although providing insight into the operational principles, the prototype machines did not achieve the desired performance in both steady state and dynamic situations which is required of a practical ASD or VSG system. The performance of the machine can be significantly improved in terms of efficiency, torque production and other aspects through stator and rotor redesign. Research was thus planned for improving the machine performance and it was decided to address the following aspects

(1) Modeling and analysis of the BDFM, which include

a) Detailed machine design modeling for computer aided design;

b) Dynamic modeling (or d-q modeling) and analysis of the BDFM for dynamic, stability and control studies;

c) Equivalent circuit modeling for steady state performance and machine design studies;

d) Machine electromagnetic field analysis;

e) Parameter identification of the machine using modern system identification techniques;

(2) Practical application studies, which include

a) VSG of the BDFM system for car generator application;

b) Linear BDFM for electrical railroad vehicles.

(3) Potential market studies

This thesis discusses mainly the study of dynamic and steady state modeling and analysis of the BDFM based on previous investigations of the machine modeling and design.

Literature Review

The earliest means of achieving speed control of induction motors was by use of external resistors. In order to use external resistors, wound rotor induction motors had to be utilized. To avoid the use of slip rings, researchers were looking for other alternatives. In 1893 and 1894, Steinmetz of U.S.A. and Gorges of Germany independently filed two patents to claim a new way of achieving speed control through cascade connection of two induction motors. Later, there were several attempts to develop a 'single unit' cascade induction motor to reduce the cost and improve machine performance. It was first shown by Hunt in 1907 [4] that cascading of two induction motors for the purpose of speed control could be incorporated in one machine frame through ingenious stator and rotor winding design.

Creedy [5] made significant improvements on self-cascade induction motors by designing more effective stator and rotor windings. He proposed a 6 and 2-pole machine on which the original stator of the lab machine at OSU was based. Creedy also developed a logic for effective rotor configuration design.

No additional machine design was reported until in the early 1970's when notable rotor design progress was achieved by Broadway [3]. The so-called "Broadway rotor" is a cage structure which resembles closely that of a conventional induction motor. The advantages of the cage rotor lie in its simplicity, ruggedness and ease of manufacture. While pursing the design of the machine for low speed motor and high speed generator applications, Broadway also developed steady state equivalent circuits for induction and synchronous modes of operation from the basic assumption that the

machine is equivalent to two induction motors connected on a common shaft. He claimed that the parameters used for the steady state models were based on computations using well established formulas. However, no information concerning this can be extracted from the publications [3]. In the synchronous mode of operation, Broadway restricted himself to dc excitation on the control winding, hence, he could not achieve wide range of speed control when the machine was running as a doubly-fed synchronous motor.

Synchronous behavior of the self-cascaded induction motors over wide speed ranges was studied by Smith in 1967 [6]. Starting from two separate induction motors, Smith obtained a simple equivalent circuit with which he investigated the synchronous operation of the system in steady state conditions.

Kusko [7] and Shibata [8] investigated the use of a power electronic converter to extract the slip power of this type of machine in both induction and synchronous modes of operation. The equivalent circuits used for this analysis were essentially the same as those by early researchers.

In the synchronous mode of operation, stability problems may arise when control over a wide speed range is required. The problem was studied by Cook and Smith using a linearized model based on two wound rotor induction motors [9]. The effects of parameter variation on the dynamic performance of the machine is discussed in [10]. It was shown that although unstable operation could occur in some speed ranges, simple feedback schemes could be used to stabilize the machine in the unstable regions.

A common feature of all the above analytical and experimental work is its basis on the assumption that the machine is equivalent to two magnetically separated wound rotor motors of different pole numbers electrically connected and mounted on a common shaft. Although this approach is appropriate for conceptual understanding of the operation principles of the BDFM, it is not adequate for detailed machine and drive system design.

Moreover, most published work is limited to steady state performance analyses. Dynamic characteristics, such as machine run-up, synchronization, machine response to sudden change of load torque and many others have not been addressed.

More recently, Wallace et al have developed a detailed machine design model to investigate the machine performance under all operating conditions [11]. The model was developed by considerations of basic stator coils and nested rotor loops and the interaction between them. By the use of modern digital computers, the model has been used to investigate the dynamic performance of the machine by providing time domain solutions to every stator coil group and rotor loop currents, electromagnetic torque as well as shaft position and speed [12]. The simulation model has also been successfully employed to investigate the stator and rotor design based on steady state performance evaluations.

In [13,15], stator winding design is considered by means of variation of coil span, distribution of windings, alternative coil-group connections and adoption of isolated windings. The study concludes that the isolated winding option for the two stator systems gives a better overall performance for two given operational conditions at constant load torque.

The design of more effective rotor configurations is discussed in [14,15]. The best alternative for the rotor structure is selected in such a way that for each option the torque contribution from each individual short circuited loop is computed and the overall machine efficiency is evaluated for two given control frequencies. Based on the computer simulation results,for the most promising of its rotor structures examined, the machine efficiency is increased, on the average, by more than ten percent for the two given control frequencies compared with the basic Broadway design.

In addition to utilizing the detailed model for machine design, electromagnetic field analysis has also been carried out by Alexander [16], which, to a large extent, enhances the understanding by providing fundamental insight into the operation of the BDFM. The study also provides information about how to design the machine more effectively.

The Approach of this Research

In this thesis, a simplified dynamic model is developed and used to perform dynamic simulation in both induction and synchronous modes of operation [17].

Conventional approaches consider the BDFM as two magnetically separated wound rotor induction machines connected electrically on the rotors. This enables well established induction motor d-q models to be applied directly to perform d-q analysis. Unlike these previous approaches, the d-q model described here is obtained from the direct mathematical transformation of the detailed machine design model. Since the detailed machine design model, under certain assumptions, is a true mathematical representation of the BDFM the simplified model must also be valid for describing the dynamic behavior of the machine with specified accuracies.

The reason for adopting this approach is based on the argument that although the BDFM is electrically equivalent to two wound rotor induction machines in cascade connection, in practice there exists in the single-frame machine only one rotor capable of providing coupling to both stator systems. The development of the Broadway rotor makes it even more difficult, if not impossible, to separate physically the cage structure to obtain the two equivalent three phase windings and their parameters. Therefore, for cage rotor BDFM, it is appropriate to work from the original physical configuration of the machine to develop analytical tools.

As will be shown in the next Chapter, the BDFM under consideration possesses a much more complex winding structure than those of most other AC electric machines. Hence, the performance equations for describing the behavior of the machine are much higher in order than those of other machines. For the detailed representation of the BDFM, it has been shown that the machine is represented by a set of 35th order nonlinear differential equations in machine variables. To transform these equations into a two-axis model, which is the minimum order dynamic representation of the BDFM, will undoubtedly provide an ultimate challenge. In addition, the necessity for obtaining the model parameters from the detailed model through a rigorous computational process adds even more complexity.

The main advantage of the modeling approach lies in the fact that it allows for not only the investigation of the dynamic behavior of the machine but also the computation of the machine parameters from machine geometry and the d-q model parameters from the rules of the transformation process. This is believed to be essential in the present

situation when parameter identification techniques for the BDFM are still being developed.

The development of the two-axis model results in a substantial order reduction compared with that of the detailed model. Thus, it can be used for development of control strategies for the BDFM as a possible alternative drive system.

The two-axis model has been used to perform dynamic simulation studies and the results are compared with the available test data [18]. Dynamic simulations performed include machine run-up in induction mode, dc and ac synchronization and synchronous behavior of the machine.

Steady state equivalent circuits for different modes of operation have also been derived from the two-axis representation. These steady state models, although derived using simplifying assumptions, can be shown to represent the fundamental nature and the basic operational principles of the BDFM and have thus improved upon the traditionally used equivalent circuits [3,6,7,8] by providing for all possible modes of operation. A method for solving the steady state equations in synchronous mode of operation for ASD applications of the system is developed and used to carry out steady state performance analysis.

Stability analysis of the BDFM under the synchronous mode of operation is also carried out using the linearized version of the two-axis model [19]. The analysis is based on the Lyapunov's indirect method in which the original nonlinear two-axis model is linearized around some equilibrium point. Since the two-axis model has to be expressed exclusively in the rotor reference frame, the resultant linearized system is

found to be time-varying and commonly used eigenvalue analysis cannot be performed directly. A new method is thus proposed in which eigenvalue analysis is carried out based on a transformed linear time-invariant model using the generalized theory of Floquet. The theoretical analysis is correlated with test data and predictions given by the original nonlinear two-axis model.

Outline of the Thesis

Following the Introduction, the basic structure and operational principles of the BDFM are discussed in Chapter 1. In Chapter 2, the dynamic equations of the BDFM in machine variables are derived followed by the machine parameter computation in Chapter 3. In Chapter 4, a two-axis model and its parameters are developed and computed. Dynamic simulation of the BDFM is presented in Chapter 5 and steady state models and performance analyses are given in both the induction and the synchronous modes of operation in Chapter 6. Chapter 7 discusses the stability analysis of the BDFM under the synchronous mode of operation.

1. THE STRUCTURE AND THE OPERATIONAL PRINCIPLES OF THE BDFM

In this chapter, the basic structure of the BDFM is described in detail, followed by a discussion of the operational principles of the BDFM.

1.1 Stator Winding Configurations

The basic structure of the stator windings, due to the work by Hunt and Creedy, can have two notable forms: a common winding structure and a separate (or isolated) winding structure [15]. The first OSU laboratory prototype was constructed based on the former and the second on the latter. Since this research work was begun when the first machine was in use, the entire analyses of the machine started by consideration of the common winding option. It will be shown later that under certain assumptions these two forms of winding structure are functionally identical. However, it is noted that it is much easier to analyze the isolated winding configuration than the common winding case.

Fig. 1-1 shows the basic stator and rotor configurations of the 6-pole and 2-pole experimental BDFM under consideration. The machine has a double layer winding in 36 stator slots. 36 individual coils are connected into 9 coil groups, which, in turn, are arranged in three Y-connected sets. These coils groups can be considered as being positioned at 0°, 40° and 80° degrees from a reference axis. Two independent three phase supplies representing the 60Hz utility grid and the output of an adjustable voltage, adjustable frequency power converter are applied to the six terminals, namely A,B,C and a,b,c, respectively. The distribution and interconnection of the coil groups are such that balanced three phase currents flowing from

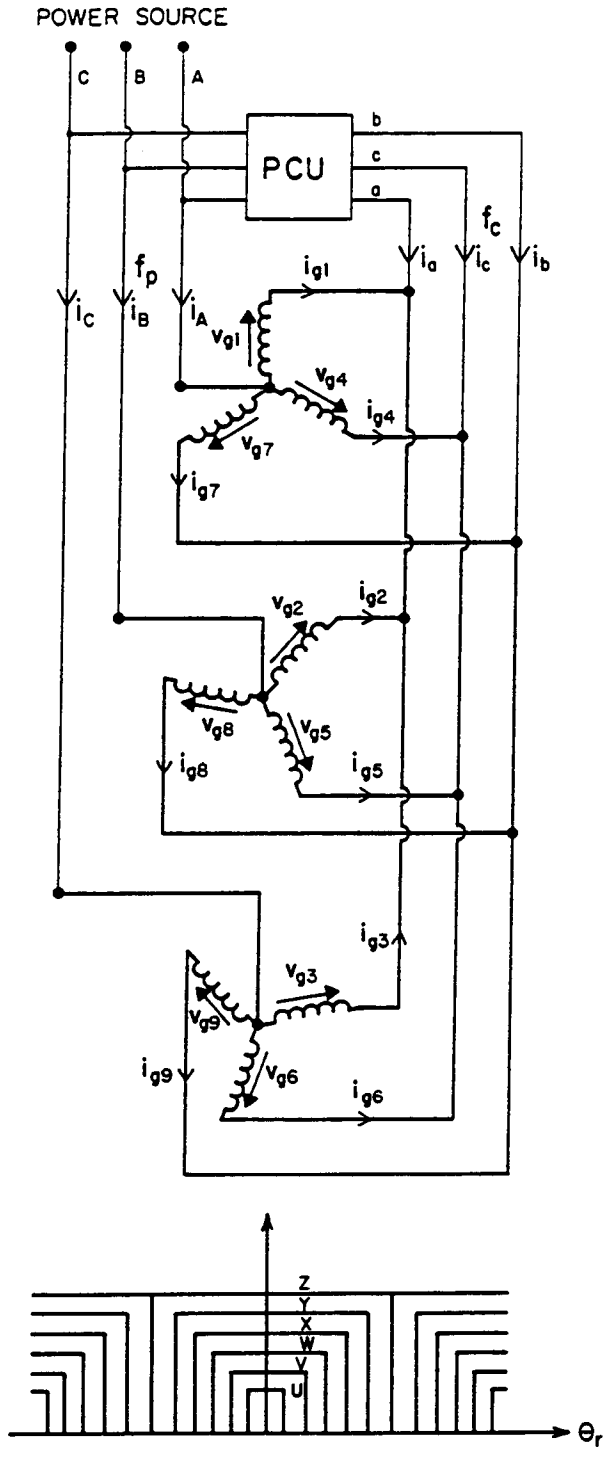

Fig. 1-1 Stator and rotor configurations of the 6- and 2-pole BDFM

the grid produce an airgap field of 6-poles, whereas currents supplied by the power electronic converter produce an airgap field of 2-poles.

The purpose of two sets of stator winding configuration described above is to avoid the use of slip rings that would be necessary for either cascade connection of two individual induction motors or a conventional doubly-fed generator or motor. Thus, slip-power recovery can be realized in normal operational conditions through one set of stator windings.

From the design point of view, the advantage of the common winding scheme has the feature of increasing usage of stator slot space. On the other hand, however, due to the connection constraints, circulating currents result because of inherent winding unbalances [16].

1.2 Cage Rotor Structures

In order to support the two airgap rotating fields of different pole numbers produced by the stator windings, a special rotor structure is required. In his original work, Hunt developed a wound rotor structure. Due to the work by Creedy and Broadway [5,3], the rotor has become mechanically simple enough to be die-cast. For the experimental prototype, there are four nests, N_1, N_2, N_3, N_4 , made up of the cage bars, also denoted as the Z loop. Within each nest there are five short-circuited loops, Y, X, W, V, U. This structure satisfies the requirement that the minimum number of cage bars must be equal to the mean of the two stator pole numbers.

1.3 Operational Principles of the BDFM

Since the BDFM is essentially composed of two induction motors in cascade connection, its characteristics should resemble those of conventional induction motors. However, the presence of two stator fields

rotating at two different speeds and their corresponding rotor fields make the machine analysis more complicated than either induction or synchronous machines in both steady state and dynamic conditions.

In doubly-fed operation, the two stator rotating fields are caused by the two independent sets of excitation voltages applied to the two stator winding systems. Ideally, these systems should be independent of one another because they compose different pole numbers. However, in practice they are slightly coupled through unbalances and harmonics in addition to their fundamental interaction via the rotor circuits. Nevertheless, throughout the thesis, it is assumed that the direct coupling between the two stator systems is negligible. As a result of this assumption, the original 9 coil group stator windings can be regarded as being **two independent 3-ϕ windings** namely ABC for the 6-pole and abc for the 2-pole. The two independent three phase windings are obtained as follows:

When energized from the 6-pole or ABC side, the machine presents a short circuit from the 2-pole or abc side as shown in Fig. 1-2(a). It can be seen that the equivalent A, B and C phases are composed of coil groups 1-4-7, 2-5-8 and 3-6-9, respectively. On the other hand, when the 2-pole or abc side is subject to an applied voltage, no current should be seen flowing out from the 6-pole or ABC side to the power supply. When the 6-pole or ABC side is short circuited, the equivalent a, b and c phases are formed. The a-phase is composed of coil groups 1-2-3, b-phase, coil groups 4-5-6 and c-phase coil groups 7-8-9. The results are also shown in Fig. 1-2(a). The two three phase systems are further illustrated in Figs. 1-2(b) and 1-2(c). It is emphasized that the cage rotor is left unchanged from its original physical configuration.

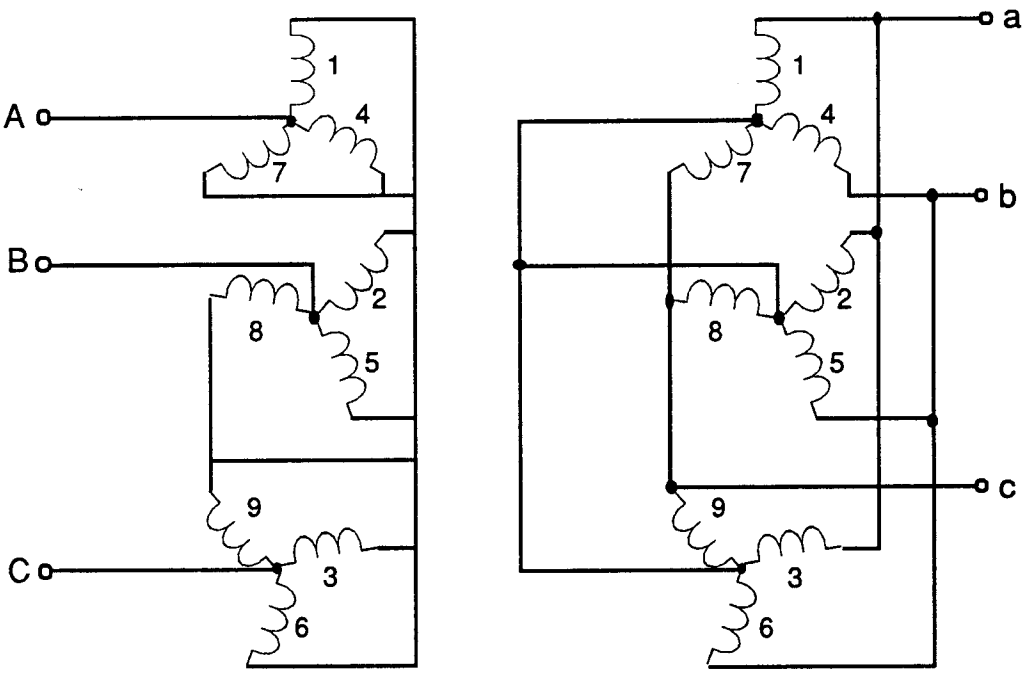

Fig. 1-2(a) Coil groups and equivalent 6- and 2-pole phases

As stated previously, the 6-pole A-phase consists of coil groups 1-4-7 each of which is, in turn, composed of four single coils positioned in proper stator slots and connected in series. Fig. 1-3 shows the 6-pole A-phase spatial MMF distribution as a result of the superposition of single coil and coil group MMF distribution. It can be seen that the 6-pole A-phase MMF is distributed spatially with a $3\theta_r$ variation, where θ_r is the rotor angle in mechanical degrees.

The 2-pole a-phase MMF is shown in Fig. 1-4 which results from currents flowing in the equivalent 2-pole a-phase winding. Since the winding is formed by coil groups 1-2-3 that have positive mutual coupling between them, the resultant MMF magnitude is much higher than that of the 6-pole A-phase. Within 0° to 360°, the MMF has one cycle of variation.

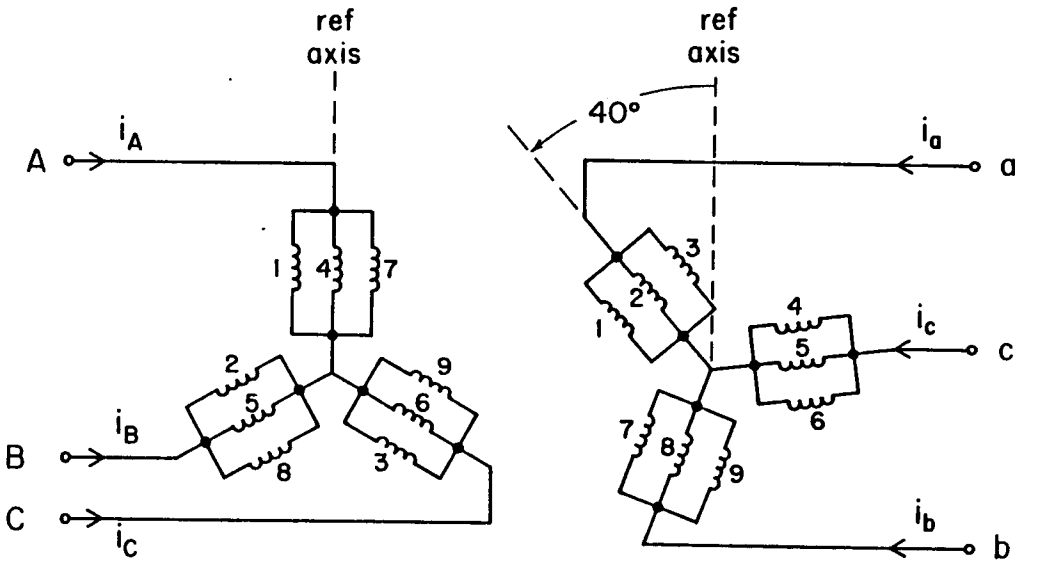

Fig. 1-2(b) Coil groups and equivalent 6- and 2-pole phases

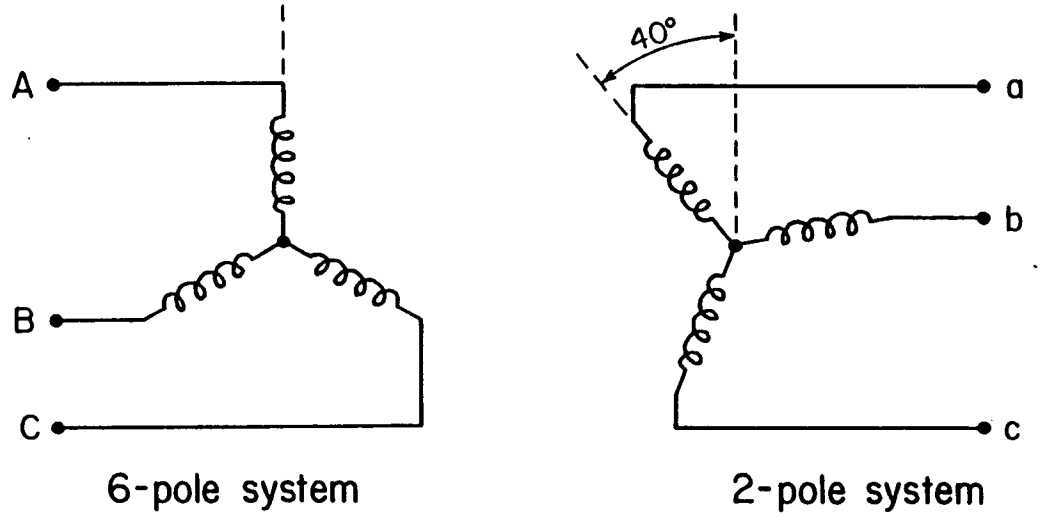

Fig. 1-2(c) Equivalent 6- and 2-pole phases

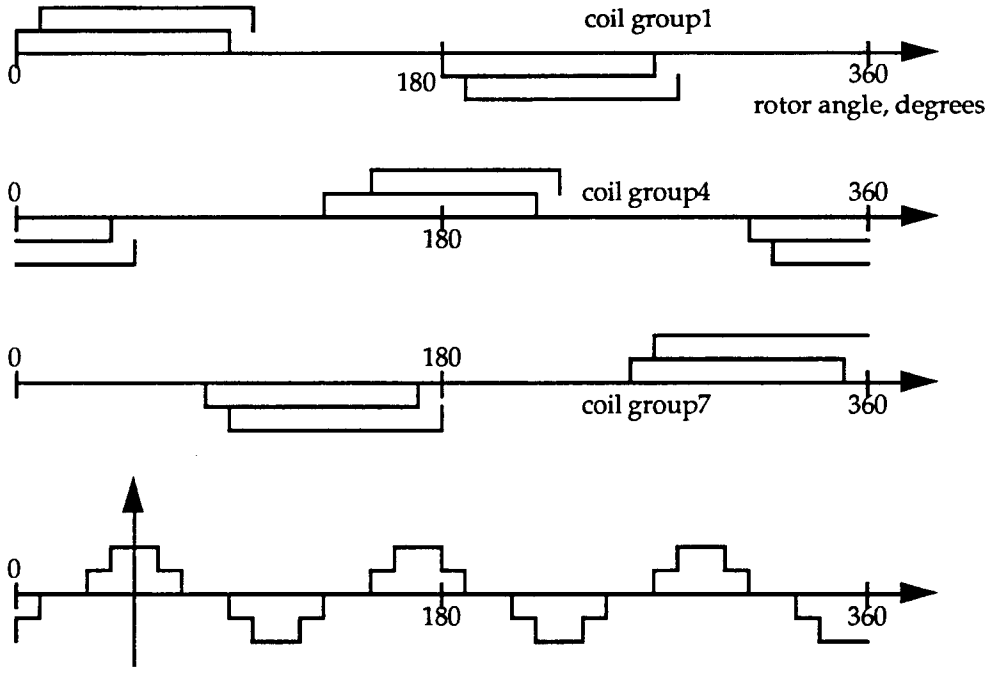

Fig. 1-3 Single coil, coil group and 6-pole A-phase MMF distribution

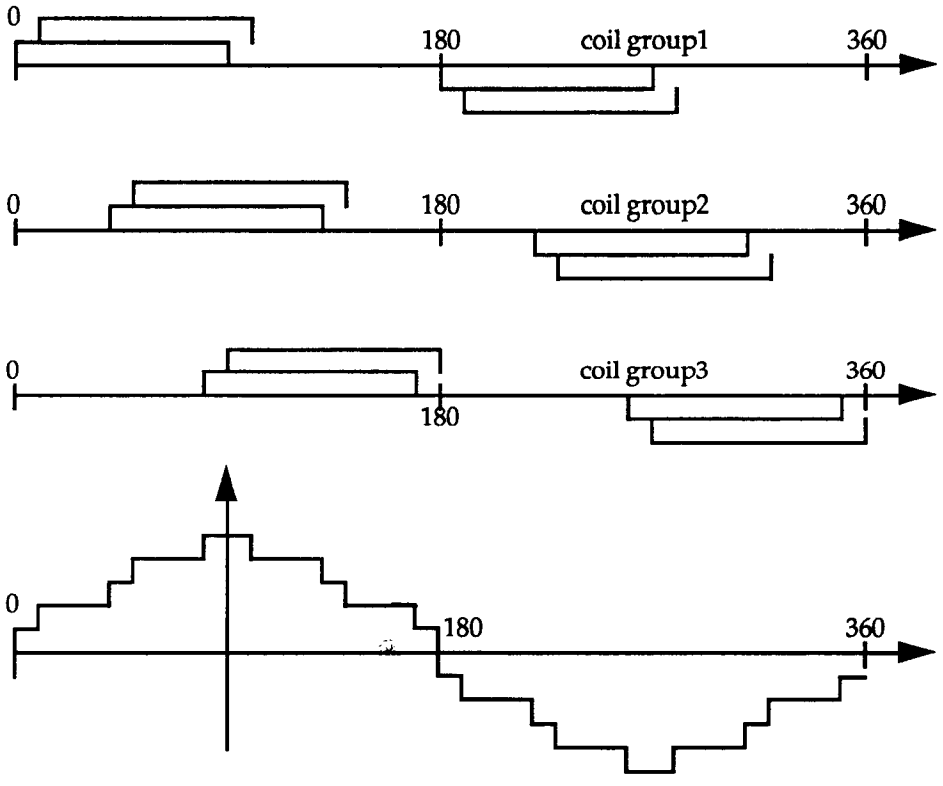

Fig. 1-4 Single coil, coil group and 2-pole a-phase MMF distribution

B and C-phase MMF distributions for the 6-pole stator system (or b and c phase MMF's for the 2-pole stator system) are shifted by 120° spatially with respect to that of the A-phase (or a-phase).

When balanced three phase sinusoidal currents are flowing in the two 3-ϕ windings, two rotating fields are established. Depending upon the sequences of the two sets of input voltages, the two rotating fields can be either in the same direction or in the opposite direction. In either scheme, the total air gap MMF is the sum of the two. Unless otherwise stated, the two fields are considered to be rotating in the opposite direction.

In response to the two stator fields of different rotating speeds, the rotor must be capable of producing two rotating fields to support the stator fields. The electromagnetic field analysis results show [16] that the requirements can be met with the cage structure proposed by Broadway. The two rotating fields produced by the rotor are due to the induced currents in the short-circuited rotor loops. The currents can be thought of as being composed of two components, each of which results from one stator rotating field. In steady state operational conditions, they may have different or the same frequency, from which the concept of modes of operation is established.

1.4 Modes of Operation of the BDFM

Both theoretical and experimental results have shown that the BDFM exhibits two distinct modes of operation: the induction mode (I.M.) and the synchronous mode (S.M.). In the former mode,the machine is fed from one set of stator windings and the other set may be connected in one of the following ways:

(1) open circuited;

(2) short circuited;

(3) connected to a passive network to dispatch slip power and perform speed control;

(4) connected to a power electronic converter to extract slip power.

Except the first case where the machine behaves essentially like a 6-pole induction motor, there are induced three phase currents in the unexcited windings which act upon the system to produce unusual effects. In the early stage of development of the system, speed control of self-cascaded induction motors was by means of the third method of winding connections since sources with variable frequency and voltage were not readily available at the time of Hunt and Creedy. Today, with the state-of-the-art power electronic converters, although this mode of operation is not a major means of achieving speed control, it is found to be an intermediate mode of operation through which a more preferable mode can be achieved. Similar to the induction motor torque speed characteristics, the shaft speed in this mode of operation is dependent on the load conditions.

The induction mode of operation (also referred to as asynchronous mode) may also take place when the BDFM is doubly-fed. The fundamental difference between the singly-fed induction mode and doubly-fed induction mode is that in the former the rotor currents have only one frequency while in the latter two frequencies co-exist. In the case where the two fields are in the opposite direction of rotation, this mode of operation was found to cause power losses, pulsating torques and fluctuating speeds. Thus, this mode of operation, under any normal circumstances, should be avoided.

The synchronous mode of operation is established when the frequencies of the rotor currents induced by the two counter-rotating fields of the two stator systems become identical. In the synchronous mode of operation, the two sets of stator windings are fed from isolated sources of different frequencies. Like conventional synchronous machines, the BDFM requires certain synchronization procedures [1]. Once synchronous operation is established, the shaft speed of the machine is independent of the load conditions unless a severe disturbance occurs. Compared with the induction mode of operation, synchronous mode is highly preferred since precise open loop speed control can easily be obtained. Table I summarizes the different modes of operation for the experimental BDFM, which has 6-pole and 2-pole stator winding sets and a Broadway rotor (cage rotor).

Table I Operation modes of the BDFM in steady state conditions

	6-pole stator	2-pole stator	cage rotor
I.M.	Excited with f_6	Not excited	One freq f_r
I.M.	Excited with f_6	Excited with f_2	Two freq. f_{r6}, f_{r2}
S.M.	Excited with f_6	Excited with f_2	One freq. $f_{r6}=f_{r2}$

Modes of operation of the BDFM, under certain conditions, can be changed from one form to another through a transition period as can be observed in the laboratory. From a simulation point of view, this cannot be realized using steady state models on which most previous work has been based. Indeed, development of a dynamic model will make it possible to study the machine behavior in a more general way instead of looking into the modes of operation of the machine separately.

2. DYNAMIC MODELING OF BRUSHLESS DOUBLY-FED MACHINES IN MACHINE VARIABLES

The voltage equations to be developed in this Chapter are modified equations of the BDFM described in [11,12] in order that they can be transformed into a two-axis model. In order to derive the voltage equations for the Brushless Doubly-Fed machines, the following assumptions are made.

(1) The magnetic and electric circuits are linear. Saturation is neglected.

(2) Spatial harmonics, other than the third harmonic of the 2-pole system which corresponds to the 6-pole system fundamental, are negligible.

(3) Direct coupling between the 6-pole and the 2-pole systems is negligible.

It is noticed that assumptions similar to (1) and (2) are usually made when analysis of electric machinery is carried out in the two-axis reference frame. The third assumption which has been made in the previous Chapter is repeated again for completeness.

2.1 Voltage Equations of the Brushless Doubly-Fed Machines

Figs 2-1 and 2-2 show the idealized BDFM under consideration. It is noticed that in Figs 2-1 and 2-2 the 6- and the 2-pole stator systems have been separated and the distributed winding configurations of the original winding structure replaced by sinusoidally distributed, windings with the 6-pole A-phase winding taken as a reference axis.

Unlike the stator winding structures, of which three magnetic axes are

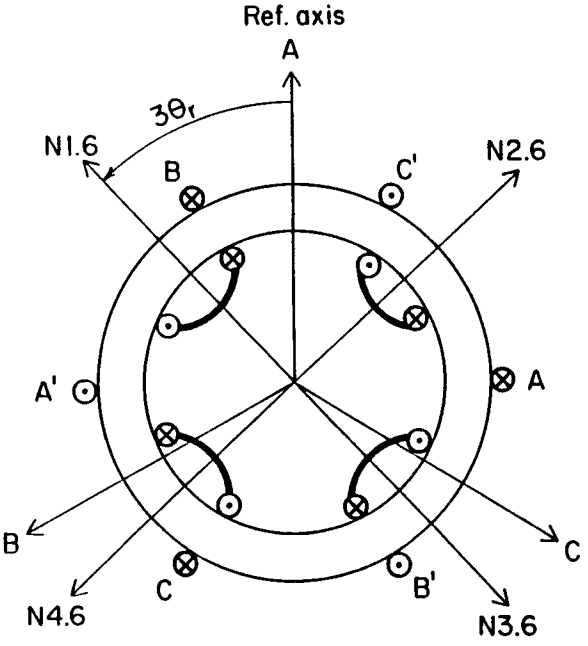

Fig. 2-1 Idealized BDFM 6-pole system

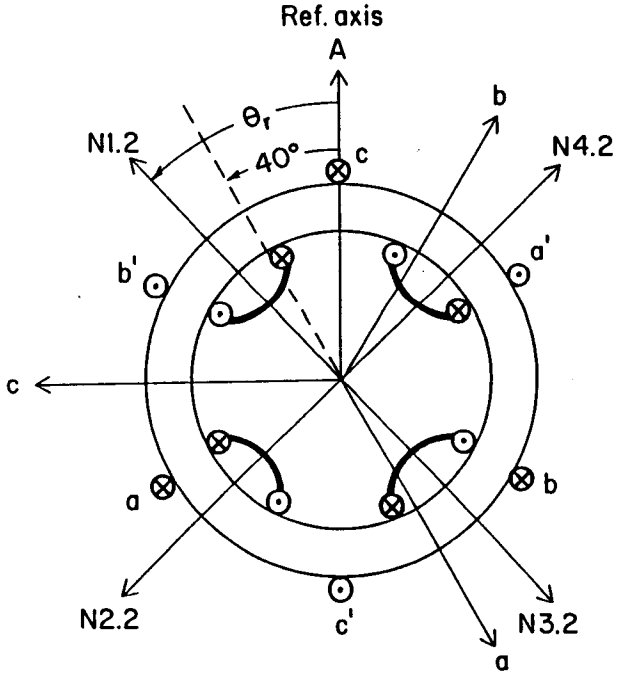

Fig. 2-2 Idealized BDFM 2-pole system

displaced 120° apart in space, the rotor winding is composed of short circuited loops and four magnetic axes are 90° apart spatially. The rotor displacement angle θ_r is defined as the angle between the reference axis A and the axis of nest 1, N1.6. Note that in Fig. 2-1, the axis of nest 2, N2.6, is lagging N1.6 by 90° spatially while in Fig. 2-2 N2.2 is leading N1.2 by 90°. This is due to the fact that θ_r is expressed in mechanical degrees and for 6-pole system 90° mechanical degrees corresponds to 270° electrical degrees.

Based on the two figures, the voltage equations in machine variables can be expressed as

$$\begin{bmatrix} \mathbf{v}_{s6} \\ \mathbf{v}_{s2} \\ \mathbf{v}_r \end{bmatrix} = \begin{bmatrix} \mathbf{Z}_{s6} & \mathbf{0} & \mathbf{Z}_{s6r} \\ \mathbf{0} & \mathbf{Z}_{s2} & \mathbf{Z}_{s2r} \\ \mathbf{Z}^t_{s6r} & \mathbf{Z}^t_{s2r} & \mathbf{Z}_r \end{bmatrix} \begin{bmatrix} \mathbf{i}_{s6} \\ \mathbf{i}_{s2} \\ \mathbf{i}_r \end{bmatrix} \tag{2-1}$$

In the above matrix equations, the subscripts s6, s2 denote variables and parameters associated with 6-pole (ABC) and 2-pole (abc) stator circuits and subscript r denotes variables and parameters associated with the cage rotor circuits. $\mathbf{v}_{s6}$,$\mathbf{v}_{s2}$ represent 6- and 2-pole phase voltage vectors while $\mathbf{v}_r$ stands for the rotor loop voltage vector. Since all the rotor loops are short circuited, $\mathbf{v}_r = 0$. Three current vectors, $\mathbf{i}_{s6}$, $\mathbf{i}_{s2}$ and $\mathbf{i}_r$ describe the 6 and 2-pole phase currents and the rotor loop currents, respectively. Notice that the mutual impedance matrices between the two independent stator systems are zero. This results from the third assumption made at the beginning of this Chapter. The parameter matrices $\mathbf{Z}_{s6}$, $\mathbf{Z}_{s2}$, $\mathbf{Z}_{s6r}$, $\mathbf{Z}_{s2r}$ and $\mathbf{Z}_r$ are described in detail below.

2.1.1 6-pole and 2-pole Stator Impedance Matrices

The 6 and the 2-pole stator impedance matrices, denoted as $\mathbf{Z}_{s6}$, $\mathbf{Z}_{s2}$, are constant 3 by 3 matrices defined by

$$Z_{s6} = \begin{bmatrix} r_6+L_Ap & M_{AB}p & M_{AC}p \\ M_{BA}p & r_6+L_Ap & M_{BC}p \\ M_{CA}p & M_{CB}p & r_6+L_Ap \end{bmatrix} \quad (2\text{-}2)$$

and

$$Z_{s2} = \begin{bmatrix} r_2+L_ap & M_{ab}p & M_{ac}p \\ M_{ba}p & r_2+L_ap & M_{bc}p \\ M_{ca}p & M_{cb}p & r_2+L_ap \end{bmatrix} \quad (2\text{-}3)$$

where r_6 and r_2 are the phase resistance of the 6-pole or the 2-pole system winding. $L_A = L_{Am} + L_{l6}$ and $L_a = L_{am} + L_{l2}$ represent the phase self inductances and L_{Am} and L_{am} are the phase magnetizing inductances of the 6- and 2-pole systems, respectively. L_{l6}, L_{l2} stand for the phase leakage inductances. M's represent the mutual inductances between ABC or abc phases.

Since the 9 coil groups form two balanced three phase systems, the mutual inductances in each of the matrices are all equal. It is noted that the impedance matrices of either 6 or 2-pole stator system in (2-2) or (2-3) are similar to that of a conventional induction motor. Moreover, sinusoidal distribution of stator windings of the two systems suggests that

$$M_{AB} = -0.5L_{Am}, \quad M_{ab} = -0.5L_{am} \quad (2\text{-}4)$$

2.1.2 Mutual Impedance Matrices between Stator Phases and Nested Rotor Loops

Z_{s6r} and Z_{s2r} designate the mutual impedance matrices between the two sets of 3-ϕ stator windings and the nested rotor loops. Since there are in total 24 rotor loops, Z_{s6r} and Z_{s2r} are 3 by 24 matrices, the entries of which are dependent on the rotor position with respect to the stator reference axis. Z_{s6r} and Z_{s2r} can be partitioned further as :

$$Z_{s6r} = p[\, L_{s6rZ}\ L_{s6rY}\ L_{s6rX}\ L_{s6rW}\ L_{s6rV}\ L_{s6rU}\,] \tag{2-5}$$

for the 6-pole system and rotor nested loop mutual impedance matrix and

$$Z_{s2r} = p[\, L_{s2rZ}\ L_{s2rY}\ L_{s2rX}\ L_{s2rW}\ L_{s2rV}\ L_{s2rU}\,] \tag{2-6}$$

for the 2-pole system and rotor nested loop mutual impedance matrix where in (2-5) and (2-6), L_{s6ri} and L_{s2ri}, i=Z,Y,X,W,V,U represent the mutual inductance matrices between stator phases and the similar rotor loops in different nests. Since the BDFM rotor has four nests, L_{s6ri} and L_{s2ri} are 3 by 4 matrices. The complete expansions of L_{s6ri} and L_{s2ri} are typically

$$L_{s6ri} = M_{s6ri} \begin{bmatrix} \cos 3\theta_r & \sin 3\theta_r & -\cos 3\theta_r & -\sin 3\theta_r \\ \cos(3\theta_r - 120^\circ) & \sin(3\theta_r - 120) & -\cos(3\theta_r - 120^\circ) & -\sin(3\theta_r - 120^\circ) \\ \cos(3\theta_r + 120^\circ) & \sin(3\theta_r + 120^\circ) & -\cos(3\theta_r + 120^\circ) & -\sin(3\theta_r + 120^\circ) \end{bmatrix}$$

$$= M_{s6ri}\,[\, f(3\theta_r)\,] \tag{2-6}$$

for 6-pole stator phase and rotor loop mutual inductances and

$$L_{s2ri} = M_{s2ri} \begin{bmatrix} -\cos[\theta_r - 40^\circ] & \sin[\theta_r - 40^\circ] & \cos[\theta_r - 40^\circ] & -\sin[\theta_r - 40^\circ] \\ -\cos[(\theta_r - 40^\circ) - 120^\circ] & \sin[(\theta_r - 40^\circ) - 120^\circ] & \cos[(\theta_r - 40^\circ) - 120^\circ] & -\sin[(\theta_r - 40^\circ) - 120^\circ] \\ -\cos[(\theta_r - 40^\circ) + 120^\circ] & \sin[(\theta_r - 40^\circ) + 120^\circ] & \cos(\theta_r - 40^\circ) + 120^\circ] & -\sin[(\theta_r - 40^\circ) + 120^\circ] \end{bmatrix}$$

$$= M_{s2ri}\,[g(\theta_r)] \tag{2-7}$$

for 2-pole stator phase and rotor loop mutual inductances.

In (2-6) and (2-7), M_{s6ri} and M_{s2ri}, i=Z,Y,X,W,V,U are the magnitudes of the sinusoidal mutual inductance functions, which result from the Fourier analysis of the nonsinusoidal variations of the stator phase rotor loop mutual inductances.

The mutual inductance matrices Z^t_{s6r} and Z^t_{s2r} are the transpose of Z_{s6r} and Z_{s2r}, respectively.

2.1.3 Rotor Circuit Impedance Matrix

Because its function is absolutely unique in electric machine operating principles, the BDFM rotor has configurations that are not readily analyzable by conventional means. It can be shown [11], however, that it is appropriate to represent the cage rotor in terms of a series of coupled mesh loop circuits as can be shown in Fig. 2-3 and Fig. 2-4, in which only three out of six loops in each nest are shown.

It is seen from Fig. 2-4 that each rotor loop has a resistance and self inductance and there exists mutual inductance between loops in the same nest. In addition, there is also mutual inductance between adjacent nests. Since the rotor loops are all short circuited at the common endrings, there is also common endring resistance. Taking all the rotor loops into account, we can express the rotor impedance matrix as a 24 by 24 matrix, which is described in detailed in [11,12]. In order to develop the two-axis model in Chapter 4, the rotor impedance matrix needs to be rearranged from its original structure. Denoting the rotor impedance matrix as Z_r which can be concisely expressed by the following expression

$$Z_r = \{ Z_{ij} \} \tag{2-8}$$

where i and j are rotor loop indentifiers, i.e. i, j= Z,Y,X,W,V,U.

It should be noted that in (2-8) each element of Z_r, Z_{ij}, is also a 4 by 4 symmetrical impedance matrix, each of which is defined as follows:

(1) for i=j≠Z, i, j=Y,X,W,V,U

$$Z_{ii} = \begin{bmatrix} r_{ii}+L_{ii}p & -M_{ii}p & -M_{ii}p & -M_{ii}p \\ -M_{ii}p & r_{ii}+L_{ii}p & -M_{ii}p & -M_{ii}p \\ -M_{ii}p & -M_{ii}p & r_{ii}+L_{ii}p & -M_{ii}p \\ -M_{ii}p & -M_{ii}p & -M_{ii}p\,p & r_{ii}+L_{ii}p \end{bmatrix} \tag{2-9}$$

where r_{ii} and L_{ii} designate loop resistance and self inductance, respectively. M_{ii} represents the mutual inductance between the similar loops in different nests, as is illustrated in Fig. 2-4.

Eqn. (2-9) describes five diagonal elements (five loops) in Z_r.

(2) for i=j=Z

$$Z_{zz} = \begin{bmatrix} r_{zz}+L_{zz}p & -r'_{zz}-(L'_{zz}+M_{zz})p & -M_{zz}p & -r'_{zz}-(L'_{zz}+M_{zz})p \\ -r'_{zz}-(L'_{zz}+M_{zz})p & r_{zz}+L_{zz}p & -r'_{zz}-(L'_{zz}+M_{zz})p & -M_{zz}p \\ -M_{zz}p & -r'_{zz}-(L'_{zz}+M_{zz})p & r_{zz}+L_{zz}p & -r'_{zz}-(L'_{zz}+M_{zz})p \\ -r'_{zz}-(L'_{zz}+M_{zz})p & -M_{zz}p & -r'_{zz}-(L'_{zz}+M_{zz})p & r_{zz}+L_{zz}p \end{bmatrix} \quad (2\text{-}10)$$

where $r_{zz}+L_{zz}p$ is the "Z" loop impedance and $-(r'_{zz}+L'_{zz}p)$ is defined as the common bar impedance.

This matrix describes the impedance of the outermost loop or cage, i.e. the "Z" loop matrix. It is noted that besides the loop resistance and self inductance, the Z loop contains common bars which have been taken into account.

(3) for $i \neq j$, i, j=Z,Y,X,W,V,U

$$Z_{ij} = \begin{bmatrix} r_{ij}+M_{ij}p & -M'_{ij}p & -M'_{ij}p & -M'_{ij}p \\ -M'_{ij}p & r_{ij}+M_{ij}p & -M'_{ij}p & -M'_{ij}p \\ -M'_{ij}p & -M'_{ij}p & r_{ij}+M_{ij}p & -M'_{ij}p \\ -M'_{ij}p & -M'_{ij}p & -M'_{ij}p & r_{ij}+M_{ij}p \end{bmatrix} \quad (2\text{-}11)$$

where r_{ij} is the "mutual" resistance in one nest and M_{ij} expresses the mutual inductance between loops in the same nests. M'_{ij} represents the mutual inductance between loops in different nests.

There are fifteen possible combinations of i, j. Thus, this matrix presents 15 submatrices, i.e. the upper diagonal elements of Z_r. Notice also that $Z_{ji}=Z_{ij}$, for $i \neq j$, which expresses another 15 submatrices, i.e. the lower diagonal elements of Z_r.

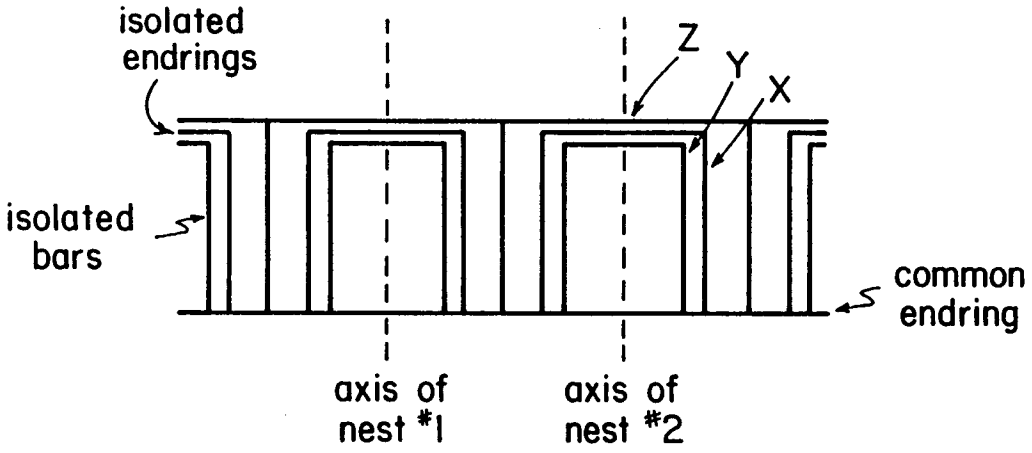

Fig. 2-3 Cage rotor structures of the BDFM

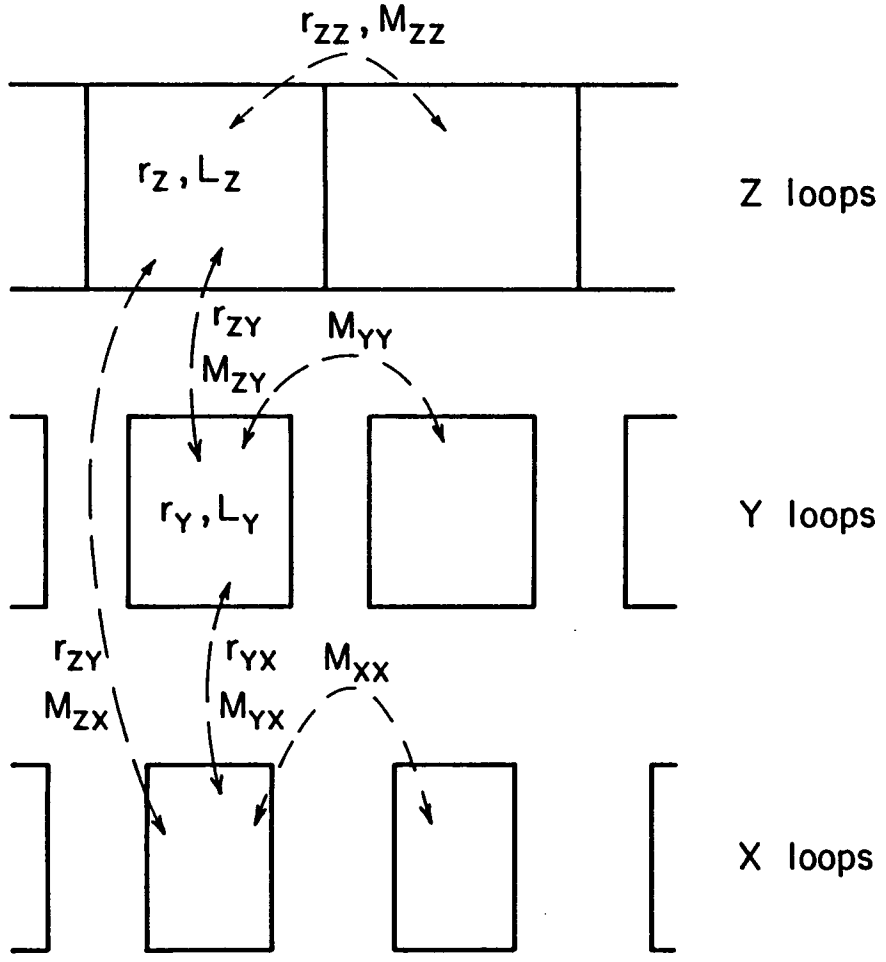

Fig. 2-4 Mesh loop circuit model of the cage rotor of the BDFM

3. PARAMETER COMPUTATIONS OF THE BDFM IN MACHINE VARIABLES

Parameter computations for the BDFM voltage equations are presented in this Chapter. It can be shown that parameter computation of the BDFM plays an essential role in the dynamic modeling process since no information concerning parameter identification for the BDFM has been found in the literature. Commonly used parameter identification techniques for both synchronous and induction machines can not, in general, be applied to the BDFM parameter identification process. A mistake that can be easily made in parameter identification procedure is to attempt to use a model, which is valid for only one particular operational mode, to identify machine parameters. This model, under machine testing process, may be completely invalid, which often results in meaningless results. Research is now underway to use modern system identification techniques to accomplish the task.

An alternative for obtaining machine parameters is to employ computational methods from which parameters of the machine are calculated based on machine geometry. An apparent advantage of this approach is that it relates the **true machine parameters,** such as winding resistance, self and mutual inductances and mutual inductances between stator and rotor windings, with the machine performance in both dynamic and steady state operational conditions.

As mentioned in the Introduction, by consideration of the interaction between basic stator winding and nested rotor loops, a detailed machine design model has been developed. The machine parameters have all been

computed and assembled into four impedance matrices, namely the stator impedance $\mathbf{Z'}_{ss}$, the stator-rotor mutual impedance matrix $\mathbf{Z'}_{sr}$, the rotor-stator impedance matrix $\mathbf{Z'}_{rs}$ and finally the rotor impedance matrix $\mathbf{Z'}_{rr}$ [11,12]. Since the BDFM equation in machine variables described in this thesis is a modified version of that given in [11,12], the parameter matrices must also be modified accordingly.

It is the purpose of this Chapter to develop additional computational techniques for evaluation of machine parameters for the modified BDFM equation, which is more suitable for the development of the two-axis model.

It is assumed that the four parameter matrices from the detailed model $\mathbf{Z'}_{ss}$, $\mathbf{Z'}_{sr}$, $\mathbf{Z'}_{rs}$, and $\mathbf{Z'}_{rr}$ parameter matrices are given and it will be shown that all the parameters in the BDFM Eqn. (2-1) can be calculated according to the given information and later developed into the d-q model parameters (see Chapter 4).

3.1 Parameter Computation of the 6-pole Stator Windings

Previous work has been done to calculate the machine parameters at the coil group level [11]. The equivalent 6- and 2-pole phase quantities can be identified if the coil group impedance matrix is known. Fig. 3-1 shows the equivalent 6- pole three phase (ABC) windings in term of the 9 coil groups. When each of the 6-pole phases is energized independently, we can write a series of equations to calculate the parameters. Since the 6-pole system is completely balanced, only two quantities, the self impedance of one phase and the mutual impedance between two phases, are needed to be computed.

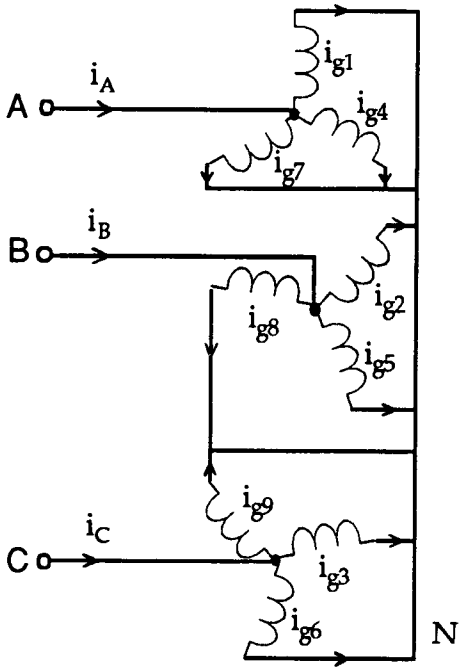

Fig. 3-1 Equivalent 6-pole phases in terms of 9 coil groups

Suppose that 6-pole A-phase is subject to an applied voltage v_{AN}, we have from Fig. 3-1

$$\begin{bmatrix} v_{AN} \\ v_{AN} \\ v_{AN} \end{bmatrix} = \begin{bmatrix} r_g+L_gp & Mp & Mp \\ Mp & r_g+L_gp & Mp \\ Mp & Mp & r_g+L_gp \end{bmatrix} \begin{bmatrix} i_{g1} \\ i_{g4} \\ i_{g7} \end{bmatrix} \tag{3-1}$$

where (r_g+L_gp) is the impedance of one coil group. $M=M_{14}=M_{17}=M_{47}$ is the mutual inductance between coil groups 1, 4 and 7. Adding the three equations together and also noting that $i_A= i_{g1}+i_{g4}+i_{g7}$, we get

$$v_{AN}=\frac{1}{3}\,[r_g+(L_g+2M)p]\,i_A = [r_6 + (L_{l6} + L_{Am})p]\,i_A = Z_A\,i_A \tag{3-2}$$

Thus, the equivalent per phase impedance is obtained. Comparing (3-1) and (3-2), we also get

$$i_{g1} = i_{g4} = i_{g7} = \frac{1}{3}\,i_A \tag{3-3}$$

Equation (3-3) suggests that i_A is distributed evenly in coil groups 1, 4 and 7.

The mutual inductance between the 6-pole phases is next computed. The induced voltage in the B-phase due to the applied voltage v_{AN} is

$$v_{BN} = M_{12}\,p(i_{g1})+M_{42}\,p(i_{g4})+M_{72}p(i_{g7}) \tag{3-4}$$

Using (3-3), we have

$$v_{BN} = \frac{1}{3}(M_{12}+M_{42}+M_{72})p(\,i_A) = M_{AB}p(i_A) \tag{3-5}$$

since $M_{AB}=M_{AC}=M_{BC}$ and the mutual inductances are reciprocal, the 6-pole inductance matrix can been formed from the two calculated values. This matrix together with coil resistance is assembled into the 6-pole impedance matrix denoted by z_{s6} as has been given in (2-2).

3.2 Parameter Computation of the 2-pole Stator Windings

Fig. 3-2 shows the equivalent abc phases in terms of 9 coil groups. Suppose that 2-pole a-phase is energized alone. The following two equations can be written

$$\begin{bmatrix} -v_{an} \\ -v_{an} \\ -v_{an} \end{bmatrix} = \begin{bmatrix} r_g+L_gp & M_{12}p & M_{13}p \\ M_{21}p & r_g+L_gp & M_{23}p \\ M_{31}p & M_{32}p & r_g+L_gp \end{bmatrix} \begin{bmatrix} i_{g1} \\ i_{g2} \\ i_{g3} \end{bmatrix} \tag{3-6}$$

and

$$i_a = -\,(\,i_{g1}+i_{g2}+i_{g3}\,) \tag{3-7}$$

Since $M_{12} = M_{23}$, but $M_{13} \neq M_{12}$, Eqn. (3-6) can not be solved explicitly. Therefore, an assumption as to how the current is distributed in the windings has to be made. From the partial symmetry of the three windings, it is known that $i_{g1}=i_{g3}$. In the 2-pole impedance matrix computations, it is assumed that the currents in the 1, 2 and 3 coil groups are distributed in the following way

$$i_{g1} = i_{g3} = -\frac{2}{7} i_a \tag{3-8}$$

and

$$i_{g2} = -\frac{3}{7} i_a \tag{3-9}$$

Knowing these conditions, we can express v_{an} in terms of i_a only,

$$v_{an} = \frac{1}{3} \{r_g + [L_g + \frac{2}{7}(M_{21}+M_{31})p + \frac{3}{7}(M_{12}+M_{32})p + \frac{2}{7}(M_{13}+M_{23})p]\} i_a \tag{3-10}$$

since $M_{12} = M_{21} = M_{23} = M_{32}$ and $M_{13}=M_{31}$, (3-10) can also be written as

$$v_{an} = \frac{1}{3} [r_g + (L_g + \frac{10}{7} M_{12} + \frac{4}{7} M_{13})p] i_a$$

$$= [r_2 + (L_{12} + L_{am})p] i_a = Z_a i_a \tag{3-11}$$

Other ratios of the current distribution may also be assumed, but they do not affect the value of the impedance, Z_a , significantly.

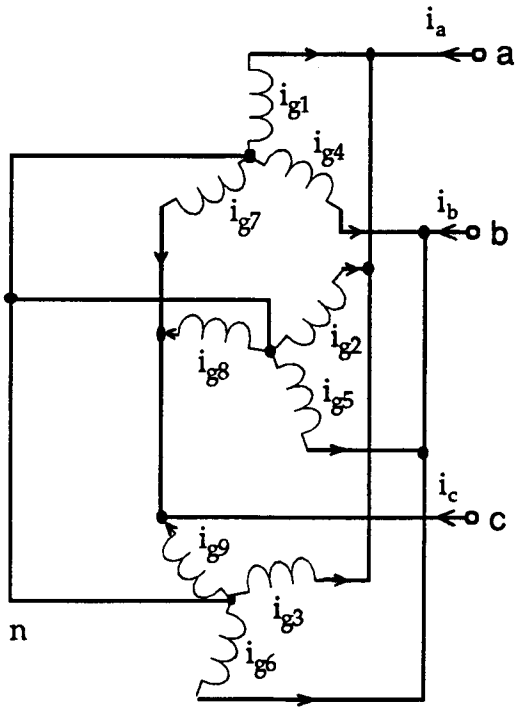

Fig. 3-2 Equivalent 2-pole phases in terms of 9 coil groups

The mutual inductance between abc phases can be computed by first considering applying a voltage to a-phase and then calculating the induced voltages on the b-phase. The following equations are derived

$$\begin{bmatrix} -v_{bn} \\ -v_{bn} \\ -v_{bn} \end{bmatrix} = \begin{bmatrix} M_{14}p & M_{24}p & M_{34}p \\ M_{15} & M_{25}p & M_{35}p \\ M_{16}p & M_{26}p & M_{36}p \end{bmatrix} \begin{bmatrix} i_{g1} \\ i_{g2} \\ i_{g3} \end{bmatrix} \tag{3-12}$$

and

$$i_a = -(i_{g1}+i_{g2}+i_{g3}) \tag{3-13}$$

Combining the three equations in (3-12) leads to

$$-v_{bn}= \frac{1}{3} [(M_{14}+M_{15}+M_{16})p(i_{g1})+(M_{24}+M_{25}+M_{26})p(i_{g2})+(M_{34}+M_{35}+M_{36})p(i_{g3})] \tag{3-14}$$

Similarly, the induced voltage v_{cn} due to the applied v_{an} is

$$\begin{bmatrix} -v_{cn} \\ -v_{cn} \\ -v_{cn} \end{bmatrix} = \begin{bmatrix} M_{17}p & M_{18}p & M_{19}p \\ M_{27}p & M_{28}p & M_{29}p \\ M_{37}p & M_{38}p & M_{39}p \end{bmatrix} \begin{bmatrix} i_{g1} \\ i_{g2} \\ i_{g3} \end{bmatrix} \tag{3-15}$$

or

$$-v_{cn}= \frac{1}{3} [(M_{17}+M_{18}+M_{19})p(i_{g1})+(M_{27}+M_{28}+M_{29})p(i_{g2})+(M_{37}+M_{38}+M_{39})p(i_{g3})] \tag{3-16}$$

v_{cn} may also be expressed if the b-phase is subject to an applied voltage v_{bn}

$$-v_{cn}= \frac{1}{3} [(M_{47}+M_{48}+M_{49})p(i_{g4})+(M_{57}+M_{58}+M_{59})p(i_{g5})+(M_{67}+M_{68}+M_{69})p(i_{g6})] \tag{3-17}$$

With any of the above equations, the mutual inductance among abc phases could be obtained, provided that the phase current can be expressed in term of coil group currents. Again, we assume that

$$i_{g1} = i_{g3} = -\frac{2}{7} i_a \tag{3-18}$$

and

$$i_{g2} = -\frac{3}{7} i_a \tag{3-19}$$

or

$$i_{g4} = i_{g6} = -\frac{2}{7} i_b \tag{3-20}$$

and

$$i_{g5} = -\frac{3}{7} i_b \tag{3-21}$$

for (3-17), the mutual expression is

$$M_{ab}=M_{ac}= M_{bc}= \frac{1}{21} [2(M_{17}+M_{18}+M_{19})+3(M_{27}+M_{28}+M_{29})+2(M_{37}+M_{38}+M_{39})] \tag{3-22}$$

Similar to the formulation of the 6-pole stator impedance matrix $\mathbf{Z}_{s6}$, $\mathbf{Z}_{s2}$ is established as is given in (3-3).

3.3 Mutual Inductances between Two Stator Windings and Rotor Loops

Computation of rotor angle dependent mutual inductances between 6- and 2-pole stator system and nested rotor loops starts with consideration of single stator coil and nested rotor loop mutual inductances which are available from previous work [11]. The mutual inductances are computed numerically using a modified subroutine program developed for the detailed dynamic model.

Fig. 3-3 shows a plot of the mutual inductances between single coil 1 and 6 rotor loops in nest 1 as a function of rotor angle θ_r in mechanical degrees. Obviously, mutual inductances between coil group 1, $M_{cg}(\theta_r)$, which is composed of four single coils positioned at 0°, 10°, 180° and 190°, respectively, and the 6 rotor loops can be calculated by utilizing the internal connection matrix $\mathbf{C}_1$ [11,12]. Since the four single coils are connected in series, $M_{cg}(\theta_r)$ is simply the sum of the four mutual inductances at every rotor angle $0^\circ \le \theta_r \le 360^\circ$. The results are shown in Fig. 3-4. Other coil

group rotor loop mutual inductances may also be computed by repeating the above procedure using C_1 .

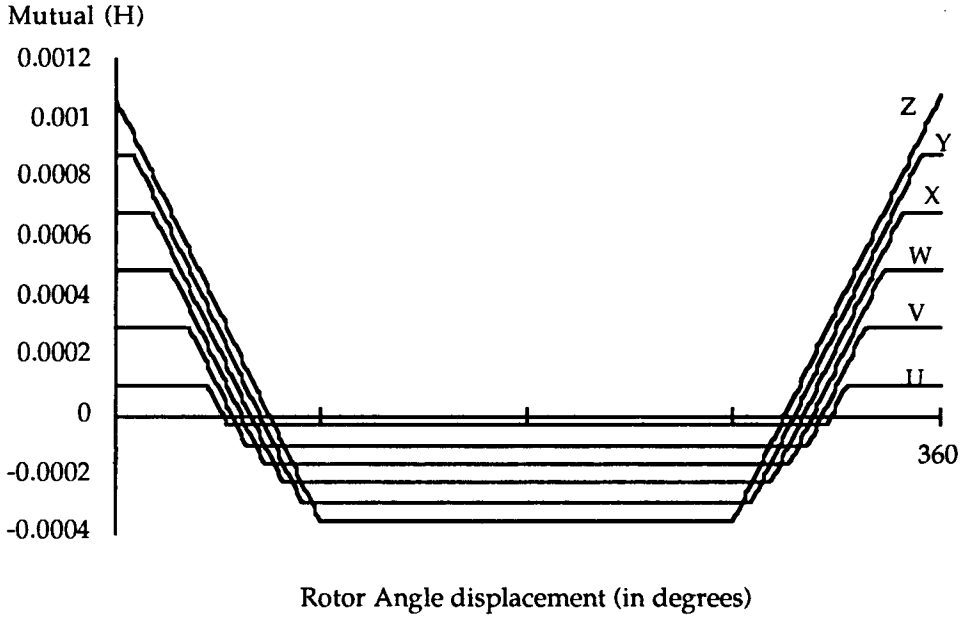

Fig. 3-3 Mutuals between single stator coil and nested rotor loops

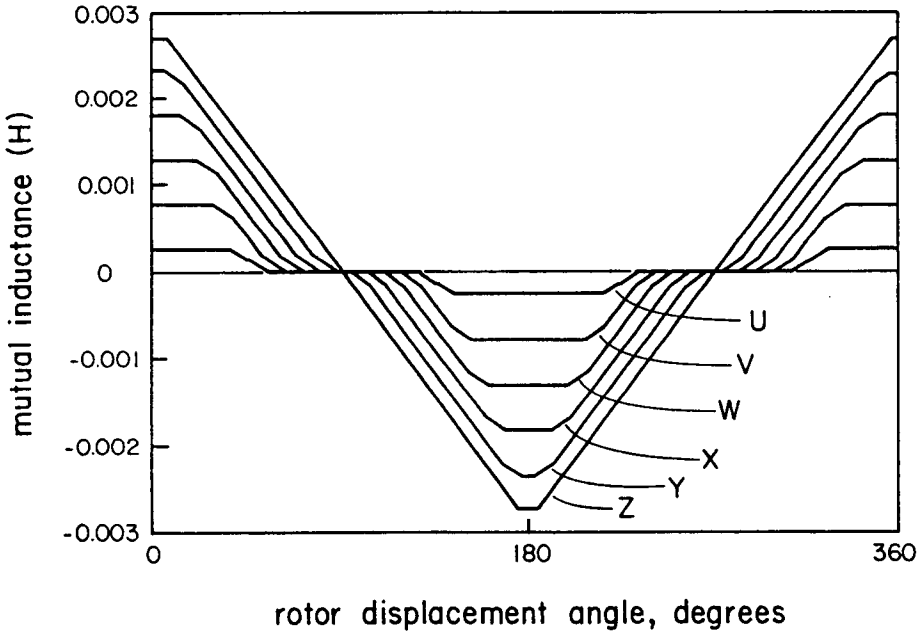

Fig. 3-4 Mutuals between coil group and nested rotor loops

The mutual inductances between equivalent 6- and 2-pole phases and nested rotor loops are calculated next. For the 6-pole rotor loop system, equivalent A, B, C phases are formed by coil groups 1-4-7, 2-5-8 and 3-6-9, respectively. In order to derive the expression for the equivalent mutual inductances between ABC phases and rotor loops in the four nests, consider Fig. 3-5

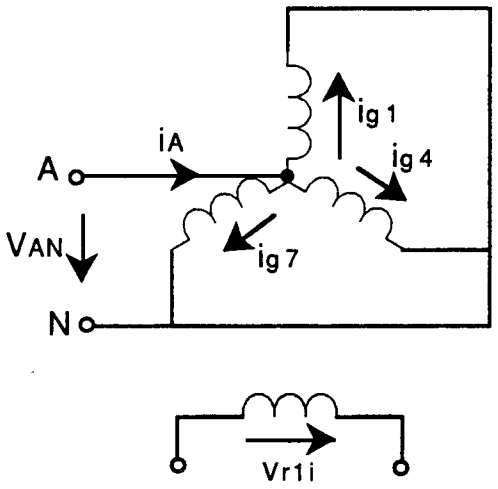

Fig. 3-5 Mutuals between A-phase and rotor "ith" loop in nest 1

With all the rotor loops open-circuited, the induced voltages in the rotor "ith" loop, i=Z,Y,X,W,V,U, in nest 1 due to the applied voltage v_{AN} alone are

$$v_{r1i} = p[M_{1\text{-}i}(\theta_r)i_{g1}] + p[M_{4\text{-}i}(\theta_r)i_{g4}] + p[M_{7\text{-}i}(\theta_r)i_{g7}] \qquad (3\text{-}23)$$

where $M_{1\text{-}i}(\theta_r)$, $M_{4\text{-}i}(\theta_r)$, $M_{7\text{-}i}(\theta_r)$ are the rotor angle dependent mutual inductances between coil groups 1, 4 and 7 and rotor "ith" loop in nest 1, respectively.

Since

$$i_{g1} = i_{g4} = i_{g7} = \frac{1}{3} i_A \qquad (3\text{-}24)$$

(3-23) leads to $$v_{r1i} = p\{ \frac{1}{3} [M_{1\text{-}i}(\theta_r)+M_{4\text{-}i}(\theta_r)+M_{7\text{-}i}(\theta_r)] \, i_A \}$$

$$=p[M_{A\text{-}i}(3\theta_r) \, i_A] \qquad (3\text{-}25)$$

Thus, the equivalent 6-pole A-phase rotor "ith" loop mutual inductance, $M_{A\text{-}i}(3\theta_r)$, is found to be equal to the mean of $M_{1\text{-}i}(\theta_r)$, $M_{4\text{-}i}(\theta_r)$, $M_{7\text{-}i}(\theta_r)$. Fig. 3-6 is a plot of the mutual inductance $M_{A\text{-}i}(3\theta_r)$ as a function of rotor angle θ_r. It is seen that the nonsinusoidal function has a $3\theta_r$ variation. Mutual inductances between A-phase and rotor loops in nests 2, 3 and 4 are obtained by simply shifting 90°, 180° and 270° with respect to $M_{A\text{-}i}(3\theta_r)$, respectively. B-phase and C-phase rotor loop mutual inductances can easily be computed using the technique developed above.

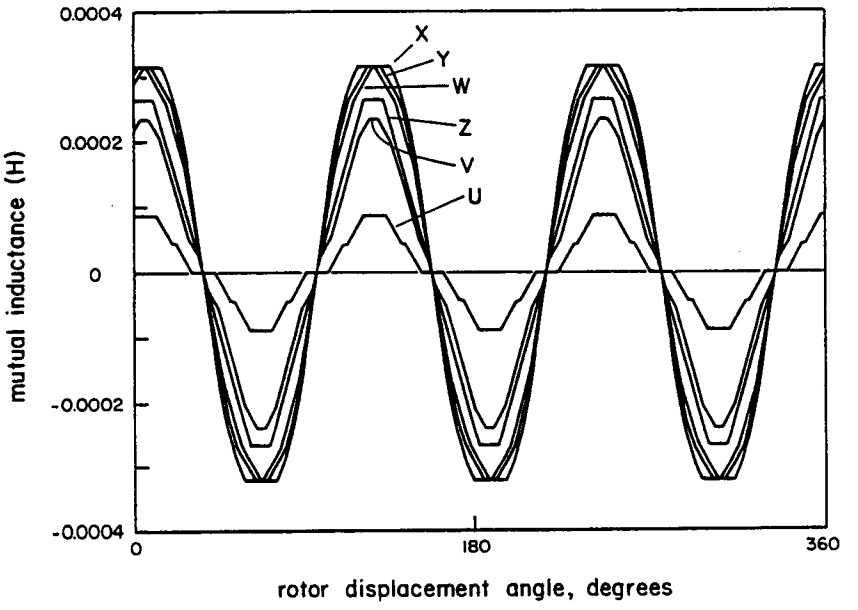

Fig. 3-6 6-pole A-phase rotor loop (in nest 1) mutual inductances

Computation of the equivalent 2-pole nested rotor loop mutual inductances is considered next. Fig. 3-7 shows the 2-pole equivalent a-phase and the rotor "ith" loop in nest 1.

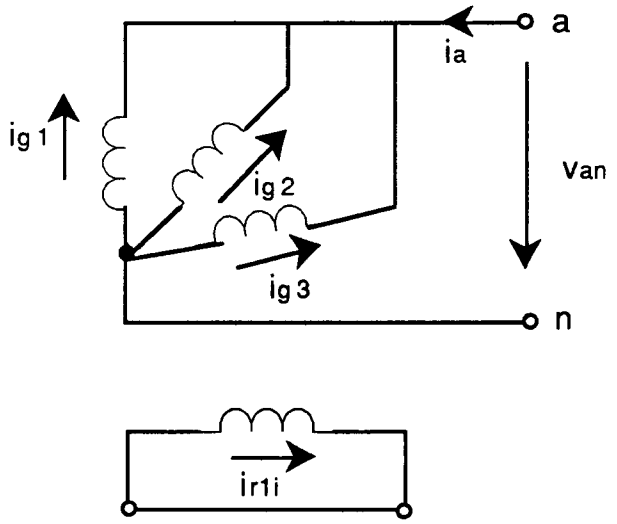

Fig. 3-7 Mutuals between 2-pole a-phase and rotor "ith"loop in nest 1

Unlike the previous case where $M_{A\text{-}i}(3\theta_r)$ can be derived readily from the rotor side equations, stator side equations must be considered. Assume that v_{an} is applied to the 2-pole a-phase and all the rotor loops except the "ith" one in nest 1 is shorted. The following equations may be written

$$\begin{bmatrix} -v_{an} \\ -v_{an} \\ -v_{an} \end{bmatrix} = \begin{bmatrix} r_g+L_gp & M_{12}p & M_{13}p \\ M_{21}p & r_g+L_gp & M_{23}p \\ M_{31}p & M_{32}p & r_g+L_gp \end{bmatrix} \begin{bmatrix} i_{g1} \\ i_{g2} \\ i_{g3} \end{bmatrix} + p \begin{bmatrix} M_{i\text{-}1}(\theta_r) & 0 & 0 \\ 0 & M_{i\text{-}2}(\theta_r) & 0 \\ 0 & 0 & M_{i\text{-}3}(\theta_r) \end{bmatrix} \begin{bmatrix} i_{r1i} \\ i_{r1i} \\ i_{r1i} \end{bmatrix} \tag{3-26}$$

Combining the three equations in (3-26) yields

$$-v_{an} = v_{seq} + p \left\{ \frac{1}{3} [M_{i\text{-}1}(\theta_r)+M_{i\text{-}2}(\theta_r)+M_{i\text{-}3}(\theta_r)]\, i_{r1i} \right\}$$

$$= v_{seq} + p\, [M_{i\text{-}a}(\theta_r)\, i_{r1i}] \tag{3-27}$$

where v_{seq} is the equivalent stator voltage due to the first term on the right hand side of (3-26), and $M_{i\text{-}a}(\theta_r)$ is thus the equivalent mutual inductance between the rotor "ith" loop in nest 1 and 2-pole a-phase. Since the mutual inductances are reciprocal, it follows that $M_{i\text{-}a}(\theta_r) = M_{a\text{-}i}(\theta_r)$, for

i=Z,Y,X,W,V,U. Fig. 3-8 shows a plot of $M_{a-i}(\theta_r)$ vs θ_r. Clearly, this nonsinusoidal function has one cycle between 0° and 360° and is shifted by 40° degrees with respect to $M_{A-i}(3\theta_r)$. Other mutual inductances are derived in the similar way which will not be repeated.

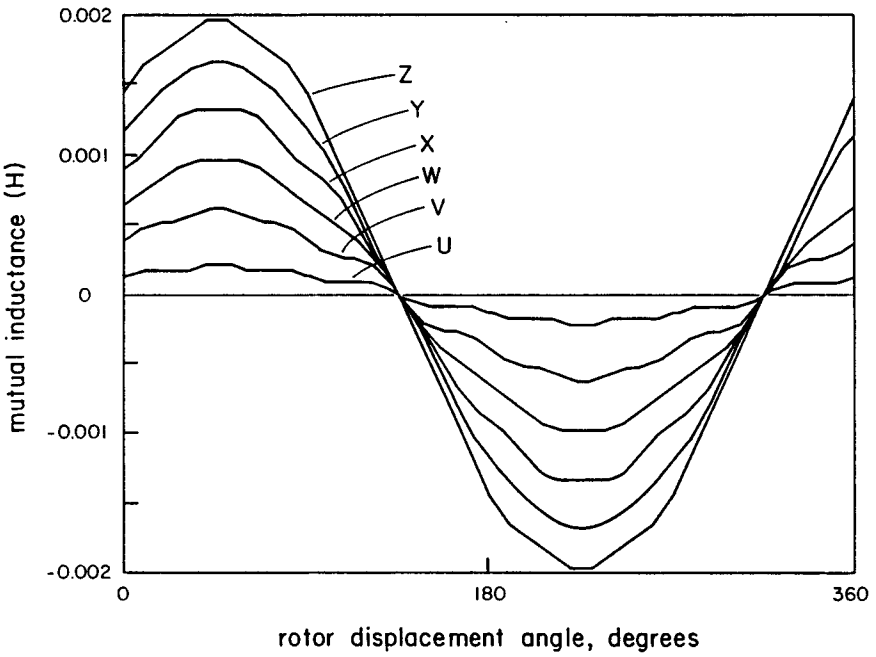

Fig. 3-8 2-pole a-phase rotor loop (in nest 1) mutual inductances

After the mutual inductances are all numerically computed, Fourier analysis is carried out to obtain the frequency spectrum of these nonsinusoidal functions. Figs 3-9 and 3-10 show the analysis results. It is clear from Figs 3-9 and 3-10 that $M_{A-i}(3\theta_r)$ is composed of the 3rd and the 9th harmonics while $M_{a-i}(\theta_r)$ contains the 1st, 5th, 7th and 11th harmonics. Only the fundamental and the third harmonic components are extracted and other high order harmonics are neglected according to the assumptions made. From the graphs, the contribution of each rotor loop to the 6 and 2-pole stator phase mutual inductances can be seen clearly.

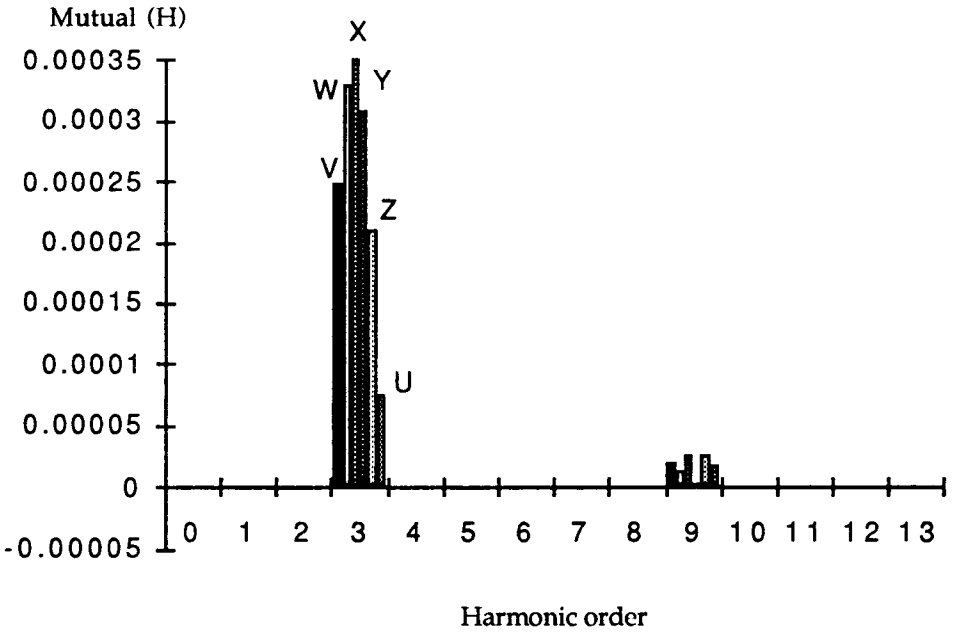

Fig. 3-9 Harmonic analysis of nonsinusoidal mutual inductances between 6-pole winding and rotor loops

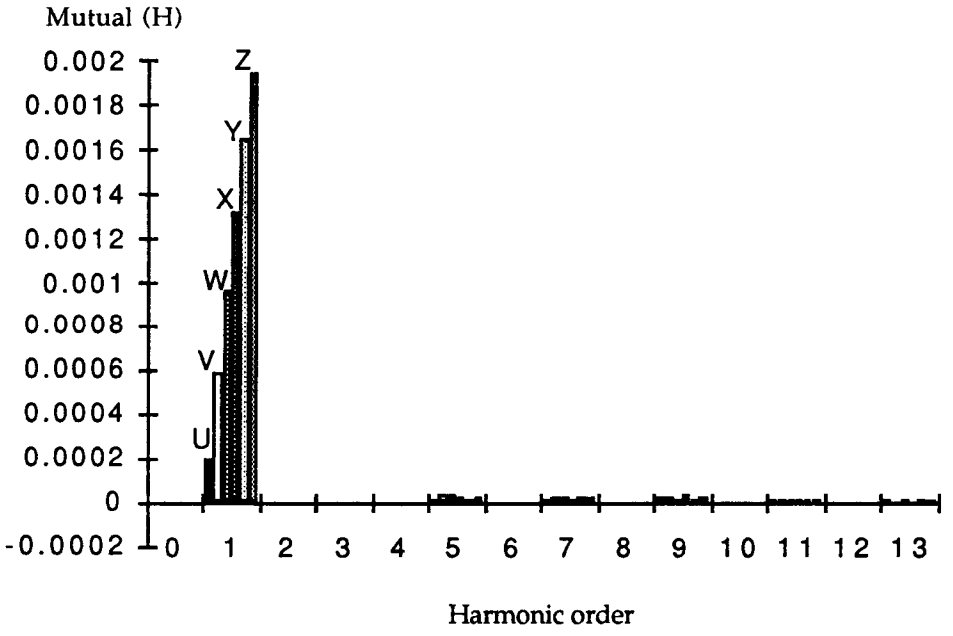

Fig. 3-10 Harmonic analysis of nonsinusoidal mutual inductances between 2-pole winding and rotor loops

3.4 Computation of Machine Parameters for an Experimental BDFM

The coil group inductance parameter matrix of the detailed model is shown below. Define

$$L'_{ss} = \{a_{ij}\} \tag{3-28}$$

where $a_{ij} = L_g$ for i =j and $a_{ij} = M_{ij}$ for $i \neq j$, represent stator coil group self-inductance and mutual inductance between coil groups, respectively. then

$$L'_{ss} = \begin{bmatrix} 0.6640 & 0.3824 & 0.0762 & -0.2294 & -0.5354 & -0.5354 & -0.2294 & 0.0762 & 0.3824 \\ 0.3824 & 0.6640 & 0.3824 & 0.0762 & -0.2294 & -0.5354 & -0.5354 & -0.2294 & 0.0762 \\ 0.0762 & 0.3824 & 0.6640 & 0.3824 & 0.0762 & -0.2294 & -0.5354 & -0.5354 & -0.2294 \\ -0.2294 & 0.0762 & 0.3824 & 0.6640 & 0.3824 & 0.0762 & -0.2294 & -0.5354 & -0.5354 \\ -0.5354 & -0.2294 & 0.0762 & 0.3824 & 0.6640 & 0.3824 & 0.0762 & 0.2294 & -0.5354 \\ -0.5354 & -0.5354 & -0.2294 & 0.0762 & 0.3824 & 0.6640 & 0.3824 & 0.0762 & -0.2294 \\ -0.2294 & -0.5354 & -0.5354 & -0.2294 & 0.0762 & 0.3824 & 0.6640 & 0.3824 & 0.0762 \\ 0.0762 & -0.2294 & -0.5354 & -0.5354 & -0.2294 & 0.0762 & 0.3824 & 0.6640 & 0.3824 \\ 0.3824 & 0.0762 & -0.2294 & -0.5354 & -0.5354 & -0.2294 & 0.0762 & 0.3824 & 0.6640 \end{bmatrix}$$

In addition, the coil group resistance is given as $r_g = 2.42\ \Omega$. By using the formulas derived in this Chapter, the BDFM equation parameters are computed as follows.

(1) 6-pole stator impedance matrix

From (3-2), it follows that

$$r_6 = \frac{1}{3} r_g = 0.807\ \Omega,\ L_A = \frac{1}{3}(L_g + 2M) = \frac{1}{3}[0.664 + 2(-0.229)] = 0.0684\ \text{H} \tag{3-29}$$

The mutual inductance between 6-pole phases is determined using (3-5)

$$\begin{aligned} M_{AB} = M_{BC} = M_{CA} &= \frac{1}{3}(M_{12} + M_{42} + M_{72}) \\ &= \frac{1}{3}(0.382+0.0762-0.5354) = -0.0255\ \text{H} \end{aligned} \tag{3-30}$$

With r_6, L_A and M_{AB}, Z_{s6} of (2-2) is formed numerically as

$$\mathbf{Z}_{s6} = \begin{bmatrix} 0.807+0.0684p & -0.0255p & -0.0255p \\ -0.0255p & 0.807+0.0684p & -0.0255p \\ -0.0255p & -0.0255p & 0.807+0.0684p \end{bmatrix} \quad (3\text{-}31)$$

(2) 2-pole stator impedance matrix

The 2-pole phase resistance r_2 is

$$r_2 = r_6 = \frac{1}{3} r_g = 0.807\ \Omega \quad (3\text{-}32)$$

The self inductance is computed using (3-11)

$$L_a = \frac{1}{3}\left(L_g + \frac{10}{7} M_{12} + \frac{4}{7} M_{13} \right) = \frac{1}{3}\left(0.664 + \frac{10}{7} 0.382 + \frac{4}{7} 0.0764 \right) = 0.4179\ \text{H} \quad (3\text{-}33)$$

The mutual inductance between 2-pole phases are all equal and calculated according to (3-22).

$$M_{ab} = M_{bc} = M_{ca} = \frac{1}{21}\left[2(M_{17}+M_{18}+M_{19})+3(M_{27}+M_{28}+M_{29})+2(M_{37}+M_{38}+M_{39})\right]$$

$$= \frac{1}{21}\left[2(-0.2294+0.0762+0.3824)+3(-0.5354-0.2294+0.0762)+\right.$$

$$\left. 2(-0.5354-0.5354-0.2294)\right] = -0.2004\ \text{H} \quad (3\text{-}34)$$

With r_2, L_a and M_{ab} , $\mathbf{Z}_{s2}$ of (2-3) is formed numerically as

$$\mathbf{Z}_{s2} = \begin{bmatrix} 0.807+0.4179p & -0.2004p & -0.2004p \\ -0.2004p & 0.807+0.4179p & -0.2004p \\ -0.2004p & -0.2004p & 0.807+0.4179p \end{bmatrix} \quad (3\text{-}35)$$

(3) The magnitudes of the rotor angle dependent mutual inductances between stator phases and rotor loops

These parameters, given in Table II, result from Fourier analysis of the nonsinusoidally varying mutual inductances between 6- and 2-pole phase and rotor loops as illustrated in Fig. 3-9 and Fig. 3-10.

Table II Magnitudes of mutual inductances between 6- and 2-pole stator phases and rotor loops

Rotor Loops	6-pole to rotor mutuals (H)	2-pole to rotor mutuals (H)
Z	0.000248	0.00200
Y	0.000329	0.00169
X	0.000350	0.00135
W	0.000308	0.00099
V	0.000210	0.00060
U	0.000075	0.00020

(4) Rotor circuit parameters

As stated previously, in order to derive the two-axis model the stator equations of the BDFM have been modified from coil group representation to equivalent phase representation. However, the rotor equations remain unchanged. The rotor circuit parameters are therefore obtained directly from the detailed model parameters. These parameters are listed below.

(i) Loop resistances, self inductances and mutual inductances between similar loops in different nests.

The parameters are given in Table III below.

Table III Loop resistances, self inductances and mutual inductances between similar loops in different nests

Resistances (μΩ)	Self inductances (μH) (including 5% leakage)	Mutuals (μH)
$r_{ZZ} = 212.0$	$L_{ZZ} = 18.8$	$M_{ZZ} = 5.978$
$r_{YY} = 188.0$	$L_{YY} = 16.3$	$M_{YY} = 4.002$
$r_{XX} = 164.0$	$L_{XX} = 13.4$	$M_{XX} = 2.421$
$r_{WW} = 140.0$	$L_{WW} = 10.1$	$M_{WW} = 1.235$
$r_{VV} = 116.0$	$L_{VV} = 6.38$	$M_{VV} = 0.444$
$r_{UU} = 92.0$	$L_{UU} = 2.23$	$M_{UU} = 0.049$

(ii) Common endring resistances ($\mu\Omega$)

$$r_{UV} = r_{UW} = r_{UX} = r_{UY} = r_{UZ} = 6.0$$
$$r_{VW} = r_{VX} = r_{VY} = r_{VZ} = 18.0$$
$$r_{WX} = r_{WY} = r_{WZ} = 30.0$$
$$r_{XY} = r_{XZ} = 42.0$$
$$r_{YZ} = 54.0$$

(iii) Mutual inductances between loops in the same nest (μH)

$M_{UV} = 2.0$	$M_{UW} = 1.9$	$M_{UX} = 1.8$	$M_{UY} = 1.7$	$M_{UZ} = 1.63$
	$M_{VW} = 5.7$	$M_{VX} = 5.4$	$M_{VY} = 5.1$	$M_{VZ} = 4.8$
		$M_{WX} = 9.14$	$M_{WY} = 8.6$	$M_{WZ} = 8.15$
			$M_{XY} = 12.1$	$M_{XZ} = 11.4$
				$M_{XZ} = 14.6$

(iv) Mutual inductances between different loops of different nests (μH)

$M'_{UV} = 0.148$	$M'_{UW} = 0.247$	$M'_{UX} = 0.345$	$M'_{UY} = 0.444$	$M'_{UZ} = 0.543$
	$M'_{VW} = 0.741$	$M'_{VX} = 1.037$	$M'_{VY} = 1.334$	$M'_{VZ} = 1.630$
		$M'_{WX} = 1.729$	$M'_{WY} = 2.223$	$M'_{WZ} = 2.717$
			$M'_{XY} = 3.112$	$M'_{XZ} = 3.804$
				$M'_{XZ} = 4.891$

By far, the BDFM dynamic model expressed in machine variables and the associated machine parameters have been derived. Eqn. (2-1) is a set of 30th order, nonlinear, ordinary differential equations which must be solved simultaneously along with two more mechanical equations in order to investigate the machine dynamics. However, in terms of stability analysis and control strategy development, (2-1) must be reduced to a manageable form, which is the subject of the rest of the thesis.

4. TWO-AXIS MODEL DEVELOPMENT AND MODEL PARAMETER COMPUTATIONS

The theory employed to derive the two-axis (d-q) model is the well known two reaction theory that calls for a change of variables of the original system equations by which the time-varying mutual inductances in the voltages equations can be eliminated.

It has been shown [22] that, for three-phase symmetrical induction machines, in order to eliminate the time-varying terms in the differential equations the reference frame can be fixed on the stator, rotor or be synchronously rotating. For synchronous machines, however, due to the saliency of their magnetic circuits, the reference frame must be fixed on the rotor.

The analysis of the BDFM in the dq domain also faces the choice of correctly selecting a reference frame in which the time-varying mutual terms due to the relative motion between the stator circuits and the rotor circuits can be eliminated. Owing to the special structure of the BDFM, it is known that there can be two synchronous speeds (two synchronously rotating reference frames) co-existing in the machine. They are due respectively to the 6-pole system excitation and 2-pole system excitation. Since the sequence of the two sets of input voltages is different , they are rotating in opposite directions with respect to one another. Moreover, since the two stator systems comprise two different pole numbers, the choice of selecting a reference frame is therefore very limited. In fact, it can be shown that it is not possible to select either stationary or synchronously rotating reference frames in the dq analysis. However, in the rotor

reference frame, since two pairs of stator fictitious windings (d and q) along with another pair of fictitious rotor windings are rotating at the speed of the rotor, no relative motion exists between these windings, thus the time-varying mutual inductances can be eliminated.

This Chapter discusses the use of dq analysis techniques to model the BDFM and its parameters in the rotor reference frame. Following the introduction, a preview of the dq modeling for the BDFM is given in 4.1 and in 4.2 the transformation matrices employed to develop the two-axis model are derived based on a generalized orthogonal transformation matrix. The development of the two-axis model is presented in section 4.3, followed by the equivalent circuits and the derivation of the torque equation in the dq domain in sections 4.4 and 4.5. Finally, the two-axis model parameters of an experimental machine are computed in 4.6.

4.1 Preview of the dq Modeling of the BDFM

As presented in the early Chapters, the process of developing the two-axis model started with a common winding structure. By assuming that the direct coupling between the two stator windings is negligible, the original stator common winding structure has been separated into two independent 3-ϕ winding systems with different pole numbers. Then, Park's transformations can be applied to transform them into two independent orthogonal sets, namely d and q plus a zero sequence if unbalanced excitation is considered.

More discussions are needed for the rotor transformation. From the basic rotor structure, it is known that there are 4 nests each of 6 loops for a total of 24 rotor loops, which might suggest that 24 rotor states could be needed to represent the rotor. However, due to the special structure of the

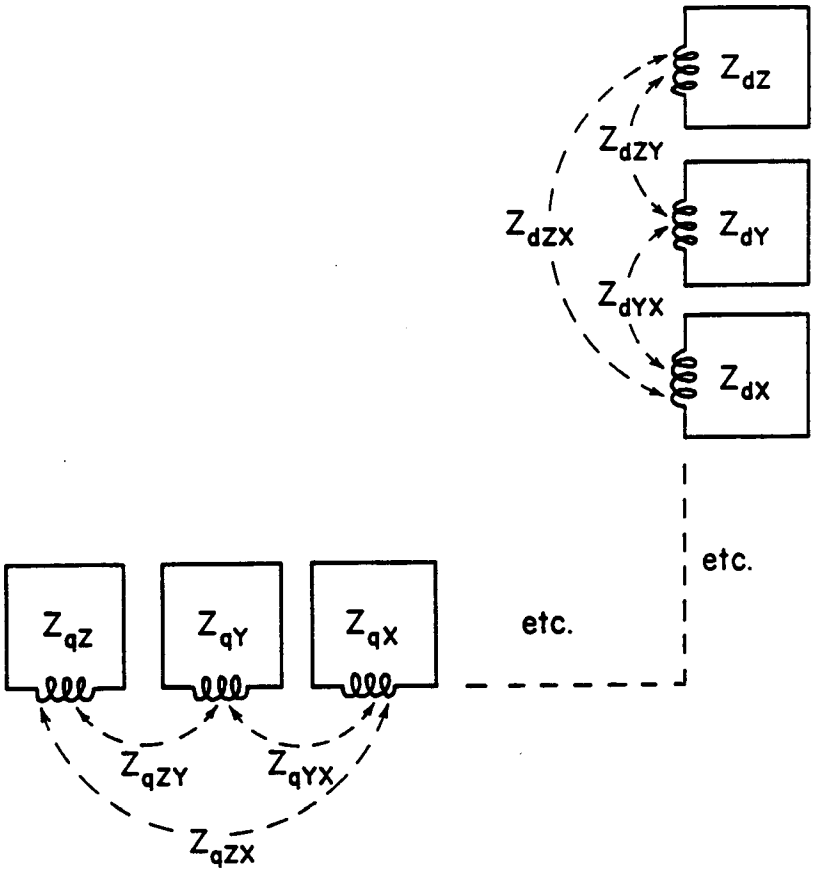

Fig. 4-1 The BDFM rotor loops represented in d-q domain

rotor, it is understood that the currents in one nest should all be in phase and 90° out of phase with respect to those in the adjacent nest in this 4 nest BDFM rotor structure. In addition, since currents in one nest are 180° out of phase with those in every other nest, the 24 rotor currents are highly linearly related. The minimum order of states can be shown to be two for this 6- and 2-pole machine.

To define the proper rotor states, we consider again Fig. 2-4 in Chapter 2. From this representation, each of the loop subsystems could be individually resolved into effective equivalent d-axis and q-axis coils as can be shown in Fig. 4-1 in which the two axes are uncoupled. For the

experimental machine, there are twelve loops on each axis (only three are illustrated) and can be summed into a mathematical equivalent system as illustrated in Fig. 4-2. This process is equivalent to adding the twelve loop currents together, that is, we can define

$$i_{qr} = k\left(\sum_i i_{r1i} - \sum_i i_{r3i}\right) \quad \text{and} \quad i_{dr} = k\left(\sum_i i_{r2i} - \sum_i i_{r4i}\right)$$

where k is a non-negative constant and the sum operates on all loops in one nest, i.e. i=Z,Y,X,W,V,U.

The two transformed stator systems are also shown in Fig. 4-2. It turns out that both the stator and the rotor transformations can be incorporated into one transformation matrix, details of which will be presented in the following sections.

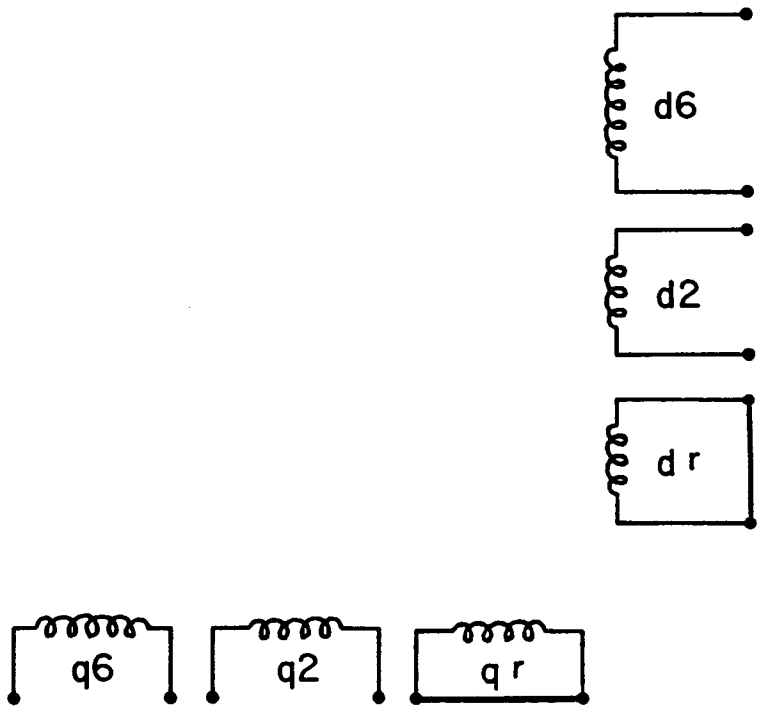

Fig. 4-2 The 6- and 2-pole BDFM in the dq domain

4.2 Transformation Matrices

The generalized transformation matrix [20] used to derive the dq model is given in (4-1).

$$C_g = \sqrt{\frac{2}{n}} \begin{bmatrix} \cos\frac{P}{2}\theta & \cos\frac{P}{2}(\theta-\psi) & \cos\frac{P}{2}(\theta-2\psi) & \cdots & \cos\frac{P}{2}[\theta-(n-1)\psi] \\ \sin\frac{P}{2}\theta & \sin\frac{P}{2}(\theta-\psi) & \sin\frac{P}{2}(\theta-2\psi) & \cdots & \sin\frac{P}{2}[\theta-(n-1)\psi] \\ \sqrt{\frac{1}{2}} & \sqrt{\frac{1}{2}} & \sqrt{\frac{1}{2}} & \cdots & \sqrt{\frac{1}{2}} \end{bmatrix} \quad (4\text{-}1)$$

where P is the pole number, n denotes the number of stator windings or rotor loops and ψ represents the angle between adjacent stator windings or rotor loops.

Notice that C_g is, in general, a rectangular matrix. However, it is easy to show that the orthogonal property of (4-1) is still fulfilled, that is

$$C_g^+ = C_g^t (C_g\ C_g^t)^{-1} = C_g^t \quad (4\text{-}2)$$

where C_g^+ and C_g^t denote pseudo-inverse and transpose of C_g, respectively.

It will be shown in the later Sections that orthogonality of (4-1) plays an essential role in the d-q model derivation, particularly in the rotor variable transformation process.

Both the stator and rotor transformations are obtained by properly assigning the parameters, n, P and ψ in (4-1) as explained in detail below.

(1) 6-pole stator transformation matrix C_{s6}

Let P=6, n=3, ψ=40° and $\theta=\theta_r$ (rotor reference frame). (4-1) becomes

$$C_{s6} = \sqrt{\frac{2}{3}} \begin{bmatrix} \cos 3\theta_r & \cos(3\theta_r - 120^\circ) & \cos(3\theta_r + 120^\circ) \\ \sin 3\theta_r & \sin(3\theta_r - 120^\circ) & \sin(3\theta_r + 120^\circ) \\ \sqrt{\frac{1}{2}} & \sqrt{\frac{1}{2}} & \sqrt{\frac{1}{2}} \end{bmatrix} \tag{4-3}$$

(2) 2-pole stator transformation matrix C_{s2}

Let P = 2, n = 3, $\psi = 120^\circ$ and $\theta = (\theta_r - 40^\circ)$, we get

$$C_{s2} = \sqrt{\frac{2}{3}} \begin{bmatrix} \cos[\theta_r - 40^\circ] & \cos[(\theta_r - 40^\circ) - 120^\circ] & \cos[(\theta_r - 40^\circ) + 120^\circ] \\ \sin[\theta_r - 40^\circ] & \sin[(\theta_r - 40^\circ) - 120^\circ] & \sin[(\theta_r - 40^\circ) + 120^\circ] \\ \sqrt{\frac{1}{2}} & \sqrt{\frac{1}{2}} & \sqrt{\frac{1}{2}} \end{bmatrix} \tag{4-4}$$

(4-3) and (4-4) are easily recognized as the modified Park's transformations applied to the BDFM system of equations.

(3) 6-pole rotor transformation matrix C_{r6}

Transformation matrix C_{r6} is defined as 2 by 24 matrix which can be partitioned as

$$C_{r6} = [\, C_{r6Z} \;\; C_{r6Y} \;\; C_{r6X} \;\; C_{r6W} \;\; C_{r6V} \;\; C_{r6U} \,]^t \tag{4-5}$$

Notice that the zero sequence disappears because of the special structure of the cage rotor. It is also noted that since the 24 rotor loops are grouped into 4 nests and the winding axis of all the loops in the same nest coincide in the same direction, C_{r6i}, i = Z,Y,X,W,V,U are all identical.

Assign P = 6, n = 24 and $\psi = 90^\circ$, then each of the submatrices of C_{r6} can be expressed as

$$C_{r6i} = \sqrt{\frac{2}{24}} \begin{bmatrix} \cos 3\theta & \cos 3(\theta - 90^\circ) & \cos 3(\theta - 180^\circ) & \cos 3(\theta - 270^\circ) \\ \sin 3\theta & \sin 3(\theta - 90^\circ) & \sin 3(\theta - 180^\circ) & \sin 3(\theta - 270^\circ) \end{bmatrix} \tag{4-6}$$

in the rotor reference frame, which implies that $\theta = 0$, C_{r6i} becomes

$$C_{r6i} = \sqrt{\frac{1}{12}} \begin{bmatrix} 1 & 0 & -1 & 0 \\ 0 & 1 & 0 & -1 \end{bmatrix} \tag{4-7}$$

(4) 2-pole rotor transformation matrix C_{r2}

The rotor transformation C_{r2} is obtained by setting P = 2, $\psi = 90^{\circ}$ and n = 24. Like the previous case C_{r2i}, i=Z,Y,X,W,V,U, are all equal

$$C_{r2} = [\, C_{r2Z} \;\; C_{r2Y} \;\; C_{r2X} \;\; C_{r2W} \;\; C_{r2V} \;\; C_{r2U} \,]^{t} \tag{4-8}$$

Each of the submatrices is

$$C_{r2i} = \sqrt{\frac{2}{24}} \begin{bmatrix} \cos\theta & \cos(\theta-90^{\circ}) & \cos(\theta-180^{\circ}) & \cos(\theta-270^{\circ}) \\ \sin\theta & \sin(\theta-90^{\circ}) & \sin(\theta-180^{\circ}) & \sin(\theta-270^{\circ}) \end{bmatrix} \tag{4-9}$$

in the rotor reference frame, (4-9) becomes

$$C_{r2i} = \sqrt{\frac{1}{12}} \begin{bmatrix} 1 & 0 & -1 & 0 \\ 0 & -1 & 0 & 1 \end{bmatrix} \tag{4-10}$$

The Transformation matrices developed will be used to derive the d-q model in the following sections.

4.3 Two-Axis Model Development

From (2-1) of Chapter 2 , it is known that

$$\begin{bmatrix} \mathbf{v}_{s6} \\ \mathbf{v}_{s2} \\ \mathbf{v}_{r} \end{bmatrix} = \begin{bmatrix} \mathbf{Z}_{s6} & \mathbf{0} & \mathbf{Z}_{s6r} \\ \mathbf{0} & \mathbf{Z}_{s2} & \mathbf{Z}_{s2r} \\ \mathbf{Z}^{t}_{s6r} & \mathbf{Z}^{t}_{s2r} & \mathbf{Z}_{r} \end{bmatrix} \begin{bmatrix} \mathbf{i}_{s6} \\ \mathbf{i}_{s2} \\ \mathbf{i}_{r} \end{bmatrix} \tag{4-11}$$

In order to derive the d-q model equations in a more rigorous manner, it is assumed that the rotor loop voltages and currents can be decomposed into

$$\mathbf{v}_r = \mathbf{v}_{r6} + \mathbf{v}_{r2} \tag{4-12}$$

$$\mathbf{i}_r = \mathbf{i}_{r6} + \mathbf{i}_{r2} \tag{4-13}$$

where v_{r6} , v_{r2} and i_{r6} , i_{r2} can be thought of as being the voltage or the current components induced from the 6-pole and the 2-pole stator systems, respectively.

Equation (4-11) thus becomes

$$\begin{bmatrix} v_{s6} \\ v_{s2} \\ v_{r6} \\ v_{r2} \end{bmatrix} = \begin{bmatrix} Z_{s6} & 0 & Z_{s6r} & Z_{s6r} \\ 0 & Z_{s2} & Z_{s2r} & Z_{s2r} \\ Z^{t}_{s6r} & 0 & Z_r & 0 \\ 0 & Z^{t}_{s2r} & 0 & Z_r \end{bmatrix} \begin{bmatrix} i_{s6} \\ i_{s2} \\ i_{r6} \\ i_{r2} \end{bmatrix} \tag{4-14}$$

or more concisely,

$$\mathbf{v} = \mathbf{Z}\,\mathbf{i} = (\mathbf{r} + p\mathbf{L})\,\mathbf{i} = \mathbf{r}\,\mathbf{i} + p\,\lambda \tag{4-15}$$

where

$$\mathbf{r} = \mathrm{diag}\,(\,r_6 \;\; r_2 \;\; r_r \;\; r_r\,) \tag{4-16}$$

$$\lambda = \mathbf{L}\,\mathbf{i} = \begin{bmatrix} L_{s6} & 0 & L_{s6r} & L_{s6r} \\ 0 & L_{s2} & L_{s2r} & L_{s2r} \\ L^{t}_{s6r} & 0 & L_r & 0 \\ 0 & L^{t}_{s2r} & 0 & L_r \end{bmatrix} \begin{bmatrix} i_{s6} \\ i_{s2} \\ i_{r6} \\ i_{r2} \end{bmatrix} \tag{4-17}$$

qdo variables are related with machine variables by

$$\xi_{qdo} = C_T\,\phi_{machine} \tag{4-18}$$

where $\phi_{machine} = [\,\phi^{t}_{s6}\;\phi^{t}_{s2}\;\phi^{t}_{r6}\;\phi^{t}_{r2}\,]^{t}$ and $\xi_{qdo} = [\,\xi^{t}_{qdo6}\;\xi^{t}_{qdo2}\;\xi^{t}_{qdr6}\;\xi^{t}_{qdr2}\,]^{t}$ denote machine and d-q domain variables such as voltages, currents, flux linkages that are associated with proper stator or rotor circuits. C_T is the overall transformation defined such that

$$C_T = \mathrm{diag}(\,C_{s6}\;\;C_{s2}\;\;C_{r6}\;\;C_{r2}\,) \tag{4-19}$$

Applying C_T to (4-15) and observing that

$$C_T^{+} = C_T^{t}\,(\,C_T C_T^{t}\,)^{-1} = C_T^{t} = \mathrm{diag}(\,C_{s6}^{t}\;\;C_{s2}^{t}\;\;C_{r6}^{t}\;\;C_{r2}^{t}\,) \tag{4-20}$$

leads to

$$\mathbf{v}_{qdo} = \mathbf{C}_T \mathbf{r} \mathbf{C}_T^t \mathbf{i}_{qdo} + \mathbf{C}_T \mathbf{p}(\mathbf{C}_T^t)\lambda_{qdo} + \mathbf{p}\,\lambda_{qdo} \tag{4-21}$$

Expanding (4-21), we can obtain the following dq model equation expressed in the rotor reference frame, in which each element in the equation is understood as a matrix of proper order.

$$\begin{bmatrix} v_{qdo6} \\ v_{qdo2} \\ v_{qdr6} \\ v_{qdr2} \end{bmatrix} = \begin{bmatrix} r_6 & 0 & 0 & 0 \\ 0 & r_2 & 0 & 0 \\ 0 & 0 & C_{r6} r_r C_{r6}^t & 0 \\ 0 & 0 & 0 & C_{r2} r_r C_{r2}^t \end{bmatrix} \begin{bmatrix} i_{qdo6} \\ i_{qdo2} \\ i_{qdr6} \\ i_{qdr2} \end{bmatrix} + \{h(\omega_r)+pI\} \begin{bmatrix} \lambda_{qdo6} \\ \lambda_{qdo2} \\ \lambda_{qdr6} \\ \lambda_{qdr2} \end{bmatrix} \tag{4-22}$$

where $\mathbf{I}$ is an identity matrix and

$$h(\omega_r) = C_T\, p(C_T^t) = \begin{bmatrix} C_{s6} p(C_{s6}^t) & 0 & 0 & 0 \\ 0 & C_{s2} p(C_{s2}^t) & 0 & 0 \\ 0 & 0 & 0 & 0 \\ 0 & 0 & 0 & 0 \end{bmatrix} \tag{4-23}$$

In the d-q domain, (4-17) becomes

$$\lambda_{qdo} = L_{qdo}\, i_{qdo} = (C_T\, L\, C_T^t)\, i_{qdo} \tag{4-24}$$

or more precisely,

$$\begin{bmatrix} \lambda_{qdo6} \\ \lambda_{qdo2} \\ \lambda_{qdr6} \\ \lambda_{qdr2} \end{bmatrix} = \begin{bmatrix} C_{s6} L_{s6} C_{s6}^t & 0 & C_{s6} L_{s6r} C_{r6}^t & C_{s6} L_{s6r} C_{r2}^t \\ 0 & C_{s2} L_{s2} C_{s2}^t & C_{s2} L_{s2r} C_{r6}^t & C_{s2} L_{s2r} C_{r2}^t \\ C_{r6} L_{s6r}^t C_{s6}^t & 0 & C_{r6} L_r C_{r6}^t & 0 \\ 0 & C_{r2} L_{s2r}^t C_{s2}^t & 0 & C_{r2} L_r C_{r2}^t \end{bmatrix} \begin{bmatrix} i_{qdo6} \\ i_{qdo2} \\ i_{qdr6} \\ i_{qdr2} \end{bmatrix} \tag{4-25}$$

Computation of each of the submatrices in (4-22), (4-23) and (4-25) is now in order. Denote $C_a = C_{s6} p(C_{s6}^t)$ and $C_b = C_{s2} p(C_{s2}^t)$, then in (4-23),

$$C_a = C_{s6}p(C_{s6}^t) = \frac{2}{3}\omega_r \begin{bmatrix} \cos 3\theta_r & \cos(3\theta_r - 120^\circ) & \cos(3\theta_r + 120^\circ) \\ \sin 3\theta_r & \sin(3\theta_r - 120^\circ) & \sin(3\theta_r + 120^\circ) \\ \sqrt{\frac{1}{2}} & \sqrt{\frac{1}{2}} & \sqrt{\frac{1}{2}} \end{bmatrix} \begin{bmatrix} -\sin 3\theta_r & \cos 3\theta_r & 0 \\ -\sin(3\theta_r - 120^\circ) & \cos(3\theta_r - 120^\circ) & 0 \\ -\sin(3\theta_r + 120^\circ) & \cos(3\theta_r + 120^\circ) & 0 \end{bmatrix}$$

$$= 3\omega_r \begin{bmatrix} 0 & 1 & 0 \\ -1 & 0 & 0 \\ 0 & 0 & 0 \end{bmatrix} \tag{4-26}$$

$$C_b = C_{s2}p(C_{s2}^t) = \frac{2}{3}\omega_r \begin{bmatrix} \cos\alpha_r & \cos(\alpha_r - 120^\circ) & \cos(\alpha_r + 120^\circ) \\ \sin\alpha_r & \sin(\alpha_r - 120^\circ) & \sin(\alpha_r + 120^\circ) \\ \sqrt{\frac{1}{2}} & \sqrt{\frac{1}{2}} & \sqrt{\frac{1}{2}} \end{bmatrix} \begin{bmatrix} -\sin\alpha_r & \cos\alpha_r & 0 \\ -\sin(\alpha_r - 120^\circ) & \cos(\alpha_r - 120^\circ) & 0 \\ -\sin(\alpha_r + 120^\circ) & \cos(\alpha_r + 120^\circ) & 0 \end{bmatrix}$$

$$= \omega_r \begin{bmatrix} 0 & 1 & 0 \\ -1 & 0 & 0 \\ 0 & 0 & 0 \end{bmatrix} \tag{4-27}$$

where $\alpha_r = (\theta_r - 40^\circ)$

To compute other submatrices in (4-22) and (4-25), we substitute (4-24) back into (4-21) and combine the first and the third terms so that two impedance matrices, defined as $\mathbf{Z'}_{qdo}$ and $\mathbf{Z''}_{qdo}$ in the dq domain, are formed. In doing this, (4-21) becomes

$$\mathbf{v}_{qdo} = \mathbf{Z'}_{qdo}\,\mathbf{i}_{qdo} + \mathbf{Z''}_{qdo}\,\mathbf{i}_{qdo} = \mathbf{Z}_{qdo}\,\mathbf{i}_{qdo} \tag{4-28}$$

In (4-28)

$$\mathbf{Z'}_{qdo} = \begin{bmatrix} C_{s6}Z_{s6}C_{s6}^t & 0 & C_{s6}Z_{s6r}C_{r6}^t & C_{s6}Z_{s6r}C_{r2}^t \\ 0 & C_{s2}Z_{s2}C_{s2}^t & C_{s2}Z_{s2r}C_{r6}^t & C_{s2}Z_{s2r}C_{r2}^t \\ C_{r6}Z_{s6r}^tC_{s6}^t & 0 & C_{r6}Z_rC_{r6}^t & 0 \\ 0 & C_{r2}Z_{s2r}^tC_{s2}^t & 0 & C_{r2}Z_rC_{r2}^t \end{bmatrix} \tag{4-29}$$

with $Z_{s6} = r_6 + L_{s6}p$, $Z_{s2} = r_2 + L_{s2}p$, $Z_r = r_r + L_rp$ and

$$Z''_{qdo} = \begin{bmatrix} C_a C_{s6} L_{s6} C_{s6}^t & 0 & C_a C_{s6} L_{s6r} C_{r6}^t & C_a C_{s6} L_{s6r} C_{r2}^t \\ 0 & C_b C_{s2} L_{s2} C_{s2}^t & C_b C_{s2} L_{s2r} C_{r6}^t & C_b C_{s2} L_{s2r} C_{r2}^t \\ 0 & 0 & 0 & 0 \\ 0 & 0 & 0 & 0 \end{bmatrix} \quad (4\text{-}30)$$

In (4-29), $C_{s6}\, Z_{s6}\, C_{s6}^t$ and $C_{s2}\, Z_{s2}\, C_{s2}^t$ are 3 by 3 diagonal matrices which are expressed as

$$Z_{qdo6} = \begin{bmatrix} r_6+(L_{l6}+L_{6m}-M)p & 0 & 0 \\ 0 & r_6+(L_{l6}+L_{6m}-M)p & 0 \\ 0 & 0 & r_6+L_{l6}p \end{bmatrix} \quad (4\text{-}31)$$

also

$$Z_{qdo2} = \begin{bmatrix} r_2+(L_{l2}+L_{2m}-M')p & 0 & 0 \\ 0 & r_2+(L_{l2}+L_{2m}-M')p & 0 \\ 0 & 0 & r_2+L_{l2}p \end{bmatrix} \quad (4\text{-}32)$$

Assuming sinusoidal distribution of stator windings yields

$$L_{6m} = -2M, \quad L_{2m} = -2M' \quad (4\text{-}33)$$

where $L_{l6} = L_{6m} + 2M$, $L_{l2} = L_{2m} + 2M'$ are defined as the leakage inductances of the 6 and the 2-pole systems, respectively.

Other submatrices in (4-29) are computed as follows

$$\begin{aligned} C_{s6} Z_{s6} C_{r6}^t &= \sum_i C_{s6} Z_{s6ri} C_{r6i}^t \\ &= \left(\sum_i M_{s6ri}\right) C_{s6}\,[f(3\theta_r)]\, C_{r6Z}^t \\ &= \left(\sqrt{\frac{1}{2}} \sum_i M_{s6ri}\right) p \begin{bmatrix} 1 & 0 \\ 0 & 1 \\ 0 & 0 \end{bmatrix} \end{aligned} \quad (4\text{-}34)$$

$$C_{s2} Z_{s2r} C_{r2}^t = \sum_i C_{s2} Z_{s2ri} C_{r2i}^t$$

$$= \left(\sum_i M_{s2ri}\right) C_{s2}\,[g(\theta_r)]\, C^t_{r2Z}$$

$$= \left(\sqrt{\frac{1}{2}} \sum_i M_{s2ri}\right) p \begin{bmatrix} -1 & 0 \\ 0 & -1 \\ 0 & 0 \end{bmatrix} \tag{4-35}$$

$$C_{s6}\, Z_{s6r} C^t_{r2} = \sum_i C_{s6} Z_{s6r}\, C^t_{r2i}$$

$$= \left(\sum_i M_{s6ri}\right) C_{s2}\,[f(3\theta_r)]\, C^t_{r2Z}$$

$$= \left(\sqrt{\frac{1}{2}} \sum_i M_{s6ri}\right) p \begin{bmatrix} 1 & 0 \\ 0 & -1 \\ 0 & 0 \end{bmatrix} \tag{4-36}$$

$$C_{s2} Z_{s2r} C^t_{r6} = \sum_i C_{s6} Z_{s2r}\, C^t_{r6i}$$

$$= \left(\sum_i M_{s2ri}\right) C_{s2}\,[g(\theta_r)]\, C^t_{r6Z}$$

$$= \left(\sqrt{\frac{1}{2}} \sum_i M_{s2ri}\right) p \begin{bmatrix} -1 & 0 \\ 0 & -1 \\ 0 & 0 \end{bmatrix} \tag{4-37}$$

on the rotor side, define $Z_{qdr6} = r_{qdr6} + L_{qdr6}p$ and $Z_{qdr2} = r_{qdr2} + L_{qdr2}p$ then

$$Z_{qdr6} = C_{r6} Z_r C^t_{r6} = \sum_j \sum_i C_{r6i}\, Z_{ij}\, C^t_{r6j} \tag{4-38}$$

$$Z_{qdr2} = C_{r2}\, Z_r C^t_{r2} = \sum_j \sum_i C_{r2i}\, Z_{ij}\, C^t_{r2j} \tag{4-39}$$

where i, j = Z,Y,X,W,V,U

It is easy to show that

$$Z_{qdr6} = Z_{qdr2} = Z_{qdr} \tag{4-40}$$

(4-38) and (4-39) suggest that calculation of Z_{qdr} could be done in terms of each of the submatrices of Z_r, $\{ Z_{ij} \}$. The resultant transformed matrix is obtained by summing up each individual transformed submatrices as explained as follows

(1) for i=j, i=Z,Y,X,W,V,U

$$\sum_i C_{r2i} Z_{ii} C^t_{r2i} = \frac{1}{6} \begin{bmatrix} \sum_i [r_{ii} + (L_{ii} + M_{ii})p] & 0 \\ 0 & \sum_i [r_{ii} + (L_{ii} + M_{ii})p] \end{bmatrix} \tag{4-41}$$

(2) for i≠j, i, j=Z,Y,X,W,V,U

$$\sum_j \sum_i C_{r2i} Z_{ij} C^t_{r2j} = \frac{1}{6} \begin{bmatrix} \sum_j \sum_i [r_{ij} + (M_{ij} + M'_{ij})p] & 0 \\ 0 & \sum_j \sum_i [r_{ij} + (M_{ij} + M'_{ij})p] \end{bmatrix} \tag{4-42}$$

Let
$$Z_{qdr} = \begin{bmatrix} r_{qr} + L_{qr}p & 0 \\ 0 & r_{dr} + L_{dr}p \end{bmatrix} \tag{4-43}$$

then
$$r_{qr} = r_{dr} = r_r = \frac{1}{6} [\sum_i r_i + \sum_j \sum_i r_{ij}] \tag{4-44}$$

$$L_{qr} = L_{dr} = L_{dr} = \frac{1}{6} [\sum_i (L_i + M_{ii}) + \sum_j \sum_i (M_{ij} + M'_{ij})] \tag{4-45}$$

(4-44) and (4-45) give two explicit expressions for evaluation of rotor d-q model parameters given the actual parameters based on the machine geometry.

Finally, $C_{r6}\, Z^{t}_{s6r}\, C^{t}_{s6}$ and $C_{r2}\, Z^{t}_{s2r}\, C^{t}_{s2}$ in (4-29) are the transpose of $C_{s6}\, Z_{s6r}\, C^{t}_{r6}$ and $C_{s2}\, Z_{s2r}\, C^{t}_{r2}$, respectively.

Computation of submatrices in (4-30) is considered next. It is easy to verify the following

$$C_a C_{s6}\, L_{s6} C^{t}_{s6} = 3\omega_r \begin{bmatrix} 0 & (L_{l6}+L_{6m}-M) & 0 \\ -(L_{l6}+L_{6m}-M) & 0 & 0 \\ 0 & 0 & 0 \end{bmatrix} \tag{4-46}$$

$$C_b C_{s2}\, L_{s2} C^{t}_{s2} = \omega_r \begin{bmatrix} 0 & (L_{l2}+L_{2m}-M') & 0 \\ -(L_{l2}+L_{2m}-M') & 0 & 0 \\ 0 & 0 & 0 \end{bmatrix} \tag{4-47}$$

$$C_a C_{s6}\, L_{s6r} C^{t}_{r6} = 3\omega_r \begin{bmatrix} 0 & M_6 \\ -M_6 & 0 \\ 0 & 0 \end{bmatrix} \tag{4-48}$$

$$C_a C_{s6}\, L_{s6r} C^{t}_{s2} = 3\omega_r \begin{bmatrix} 0 & -M_6 \\ -M_6 & 0 \\ 0 & 0 \end{bmatrix} \tag{4-49}$$

$$C_b C_{s2}\, L_{s2r} C^{t}_{r2} = \omega_r \begin{bmatrix} 0 & M_2 \\ M_2 & 0 \\ 0 & 0 \end{bmatrix} \tag{4-50}$$

$$C_b C_{s2}\, L_{s2r} C^{t}_{r6} = \omega_r \begin{bmatrix} 0 & -M_2 \\ M_2 & 0 \\ 0 & 0 \end{bmatrix} \tag{4-51}$$

where in (4-48) through (4-51)

$$M_6 = \sqrt{\frac{1}{2}} \sum_i M_{s6ri} \tag{4-52}$$

also

$$M_2 = \sqrt{\frac{1}{2}} \sum_i M_{s2ri} \tag{4-53}$$

(4-54) shows the complete form of the d-q model derived by assembling all the submatrices into one matrix equation.

In the above model development process, (4-29) together with (4-30) are derived by introducing rotor auxiliary variables. The final form of the equation is obtained by eliminating the two extra states in the rotor circuit. In order to do this, constraints of the rotor states must be derived. From $\mathbf{v}_r = \mathbf{v}_{r6} + \mathbf{v}_{r2}$, it follows that

$$\mathbf{v}_r = \mathbf{v}_{r6} + \mathbf{v}_{r2} = \mathbf{C}_{r6}^t \mathbf{v}_{qdr6} + \mathbf{C}_{r2}^t \mathbf{v}_{qdr2} = \mathbf{0} \tag{4-55}$$

(4-55) expresses 24 equations. The expanded form of (4-55) is

$$\mathbf{v}_r = \begin{bmatrix} 1 & 0 \\ 0 & 1 \\ -1 & 0 \\ 0 & -1 \\ . & . \\ . & . \\ . & . \end{bmatrix} \begin{bmatrix} v_{qr6} \\ v_{dr6} \end{bmatrix} + \begin{bmatrix} 1 & 0 \\ 0 & -1 \\ -1 & 0 \\ 0 & 1 \\ . & . \\ . & . \\ . & . \end{bmatrix} \begin{bmatrix} v_{qr2} \\ v_{dr2} \end{bmatrix} = \begin{bmatrix} 0 \\ 0 \\ 0 \\ 0 \\ . \\ . \\ . \\ . \end{bmatrix} \tag{4-56}$$

which suggests that only the following two equations are linearly independent

$$v_{qr6} + v_{qr2} = v_{qr} = 0 \tag{4-57}$$

and

$$v_{dr6} - v_{dr2} = v_{dr} = 0 \tag{4-58}$$

Similarly, two linearly independent conditions for currents can also be derived from $i_r = i_{r6} + i_{r2}$,

$$i_{qr6} + i_{qr2} = i_{qr} \tag{4-59}$$

and

$$i_{dr6} - i_{qr2} = i_{dr} \tag{4-60}$$

Using these conditions, we are able to combine the four rotor side equations of (4-54) into two independent equations by adding the first and

$$
\begin{bmatrix} v_{q6} \\ v_{d6} \\ v_{o6} \\ v_{q2} \\ v_{d2} \\ v_{o2} \\ v_{qr6} \\ v_{dr6} \\ v_{qr2} \\ v_{dr2} \end{bmatrix} = \begin{bmatrix} r_6+L_{s6}p & 3L_{s6}\omega_r & 0 & 0 & 0 & 0 & M_6p & 3M_6\omega_r & M_6p & -3M_6\omega_r \\ -3L_{s6}\omega_r & r_6+L_{s6}p & 0 & 0 & 0 & 0 & -3M_6\omega_r & M_6p & -3M_6\omega_r & -M_6p \\ 0 & 0 & r_6+L_{l6}p & 0 & 0 & 0 & 0 & 0 & 0 & 0 \\ 0 & 0 & 0 & r_2+L_{s2}p & L_{s2}\omega_r & 0 & -M_2p & M_2\omega_r & -M_2p & -M_2\omega_r \\ 0 & 0 & 0 & -L_{s2}\omega_r & r_2+L_{s2}p & 0 & M_2\omega_r & M_2p & M_2\omega_r & -M_2p \\ 0 & 0 & 0 & 0 & 0 & r_2+L_{l2}p & 0 & 0 & 0 & 0 \\ M_6p & 0 & 0 & 0 & 0 & 0 & r_r+L_rp & 0 & 0 & 0 \\ 0 & M_6p & 0 & 0 & 0 & 0 & 0 & r_r+L_rp & 0 & 0 \\ 0 & 0 & 0 & -M_2p & 0 & 0 & 0 & 0 & r_r+L_rp & 0 \\ 0 & 0 & 0 & 0 & -M_2p & 0 & 0 & 0 & 0 & r_r+L_rp \end{bmatrix} \begin{bmatrix} i_{q6} \\ i_{d6} \\ i_{o6} \\ i_{q2} \\ i_{d2} \\ i_{o2} \\ i_{qr6} \\ i_{dr6} \\ i_{qr2} \\ i_{dr2} \end{bmatrix} \qquad (4\text{-}54)
$$

the third equations and subtracting the second from the fourth equation. Eqn. (4-61) gives the final form of the d-q model.

$$\begin{bmatrix} v_{q6} \\ v_{d6} \\ v_{o6} \\ v_{q2} \\ v_{d2} \\ v_{o2} \\ v_{qr} \\ v_{dr} \end{bmatrix} = \begin{bmatrix} r_6+L_{s6}p & 3L_{s6}\omega_r & 0 & 0 & 0 & 0 & M_6p & 3M_6\omega_r \\ -3L_{s6}\omega_r & r_6+L_{s6}p & 0 & 0 & 0 & 0 & -3M_6\omega_r & M_6p \\ 0 & 0 & r_6+L_{l6}p & 0 & 0 & 0 & 0 & 0 \\ 0 & 0 & 0 & r_2+L_{s2}p & L_{s2}\omega_r & 0 & -M_2p & M_2\omega_r \\ 0 & 0 & 0 & -L_{s2}\omega_r & r_2+L_{s2}p & 0 & M_2\omega_r & M_2p \\ 0 & 0 & 0 & 0 & 0 & r_2+L_{l2}p & 0 & 0 \\ M_6p & 0 & 0 & -M_2p & 0 & 0 & r_r+L_rp & 0 \\ 0 & M_6p & 0 & 0 & M_2p & 0 & 0 & r_r+L_rp \end{bmatrix} \begin{bmatrix} i_{q6} \\ i_{d6} \\ i_{o6} \\ i_{q2} \\ i_{d2} \\ i_{o2} \\ i_{qr} \\ i_{dr} \end{bmatrix} \tag{4-61}$$

4.4 An Alternative Form of the Two-axis Model and Equivalent Circuits

An alternative expression of the two-axis model can easily be obtained by combining the speed voltage terms of (4-61). It follows that

$$v_{q6} = (r_6 + L_{s6}p)\, i_{q6} + 3\omega_r\lambda_{d6} + M_6pi_{qr} \tag{4-62}$$

$$v_{d6} = (r_6 + L_{s6}p)\, i_{d6} - 3\omega_r\lambda_{q6} + M_6pi_{dr} \tag{4-63}$$

$$v_{o6} = (r_6 + L_{l6}p)\, i_{o6} \tag{4-64}$$

$$v_{q2} = (r_2 + L_{s2}p)\, i_{q2} + \omega_r\lambda_{d2} - M_2pi_{qr} \tag{4-65}$$

$$v_{d2} = (r_2 + L_{s2}p)\, i_{d2} - \omega_r\lambda_{q2} + M_2pi_{dr} \tag{4-66}$$

$$v_{o2} = (r_2 + L_{l2}p)\, i_{o2} \tag{4-67}$$

$$v_{qr} = M_6pi_{q6} - M_6pi_{q2} + (r_r + L_rp)\, i_{qr} \tag{4-68}$$

$$v_{dr} = M_6pi_{d6} + M_6pi_{d2} + (r_r + L_rp)\, i_{dr} \tag{4-69}$$

where

$$\lambda_{q6} = L_{s6}i_{q6} + M_6\, i_{qr} \tag{4-70}$$

$$\lambda_{d6} = L_{s6}i_{d6} + M_6\, i_{dr} \tag{4-71}$$

$$\lambda_{q2} = L_{s2} i_{q2} - M_2 i_{qr} \tag{4-72}$$

$$\lambda_{d2} = L_{s2} i_{d2} + M_2 i_{dr} \tag{4-73}$$

The above two-axis model suggests the equivalent circuits as shown in Fig. 4-3.

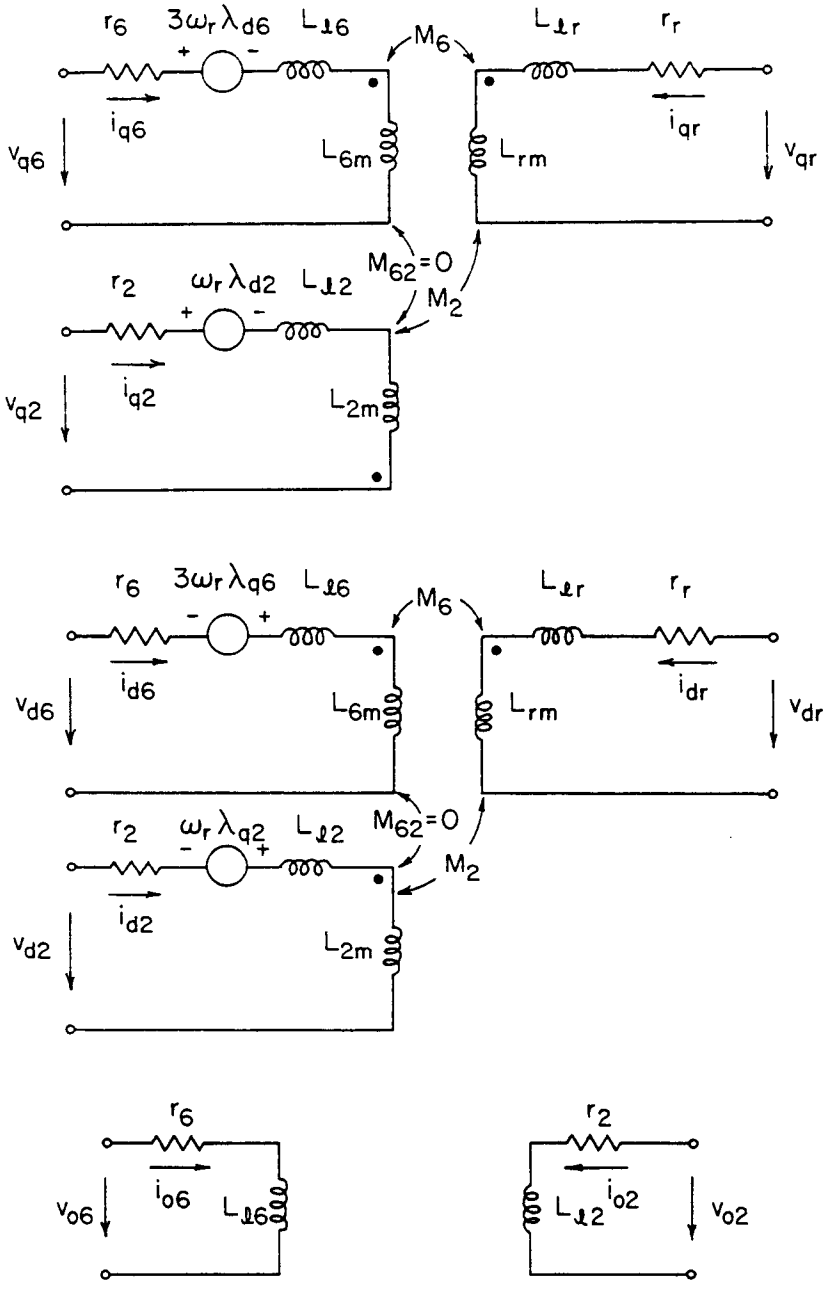

Fig. 4-3 Two-axis model equivalent circuits of the BDFM

4.5 The Torque Equation in the dq Domain

The torque equation in the d-q domain may also readily be derived from energy considerations.

From
$$T_e = (C_s^t\, i_{qdos})^t \left[\frac{\partial}{\partial \theta_r} (Z_{sr}) \right] C_r^t\, i_{qdr} \tag{4-74}$$

where
$$C_s^t = \begin{bmatrix} C_{s6}^t & 0 \\ 0 & C_{s2}^t \end{bmatrix}; \quad i_{qdos} = \begin{bmatrix} i_{qdo6} \\ i_{qdo2} \end{bmatrix};$$

$$Z_{sr} = \begin{bmatrix} Z_{s6r} & Z_{s6r} \\ Z_{s2r} & Z_{s2r} \end{bmatrix}; \quad C_r^t = \begin{bmatrix} C_{r6}^t & 0 \\ 0 & C_{r2}^t \end{bmatrix}; \quad i_{qdr} = \begin{bmatrix} i_{qdr6} \\ i_{qdr2} \end{bmatrix}$$

it follows that

$$T_e = i_{qdo6}\, C_{s6}^t \left[\frac{\partial}{\partial \theta_r} (Z_{s6r}) \right] C_{r6}^t i_{qdr6} + i_{qdo2} C_{s2}^t \left[\frac{\partial}{\partial \theta_r} (Z_{s2r}) \right] C_{r6}^t i_{qdr6} +$$

$$i_{qdo6}\, C_{s6}^t \left[\frac{\partial}{\partial \theta_r} (Z_{s6r}) \right] C_{r2}^t\, i_{qdr2} + i_{qdo2}\, C_{s2}^t \left[\frac{\partial}{\partial \theta_r} (Z_{s2r}) \right] C_{r2}^t\, i_{qdr2} \tag{4-75}$$

Simplifying (4-75) results in

$$T_e = \left(\sum_i M_{s6ri} \right) \Big\{ i_{qdo6}\, C_{s6}^t \left[\frac{\partial}{\partial \theta_r} f(3\theta_r) \right] C_{r6Z}^t\, i_{qdr6} + i_{qdo2} C_{s2}^t \left[\frac{\partial}{\partial \theta_r} g(\theta_r) \right]$$

$$C_{r6Z}^t\, i_{qdr6} + i_{qdo6}\, C_{s6}^t \left[\frac{\partial}{\partial \theta_r} f(3\theta_r) \right] C_{r2Z}^t\, i_{qdr2} + i_{qdo2} C_{s2}^t$$

$$\left[\frac{\partial}{\partial \theta_r} g(\theta_r) \right] C_{r2Z}^t\, i_{qdr2} \Big\} \tag{4-76}$$

where the matrix functions $[f(3\theta_r)]$ and $[g(\theta_r)]$ are given in (2-6) and (2-7) in Chapter 2.

The four terms in (4-76), denoted as T_{e66}, T_{e26}, T_{e62} and T_{e22}, can be verified to be of the following

$$T_{e66} = 3M_6 (i_{q6} i_{dr6} - i_{d6} i_{qr6}) \quad (4\text{-}77)$$

$$T_{e26} = M_2 (i_{q2} i_{dr6} + i_{d2} i_{qr6}) \quad (4\text{-}78)$$

$$T_{e62} = 3M_6 (-i_{q6} i_{dr2} - i_{d6} i_{qr2}) \quad (4\text{-}79)$$

$$T_{e22} = M_2 (-i_{q2} i_{dr2} + i_{d2} i_{qr2}) \quad (4\text{-}80)$$

Using rotor current constraints (4-59) and (4-60), it is easy to verify that the torque equation is of the form

$$T_e = T_{e6} + T_{e2} = 3M_6(i_{q6} i_{dr} - i_{d6} i_{qr}) + M_2(i_{q2} i_{dr} + i_{d2} i_{qr}) \quad (4\text{-}81)$$

where T_e ,T_{e6} and T_{e2} stand for the total, 6-pole and 2-pole torques, respectively. M_6 and M_2 , defined in (4-52) and (4-53), are the resulting mutual inductances between the 6-pole and the 2-pole systems and the rotor circuit in the d-q domain, respectively.

4.6 Two-Axis Model Parameters for an Experimental BDFM

Two-axis model parameters can be easily identified based on the work presented in Chapter 3 and the rules of the transformation process. In the two-axis model derivation process, the necessary formulas for computation of these parameters have already been developed. A list of these expressions is provided based on which the two-axis model parameters are computed.

(1) 6- and 2-pole stator system parameters

$$Z_{qdo6} = \begin{bmatrix} r_{q6}+L_{q6}p & 0 & 0 \\ 0 & r_{d6}+L_{d6}p & 0 \\ 0 & 0 & r_{o6}+L_{o6}p \end{bmatrix} \quad (4\text{-}82)$$

$$= \begin{bmatrix} r_6+(L_{l6}+L_{Am}-M)p & 0 & 0 \\ 0 & r_6+(L_{l6}+L_{Am}-M)p & 0 \\ 0 & 0 & r_6+L_{l6}p \end{bmatrix} \quad (4\text{-}83)$$

From $r_6 = 0.807\ \Omega$, $L_A = L_{l6} + L_{AM} = 0.0684$ H and $M = -0.0255$ H, it follows that

$$Z_{qdo6} = \begin{bmatrix} 0.807+0.0939p & 0 & 0 \\ 0 & 0.807+0.0939p & 0 \\ 0 & 0 & 0.807+0.0174p \end{bmatrix} \quad (4\text{-}84)$$

also

$$Z_{qdo2} = \begin{bmatrix} r_{q2}+L_{q2}p & 0 & 0 \\ 0 & r_{d2}+L_{d2}p & 0 \\ 0 & 0 & r_{o2}+L_{o2}p \end{bmatrix} \quad (4\text{-}85)$$

$$= \begin{bmatrix} r_2+(L_{l2}+L_{2m}-M')p & 0 & 0 \\ 0 & r_6+(L_{l2}+L_{2m}-M')p & 0 \\ 0 & 0 & r_2+L_{l2}p \end{bmatrix} \quad (4\text{-}86)$$

From $r_2 = 0.807\ \Omega$, $L_a = L_{l2} + L_{aM} = 0.4179$ H and $M' = -0.2004$ H, we also have

$$Z_{qdo2} = \begin{bmatrix} 0.807+0.6183p & 0 & 0 \\ 0 & 0.807+0.6183p & 0 \\ 0 & 0 & 0.807+0.0171p \end{bmatrix} \quad (4\text{-}87)$$

where in (4-84) and (4-87), $L_{l6} = L_{Am} + 2M$, $L_{l2} = L_{am} + 2M'$

(2) 6- and 2-pole stator phase and rotor mutual inductances

Using the data in Table II in Chapter 3 yields

$$M_6 = \sqrt{\frac{1}{2}} \sum_i M_{s6ri} = 0.001075 \text{ H} \quad (4\text{-}88)$$

also $$M_2 = \sqrt{\frac{1}{2}} \sum_i M_{s2ri} = 0.00483 \text{ H} \quad (4\text{-}89)$$

(3) Rotor parameters

From $$Z_{qdr} = \begin{bmatrix} r_{qr}+L_{qr}p & 0 \\ 0 & r_{dr}+L_{dr}p \end{bmatrix} \quad (4\text{-}90)$$

where $$r_{qr} = r_{dr} = r_r = \frac{1}{6}\left[\sum_i r_i + \sum_j \sum_i r_{ij} \right] \quad (4\text{-}91)$$

$$L_{qr} = L_{dr} = L_r = \frac{1}{6}\left[\sum_i (L_i+M_{ii}) + \sum_j \sum_i (M_{ij}+M'_{ij}) \right] \quad (4\text{-}92)$$

the rotor circuit parameters can be computed using the data given in Section 3.4 in Chapter 3 as

$$r_{qr} = r_{dr} = r_r = 327.5 \ \mu\Omega$$

and $$L_{qr} = L_{dr} = L_r = 41.7 \ \mu\text{H}$$

5. MODEL VERIFICATION - DYNAMIC SIMULATION RESULTS

Following the development of the d-q model, a computer program was written to simulate the dynamics of an experimental machine. The model equations were implemented on an HP 9000/360 workstation and integrated numerically using a 4th order Runge-Kutta algorithm. Simulation was carried out for the singly-fed and the doubly-fed modes of operation on a transient basis. Comparison of the results predicted by the d-q model and available test data was made. Some of the simulation results and test data are presented and discussed in the following sections.

5.1 The Two-Axis Model in the State Variable Form

Eqn. (5-1) is the concise form of the two-axis model Eqn. (4-61) with zero sequences omitted.

$$\mathbf{v}_{qd} = \mathbf{z}_{qd}\, \mathbf{i}_{qd} \tag{5-1}$$

By separating the coefficients of the equation into two groups comprising those that contain the operator p and those that do not, we obtain

$$\mathbf{v}_{qd} = \mathbf{z}_{qd}\, \mathbf{i}_{qd} = [\, \mathbf{R}(\omega_r) + \mathbf{L}_{qd}\, p\,]\, \mathbf{i}_{qd} = \mathbf{R}(\omega_r)\, \mathbf{i}_{qd} + \mathbf{L}_{qd}\, p(\mathbf{i}_{qd}) \tag{5-2}$$

and hence

$$p(\mathbf{i}_{qd}) = -\, \mathbf{L}^{-1}_{qd}\, \mathbf{R}(\omega_r)\, \mathbf{i}_{qd} + \mathbf{L}^{-1}_{qd}\, \mathbf{v}_{qd} \tag{5-3}$$

where in Eqn. (5-3) the state vector $\mathbf{i}_{qd}$ and the control (input) vector $\mathbf{v}_{qd}$ are defined as

$$\mathbf{v}_{qd} = [\, v_{q6}\ v_{d6}\ v_{q2}\ v_{d2}\ v_{qr}\ v_{dr}\,]^t$$

$$\mathbf{i}_{qd} = [\, i_{q6}\ i_{d6}\ i_{q2}\ i_{d2}\ i_{qr}\ i_{dr}\,]^t$$

respectively.

$$L_{qd} = \begin{bmatrix} L_{s6} & 0 & 0 & 0 & M_6 & 0 \\ 0 & L_{s6} & 0 & 0 & 0 & M_6 \\ 0 & 0 & L_{s2} & 0 & -M_2 & 0 \\ 0 & 0 & 0 & L_{s2} & 0 & M_2 \\ M_6 & 0 & -M_2 & 0 & L_r & 0 \\ 0 & M_6 & 0 & M_2 & 0 & L_r \end{bmatrix} \tag{5-4}$$

$$R(\omega_r) = \begin{bmatrix} r_6 & 3L_{s6}\omega_r & 0 & 0 & 0 & 3M_6\omega_r \\ -3L_{s6}\omega_r & r_6 & 0 & 0 & -3M_6\omega_r & 0 \\ 0 & 0 & r_2 & L_{s2}\omega_r & 0 & M_2\omega_r \\ 0 & 0 & -L_{s2}\omega_r & r_2 & M_2\omega_r & 0 \\ 0 & 0 & 0 & 0 & r_r & 0 \\ 0 & 0 & 0 & 0 & 0 & r_r \end{bmatrix} \tag{5-5}$$

The mechanical equations are given by

$$p(\theta_r) = \omega_r \tag{5-6}$$

$$Jp(\omega_r) = T_e - T_L - k_d\omega_r \tag{5-7}$$

with $$T_e = 3M_6 (i_{q6} i_{dr} - i_{d6} i_{qr}) + M_2 (i_{q2} i_{dr} + i_{d2} i_{qr}) \tag{5-8}$$

where k_d is the damping coefficient and J is the inertia.

Eqn. (5-3), together with Eqns (5-6), (5-7) and (5-8) describe fully the dynamic behavior of the BDFM system. Without loss of generality, the initial condition for the states, i_{qd}, can be assumed to be zero.

5. 2 Input Voltages to the BDFM

In addition to the assumptions made in Chapter 2, it is further assumed in the simulation that the 6-pole and the converter output voltage (the 2-pole system input voltage) are balanced three phase sinusoidal voltage sources and harmonics are neglected.

In the d-q domain, the input voltages are obtained from the two stator transformations C_{s6}, C_{s2}. In particular, with three-phase balanced excitation,

$$v_{q6} = \sqrt{\frac{3}{2}}\, V_6 \cos(\omega_6 t - 3\theta_r + \phi_6) \tag{5-9}$$

$$v_{d6} = -\sqrt{\frac{3}{2}}\, V_6 \sin(\omega_6 t - 3\theta_r + \phi_6) \tag{5-10}$$

$$v_{q2} = \sqrt{\frac{3}{2}}\, V_2 \cos(\omega_2 t + \theta_r - 40^\circ + \phi_2) \tag{5-11}$$

$$v_{d2} = \sqrt{\frac{3}{2}}\, V_2 \sin(\omega_2 t + \theta_r - 40^\circ + \phi_2) \tag{5-12}$$

and

$$v_{qr} = v_{dr} = 0 \tag{5-13}$$

where ω_6 and ω_2 represent the frequencies of the 60Hz power supply and the power converter, respectively. θ_r is the rotor angle with respect to the 6-pole stator reference axis in mechanical degrees. ϕ_6, ϕ_2 are the initial angles and V_6 , V_2 are the peak phase voltages of the two independent voltage sources.

Equations (5-9) through (5-13) give a general form of inputs and should be modified to reflect a particular type of operation. For example, for the singly-fed induction mode with short-circuited 2-pole winding,

$$v_{q2} = v_{d2} = 0 \tag{5-14}$$

In doubly-fed steady state operations, since $\theta_r = \omega_r t$ the d-q input voltages will have rotor slip frequencies defined by:

$$\omega_6 - 3\omega_r = s_1 \omega_6 \tag{5-15}$$

and

$$\omega_2 + \omega_r = \frac{\omega_2}{s_2} \tag{5-16}$$

where s_1 and s_2 are the 6 and the 2-pole rotor slips, respectively.

Particularly, in synchronous operation when the two rotor frequencies are the same, it follows that

$$\omega_6 - 3\omega_r = \omega_2 + \omega_r \tag{5-17}$$

or

$$\omega_r = \frac{\omega_6 - \omega_2}{4} \tag{5-18}$$

Thus the rotor mechanical radian frequency under the synchronous mode of operation is completely determined by the frequency of the converter output.

5.3 Dynamic Simulations of the BDFM

5.3.1 Singly-Fed Induction Mode of Operation

To be consistent with the laboratory testing procedure, in the computer simulation, the 6-pole stator set, ABC, is connected directly to the 60Hz power supply and the 2-pole terminals, abc, are short circuited. Consequently, $v_{q2}=v_{d2}=0$.

The predicted stator and rotor q axis currents during free acceleration are plotted in Fig. 5-1. Similar to a conventional 6-pole induction motor run up, substantially high but decaying currents can be seen before the machine enters steady state operation in which both the 2-pole and the rotor currents go close to zero and the 6-pole current approaches a constant value. Figs 5-2(a) and 5-2(c) show the predicted 6-pole and 2-pole line currents i_A and i_a during the start-up period. It is seen that the currents decay as the speed of the machine increases but pick up again due to the increasing interactions between the two systems around 900 r/min. The frequency of the 2-pole winding current is seen to decrease to dc close to 900 r/min, increasing again above 900 r/min before the current magnitude

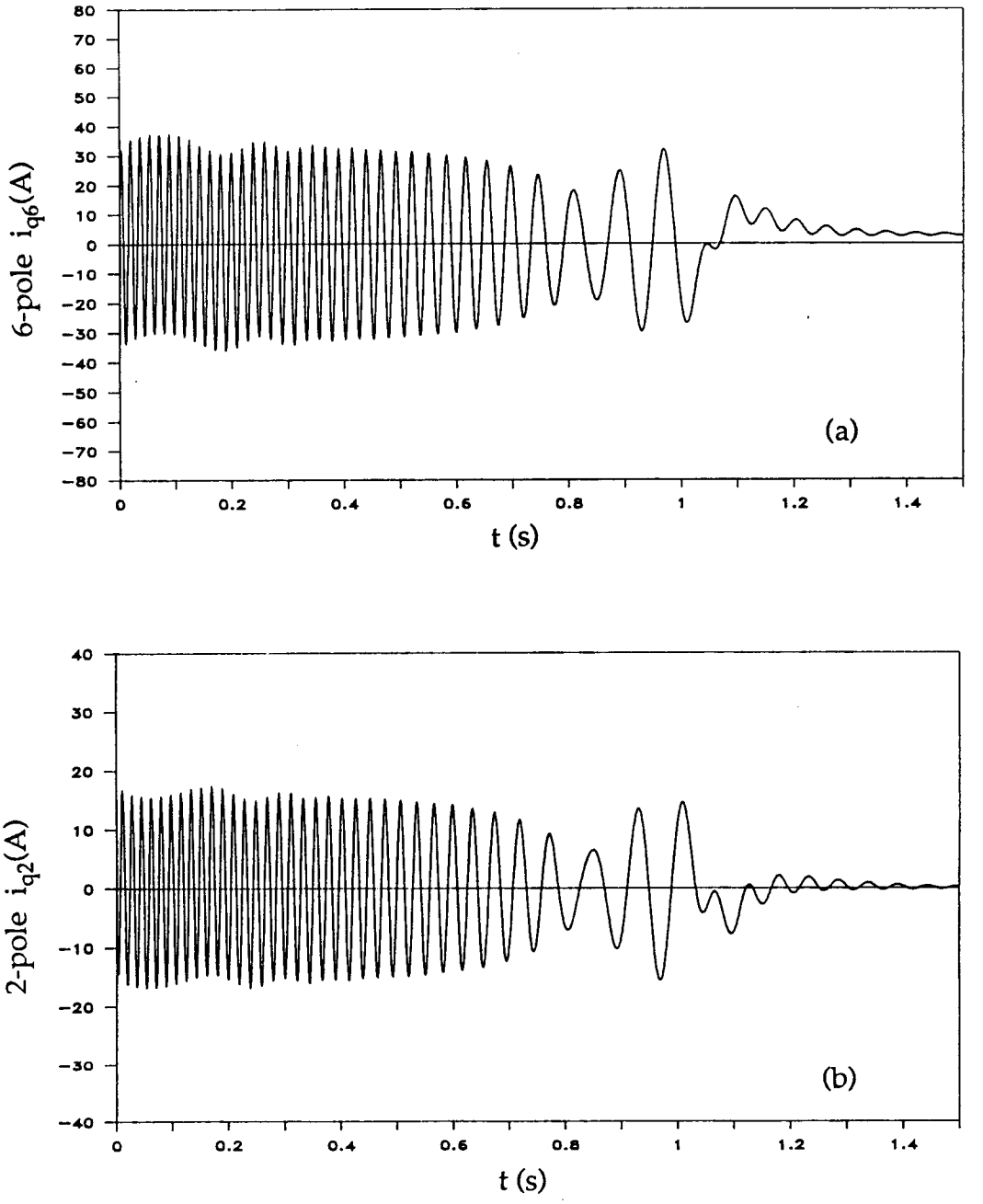

Fig. 5-1 Run-up q-axis currents and rotor speed

(a) 6-pole i_{q6}

(b) 2-pole i_{q2}

(c) rotor i_{qr}

(d) rotor speed ω_r Fig. 5-1 (continued)

Fig. 5-1 (continued)

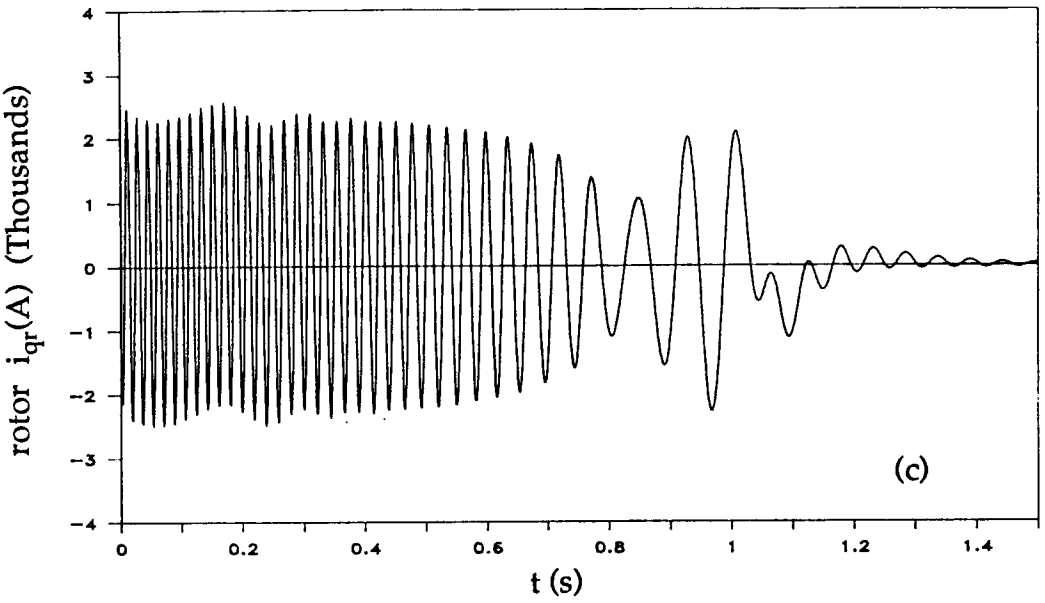

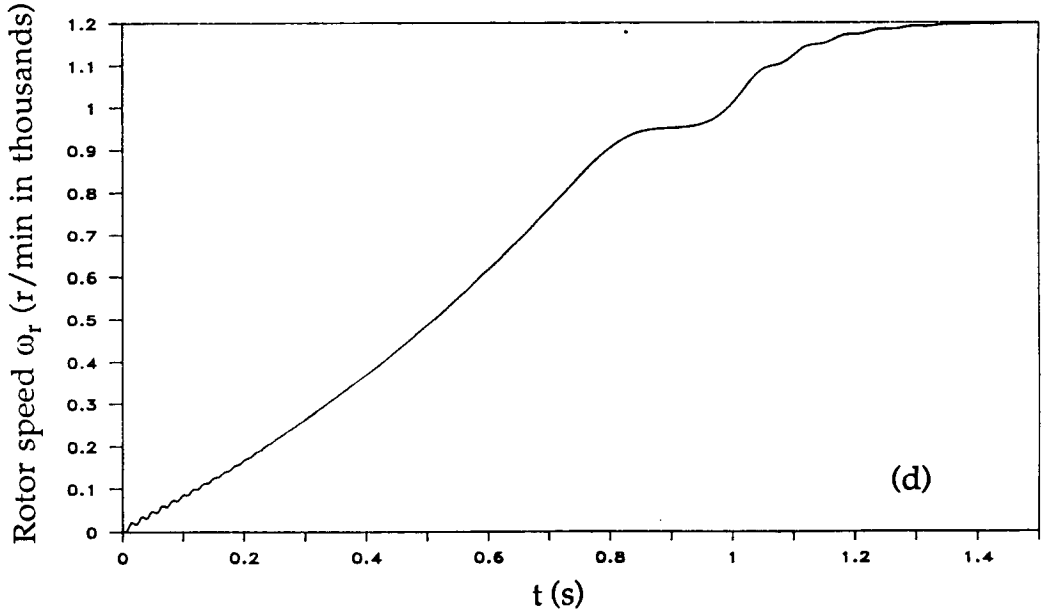

approaches zero at 1200 r/min. From the basic assumption that direct coupling between the two stator systems is negligible, it is understood that the 2-pole current i_a is due solely to the coupling between the 2-pole system and the rotor circuit. The measured transient 6-pole and 2-pole line currents are shown in Figs 5-2(b) and 5-2(d). Compared with Figs 5-2(a), 5-2(c) it is seen that there exists good correlation between these currents. It is

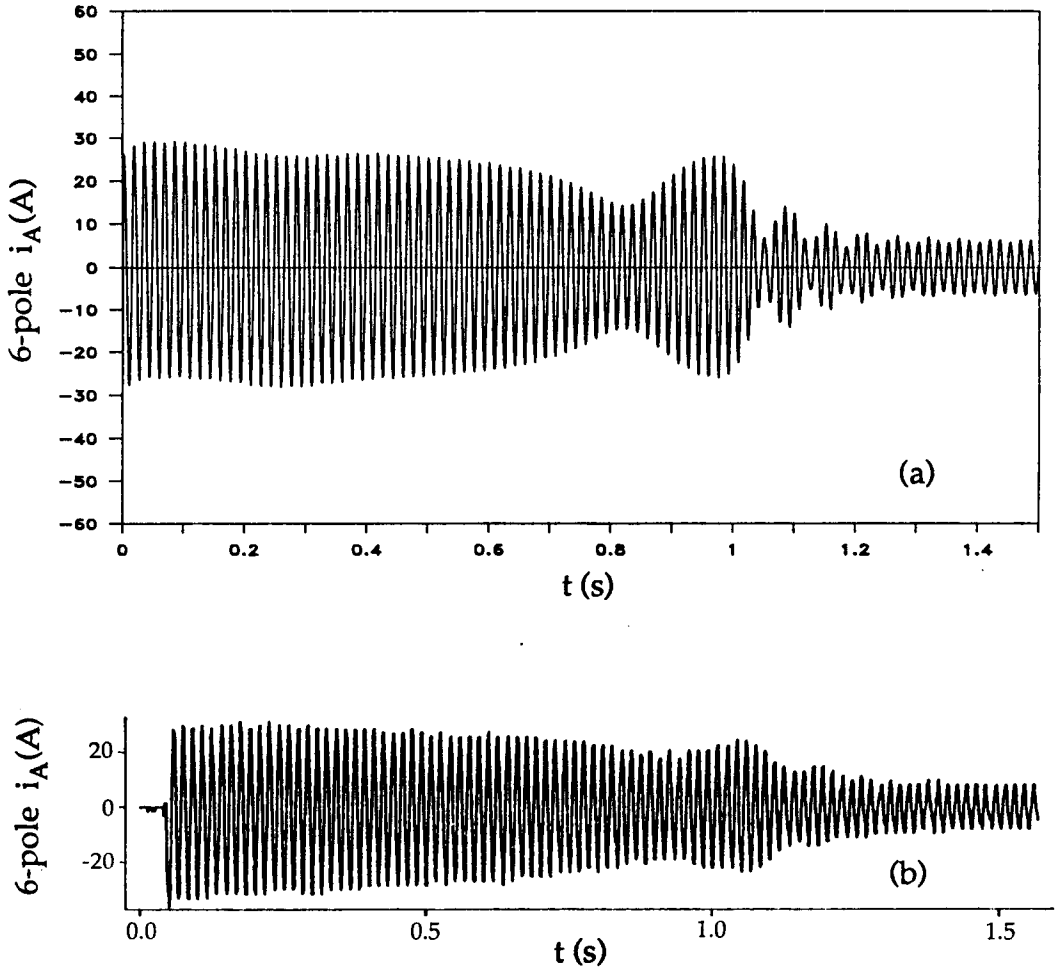

Fig. 5-2 Predicted and measured 6- and 2-pole line currents

(a) Predicted 6-pole line current (b) Measured 6-pole line current

(c) Predicted 2-pole line current (d) Measured 2-pole line current

Fig. 5-2 (continued)

Fig. 5-2 (continued)

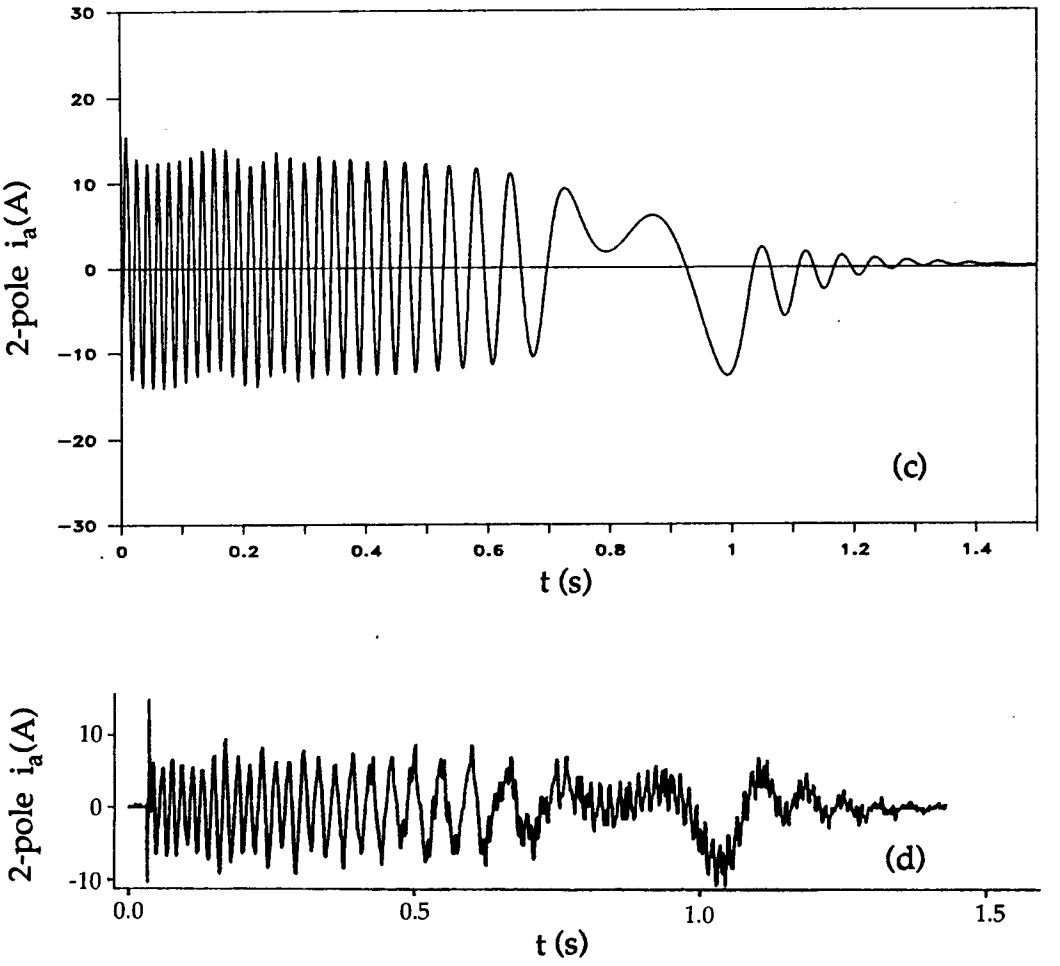

noted that while correctly predicting the fundamental nature of the machine currents, the reduced order model neglects the high order effects which are present in the measured current waveforms.

Fig. 5-1(d) is a plot of speed vs time during free acceleration. The curve resembles very closely that of an induction motor until 900 r/min when the rate of change of speed suddenly decreases. This hesitation of speed change reflects the effects of the short circuited 2-pole winding which acts

upon the system to develop a significant net torque reduction in the region of 900 r/min.

The starting torque-speed characteristic is also of great interest. Simulation results are shown in Fig. 5-3. As would be expected, the BDFM follows the torque-speed characteristic of an 8-pole induction motor (which is the sum of the pole numbers of the two systems) when the speed is less than 900 r/min. Beyond about 1000 r/min, the machine acts roughly like a 6-pole induction motor, resulting in a double-hump torque-speed characteristic (see [15]). Note that the total electrical torque,T_e, produced by the machine is composed of two components, T_{e6} and T_{e2}. T_{e6} is produced by the 6-pole system while T_{e2} is due to the 2-pole system. The interaction between the two torques and the two systems can be clearly seen.

It was also found in laboratory and computer simulation that when the starting load torque is relatively large the speed could be stabilized around 900 r/min, depending upon the loading conditions, instead of accelerating through to the full speed (about 1200 r/min).

Free acceleration and steady state operation of the BDFM provides insight into machine characteristics when compared with an induction motor. In order to achieve desired open loop precise speed control for ASD or VSG systems, synchronous operation is essential.

5.3.2 Synchronization and the Synchronous Mode of Operation

Synchronous operation can occur only when a synchronization process has been successfully carried out. There are several methods to pull the machine into synchronism [1]. Computer simulation was carried out to study synchronization of the machine using dc and ac 2-pole excitation.

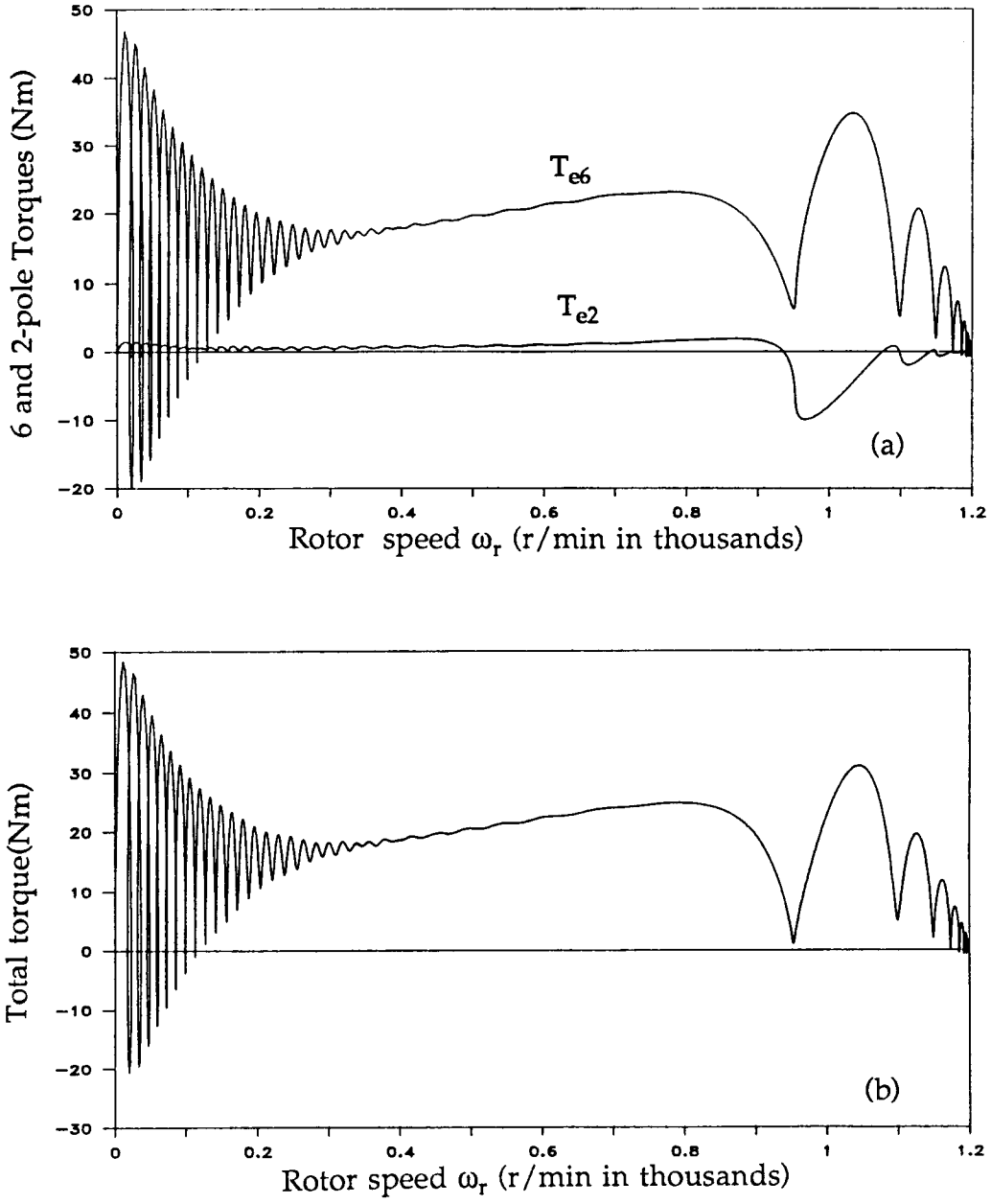

Fig. 5-3 Free acceleration torque-speed characteristics

(a) 6- and 2-pole torques, T_{e6} and T_{e2}

(b) Total torque $T_e = T_{e6} + T_{e2}$

Fig. 5-4 gives the typical simulation results using dc synchronization. Initially, the machine is running steadily in the singly-fed induction mode with 4 Nm load torque. Synchronization begins when a set of dc voltages is applied to the initially short circuited 2-pole stator windings and slowly ramped up to

$$v_{an} = V, \quad v_{bn} = v_{cn} = -\frac{V}{2} \tag{5-19}$$

where V represents a voltage level that is appropriate for successful synchronization.

This set of voltages is the limit case of a set of balanced, negative sequence three phase voltages applied to the 2-pole stator system when the frequency is approaching zero. It is seen from Fig. 5-5(a) that the machine experiences a transient period before the speed settles down at 900 r/min. The oscillation depends largely on the mechanical characteristics of the machine and the connected system. Fig. 5-5(b) shows the change of waveforms of the 2-pole a-phase current during the transition. In the single-fed induction mode of operation with load, i_a is the induced current due to the coupling between the 2-pole system and the rotor. When the motor enters synchronous operation with dc applied on the 2-pole side, i_a is an electrically forced dc current.

Synchronization can also be achieved if a set of low frequency, negative sequence ac voltages is applied to the 2-pole system terminals. In doing that, the 2-pole frequency is slowly ramped up, as is the 2-pole voltage. The voltage is applied in such a way that a constant volts/hertz ratio is maintained. Proper excitation is essential since a low ratio would not produce enough torque to bring the machine into synchronism while a large ratio can generate too much disturbance and eventually take the

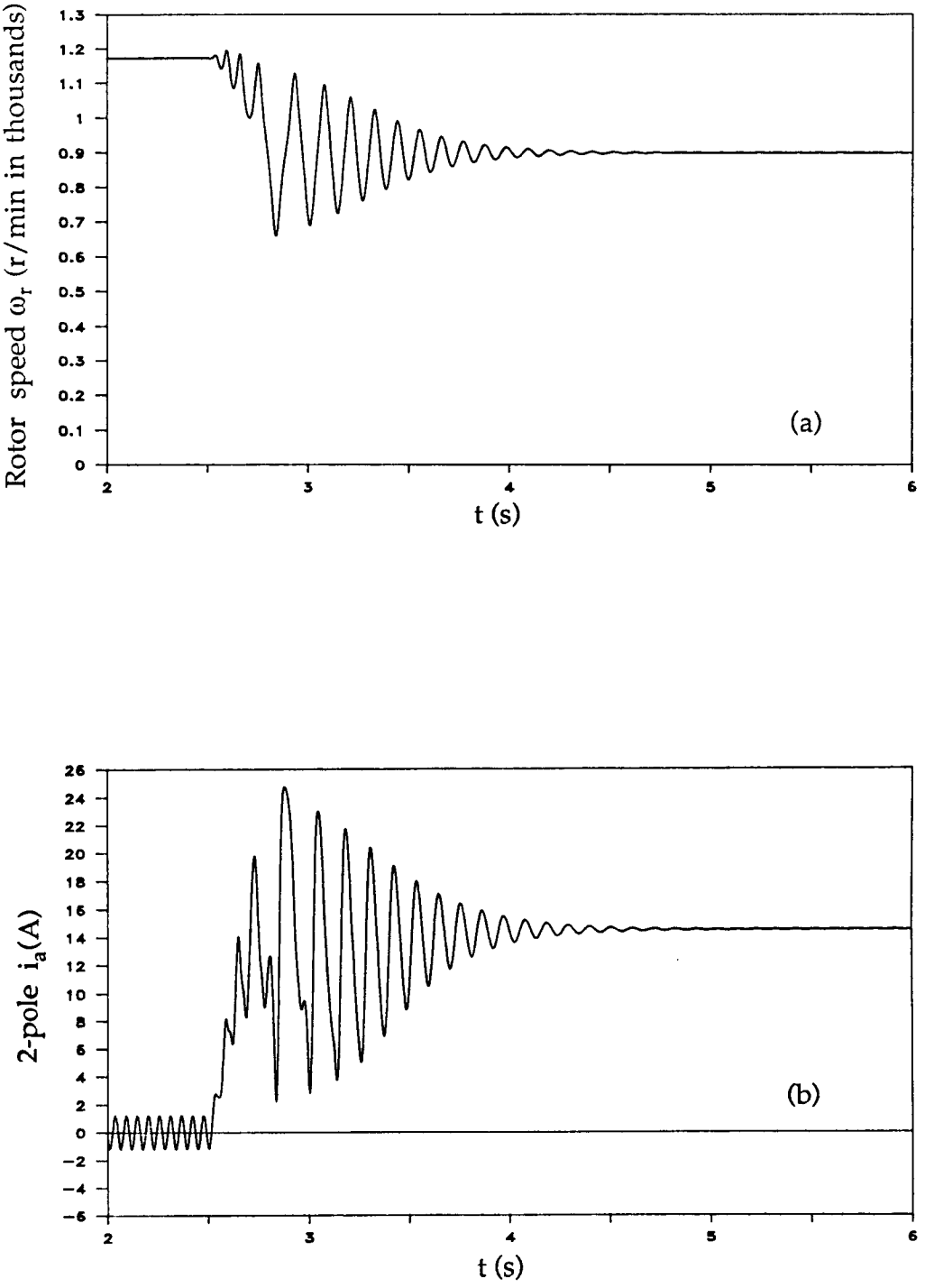

Fig. 5-4 DC synchronization simulation

(a) Speed vs time (b) 2-pole current i_a

machine into stall. Once the machine is running synchronously, the applied voltage on the 2-pole side can be reduced to a substantially lower level without losing synchronism. This is of practical importance in certain applications since reducing the excitation voltage means reducing the rating requirements of the power converter and hence its cost.

In steady state synchronous operation, the shaft speed can be determined by the following expression

$$\text{shaft speed (r/min)} = 60\,\frac{f_6 - f_2}{P_6+P_2} \tag{5-20}$$

where f_6 and f_2 denote the 6-pole utility power supply frequency and the 2-pole supply frequency from the power electronic converter, respectively. P_6 and P_2 are the pole-pair numbers for the two systems.

Fig. 5-5 shows the synchronous and fault tolerant behavior of the BDFM system. The following three situations are considered in the simulation:

(a) Machine response to a sudden reduction of 2-pole excitation voltage.

(b) Machine response to a ramp and a step change of load torque.

(c) Machine response to a sudden loss of 2-pole excitation.

Initially, the motor is running synchronously at 870 r/min (f_2=2Hz) with load torque equal to zero. At t=3.5 seconds the 2-pole excitation voltage V_2 is step changed to $0.5V_2$. This sudden change of excitation voltage results in lower 6 and 2-pole currents while the machine is still in synchronous operation.

At t=5.0 seconds, load torque is ramped up from zero to 20 Nm. Similar to conventional synchronous machines, the BDFM is seen to maintain synchronous operation at the speed of 870 r/min.

The machine response to a sudden change of load torque is illustrated at t=6.5 seconds when the load torque is rapidly reduced from 20 Nm to 10 Nm. It is seen that after the electromagnetic and electromechanical transients decay, synchronous operation is still retained.

Synchronism can be lost if a severe disturbance occurs. Fig. 5-5 also shows the machine dynamics for a sudden loss of 2-pole excitation at t=8.5 seconds when a short circuit is applied to the 2-pole terminals. An advantage of the BDFM drive system is that a loss of synchronism does not lead to a catastrophic situation and the machine can remain connected. As a result, the drive system still operates in the singly-fed induction mode and can be re-synchronized by application of appropriate 2-pole voltage and frequency.

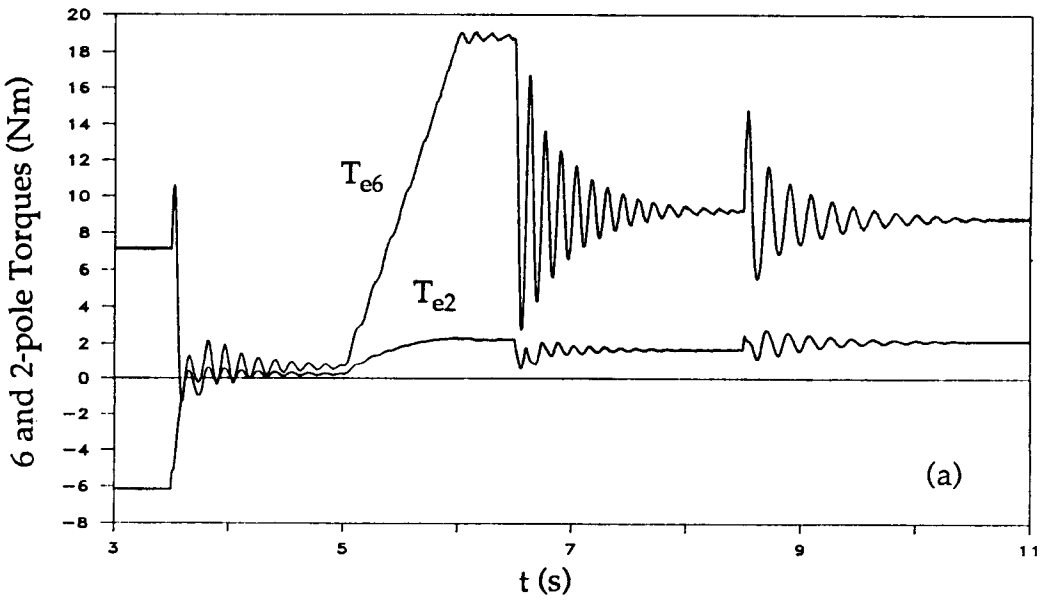

Fig. 5-5 Synchronous behavior of the BDFM

(a) 6- and 2-pole torques

(b) Total torque and load torque

(c) Rotor speed ω_r Fig. 5-5 (continued)

Fig. 5-5 (continued)

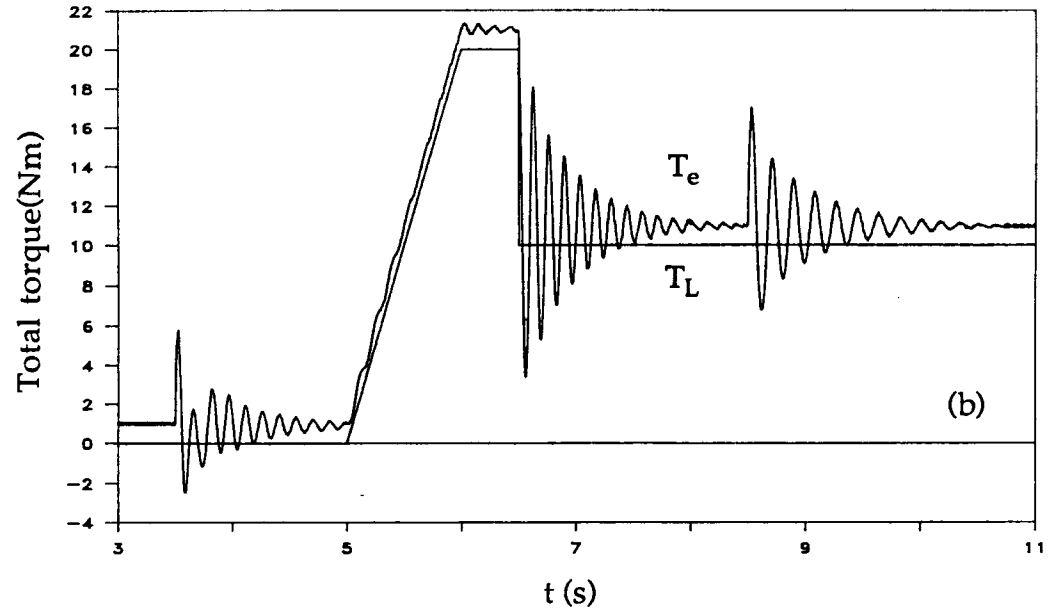

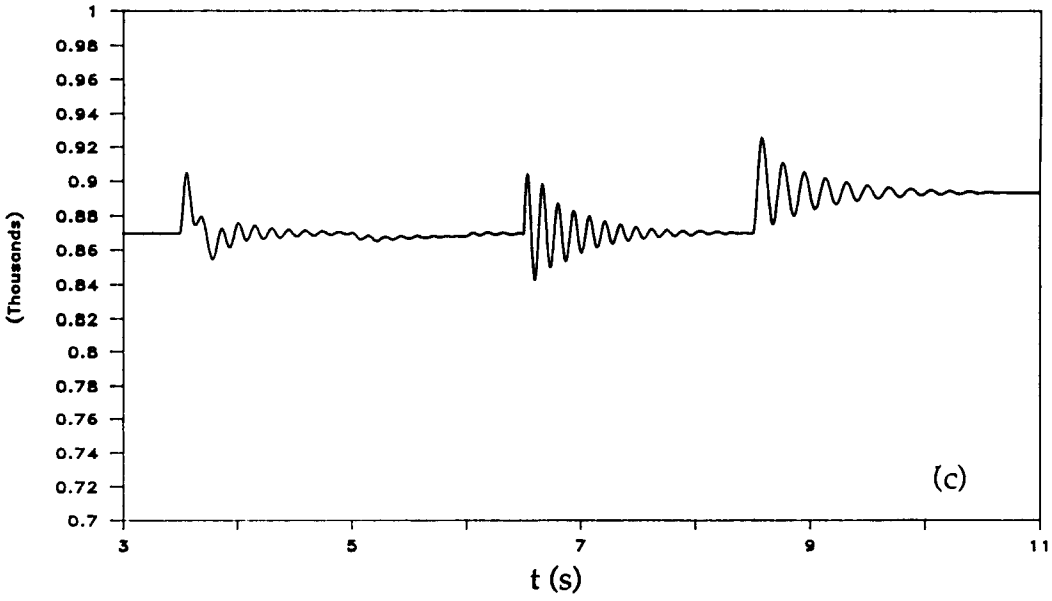

6. STEADY STATE ANALYSIS OF THE BDFM

So far the two-axis model of the BDFM has been used to predict the dynamic performance of the machine. The model may also be employed for steady state analysis. In many situations, it is desirable to analyze the machine in steady state conditions only. Hence, development of steady state models for this purpose is important.

In previous studies [3,6,7,8], steady state models were derived based on the two machine equivalence assumption and cascade connection of two induction motors were often used to analyze the machine performance. The advantage of this approach is that the machine parameters may be easily obtained using standard testing techniques. Although this approach is valid for performance evaluation of the system, the parameters used for the investigation do not necessarily represent those of a true BDFM. The results obtained may not be valid for machine and drive system design.

In this Chapter, steady state equivalent circuits are developed rigorously from the d-q representation. Since the parameters of the dq model relate directly to the true machine parameters, the direct relation between the machine performance and machine parameters is also established. It can be shown that these models improve on traditionally used equivalents by providing all possible modes of operation and relating the machine steady state performance with machine parameters. Although the circuits are derived in the dq domain, they can be transformed back to machine variables easily if necessary. Since the BDFM exhibits several modes of operation, more than one steady state equivalent circuit needs to be derived.

The development of the steady state models makes it possible to investigate steady state performance of the BDFM. However, it will be shown that certain operational modes of the machine require a special solution technique, which is also developed in this Chapter.

6.1 Steady State Models in the dq Domain

6. 1.1 The Synchronous Mode of Operation

The stator d-q variables are related with physical variables through the transformations C_{s6} and C_{s2}. In steady state operations, where $\theta_r=\omega_r t$, Eqns (5-9) through (5-12) thus become

$$v_{q6} = \sqrt{\frac{3}{2}}\ V_6 \cos[(\omega_6 - 3\omega_r)t] \tag{6-1}$$

$$v_{d6} = -\sqrt{\frac{3}{2}}\ V_6 \sin[(\omega_6 - 3\omega_r)t] \tag{6-2}$$

$$v_{q2} = \sqrt{\frac{3}{2}}\ V_2 \cos[(\omega_2+\omega_r)t-\beta] \tag{6-3}$$

$$v_{d2} = \sqrt{\frac{3}{2}}\ V_2 \sin((\omega_2+\omega_r)t-\beta] \tag{6-4}$$

with $\phi_6 = 0$ and β being the angle between the reference voltage v_{q6} and v_{q2}.

In phasor representations, (6-1) through (6-4) can be written as

$$\dot{V}_{q6} = V_{q6}\ ,\ \dot{V}_{d6}= j\dot{V}_{q6}\ ,\ \dot{V}_{q2} = V_{q2}\, e^{-j\beta},\ \dot{V}_{d2} = -\, j\dot{V}_{q2} \tag{6-5}$$

also $$\dot{I}_{d6} = j\dot{I}_{q6}, \qquad \dot{I}_{d2} = -\, j\dot{I}_{q2}, \qquad \dot{I}_{dr} = j\dot{I}_{qr} \tag{6-6}$$

where $V_{q6} = \frac{\sqrt{3}}{2}\ V_6$ and $V_{q2} = \frac{\sqrt{3}}{2}\ V_2$ are the rms voltages of the qd variables.

In the d-q domain, all the d-q quantities have the same slip frequency $s_1\omega_6 = (\omega_6-3\omega_r)=(\omega_2+\omega_r)$. Thus, replacing the differentiation operator p with $j(\omega_6-3\omega_r)$ or $j(\omega_2+\omega_r)$ and expanding the first equation of the two axis model representation (4-61), we obtain

$$\dot{V}_{q6}= [r_6+j(\omega_6-3\omega_r)L_{s6}]\,\dot{I}_{q6}+3L_{s6}\omega_r\,\dot{I}_{d6}+3M_6\omega_r\,\dot{I}_{dr}+ j(\omega_6-3\omega_r)\,M_6\,\dot{I}_{qr}$$

using (6-6) yields

$$\dot{V}_{q6}= (\,r_6 + j\,X_{s6}\,)\,\dot{I}_{q6} + j\,X_{m6}\,\dot{I}_{qr} \qquad (6\text{-}7)$$

For the 2-pole side, expanding the third equation of (4-61) yields

$$\dot{V}_{q2} = [\,r_2 +j(\omega_2 + \omega_r)L_{s2}\,]\,\dot{I}_{q2} + L_{s2}\omega_r\,\dot{I}_{d2} - j(\omega_2 + \omega_r)\,M_2\,\dot{I}_{qr} + M_2\omega_r\,\dot{I}_{dr}$$

$$= [\,r_2 + (\frac{\omega_2}{\omega_6})\,j\,X_{s2}\,]\,\dot{I}_{q2} - (\frac{\omega_2}{\omega_6})\,j\,X_{m2}\,\dot{I}_{qr} \qquad (6\text{-}8)$$

Define the total slip $s = s_1 s_2 = \dfrac{\omega_2}{\omega_6}$, with $s_1 = \dfrac{\omega_6 - 3\omega_r}{\omega_6}$ and $s_2 = \dfrac{\omega_2}{\omega_2 + \omega_r}$

being the 6-pole to rotor and 2-pole to rotor slips, respectively.

hence,

$$\dot{V}_{q2} = (\,r_2 + s\,j\,X_{s2}\,)\,\dot{I}_{q2} - s\,j\,X_{m2}\,\dot{I}_{qr} \qquad (6\text{-}9)$$

or

$$\frac{\dot{V}_{q2}}{s} = (\frac{r_2}{s} + j\,X_{s2}\,)\,\dot{I}_{q2} - j\,X_{m2}\,\dot{I}_{qr}, \quad \text{for } s \neq 0 \qquad (6\text{-}10)$$

For the rotor side, the fifth equation of (4-61) is expanded.

$$\dot{V}_{qr} = j(\omega_6 - 3\omega_r)M_6\,\dot{I}_{q6} - j(\omega_6 - 3\omega_r)M_2\,\dot{I}_{q2} + [r_r + j(\omega_6 - 3\omega_r)L_r]\,\dot{I}_{qr}$$

Simplifying the above expression yields

$$\frac{\dot{V}_{qr}}{s_1} = j\,X_{m6}\,\dot{I}_{q6} - j\,X_{m2}\,\dot{I}_{q2} + (\frac{r_r}{s_1} + j\,X_r\,)\,\dot{I}_{qr} \qquad (6\text{-}11)$$

where in equations (6-7) through (6-11), $X_{s6} = \omega_6 L_{s6}$, $X_{s2} = \omega_6 L_{s2}$, $X_{m6} = \omega_6 M_6$, $X_{m2} = \omega_6 M_2$ and $X_r = \omega_6 L_r$.

An equivalent circuit based on Eqns (6-7), (6-10) and (6-11) is given in Fig. 6-1(a). For dc excitation on the 2-pole terminals, which implies that s=0, Eqn. (6-9) becomes

$$\dot{V}_{q2} = r_2\,\dot{I}_{q2} \qquad (6\text{-}12)$$

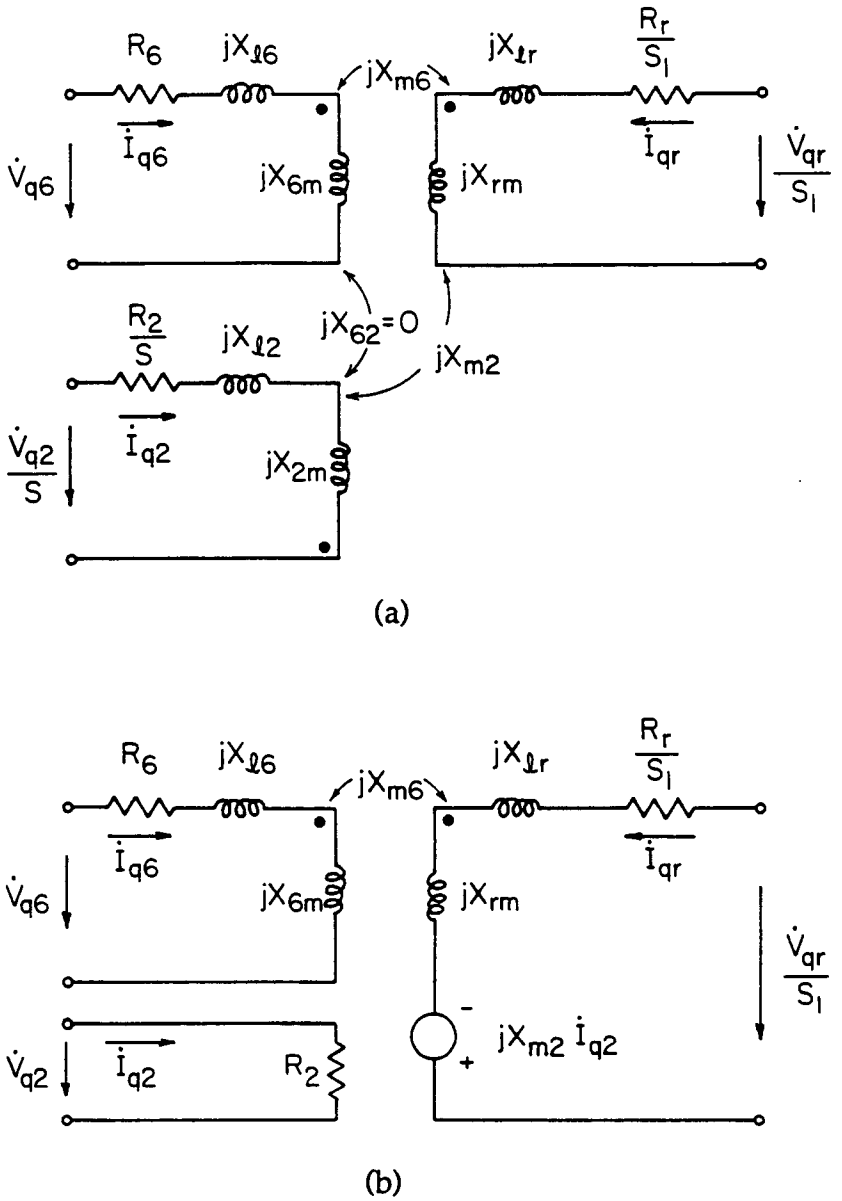

Fig. 6-1 Steady state equivalent circuits for synchronous operation

(a) ac excitation on the 2-pole system

(b) dc excitation on the 2-pole system

The equivalent circuit for this operating condition is shown in Fig. 6-1(b) from which it is seen that the 2-pole stator system becomes purely resistive.

6.1.2 Singly-Fed Induction Mode of Operation with 2-pole System Short-Circuited

A steady state equivalent circuit for the singly-fed induction mode of operation with 2-pole system short circuited may also be derived using similar techniques to those shown above. It is easy to verify the following equations:

$$\dot{V}_{q6} = (r_6 + j X_{s6}) \dot{I}_{q6} + j X_{m6} \dot{I}_{qr} \tag{6-13}$$

$$0 = (r_2 + s j X_{s2}) \dot{I}_{q2} - s j X_{m2} \dot{I}_{qr} \tag{6-14}$$

or

$$0 = (\frac{r_2}{s} + j X_{s2}) \dot{I}_{q2} - j X_{m2} \dot{I}_{qr}, \text{ for } s \neq 0 \tag{6-15}$$

$$\frac{\dot{V}_{qr}}{s_1} = j X_{m6} \dot{I}_{q6} - j X_{m2} \dot{I}_{q2} + (\frac{r_r}{s_1} + j X_r) \dot{I}_{qr} \tag{6-16}$$

It can be shown that in singly-fed induction mode of operation with 2-pole side short circuited, the relation $(\omega_6 - 3\omega_r) = (\omega_2 + \omega_r)$ still holds. However, it must be understood that ω_2 is the induced frequency. From the above expression, it follows that

$$s = \frac{\omega_2}{\omega_6} = \frac{\omega_6 - 4\omega_r}{\omega_6} \tag{6-17}$$

From equations (6-13), (6-14) and (6-16), an equivalent circuit can be obtained by short circuiting the 2-pole input terminals in Fig. 6-1(a) for 2-pole ac excitation. A special case is when the machine is running at 900 r/min. Since s=0 and $\dot{I}_{q2} = 0$, (6-14) vanishes, which means that at this speed there are no effects from the short circuited 2-pole winding on the

system. The equivalent circuit in this case is the same as that of a conventional induction motor.

The equivalent circuit expressed in terms of d axis variables can also be readily obtained. For the synchronous mode of operation, upon substituting (6-5) and (6-6) into equations (6-7),(6-9) and (6-11), we obtain

$$\dot{V}_{d6} = (r_6 + j X_{s6}) \dot{I}_{d6} + j X_{m6} \dot{I}_{dr} \tag{6-18}$$

$$\dot{V}_{d2} = (r_2 + s j X_{s2}) \dot{I}_{d2} + s j X_{m2} \dot{I}_{dr} \tag{6-19}$$

$$\frac{\dot{V}_{d2}}{s} = (\frac{r_2}{s} + j X_{s2}) \dot{I}_{d2} + j X_{m2} \dot{I}_{d2}, \quad \text{for } s \neq 0 \tag{6-20}$$

$$\frac{\dot{V}_{dr}}{s_1} = j X_{m6} \dot{I}_{d6} + j X_{m2} \dot{I}_{d2} + (\frac{r_r}{s_1} + j X_r) \dot{I}_{dr} \tag{6-21}$$

These equations can be shown to be equally valid for describing the steady state behavior of the BDFM under the synchronous mode of operation. Since d and q variables are linearly dependent in steady state operation, only one set of equations need be used.

It is important to note the advantage of deriving steady state equivalent circuits for the singly-fed induction mode and the doubly-fed synchronous mode of operation from the d-q domain in which all the quantities have the same rotor slip frequency which depends on the speed of the machine. Research is now underway to apply these steady state models expressed in both dq and machine variables for machine and control designs.

6.2 Steady State Models in Machine Variables

Steady State models or equivalent circuits expressed in actual machine variables, which are useful for correlating test data and deriving machine parameters from tests, may be obtained from dq domain models or

equivalent circuits. It is noticed that in Eqns (6-7), (6-10) and (6-11) the frequency of the phasors is

$$\omega_{rs} = \omega_6 - 3\omega_r = \omega_2 + \omega_r \tag{6-22}$$

It is thus appropriate to write (6-7), (6-10) and (6-13) in the following form

$$\begin{bmatrix} \dot{V}_{q6} \\ \frac{\dot{V}_{q2}}{s} \\ 0 \end{bmatrix} e^{j\omega_{rs}t} = \begin{bmatrix} r_6 + jX_{s6} & 0 & jX_{m6} \\ 0 & \frac{r_2}{s} + jX_{s2} & -jX_{m2} \\ jX_{m6} & -jX_{m2} & \frac{r_r}{s_1} + jX_r \end{bmatrix} \begin{bmatrix} \dot{I}_{q6} \\ \dot{I}_{q2} \\ \dot{I}_{qr} \end{bmatrix} e^{j\omega_{rs}t} \tag{6-23}$$

In order to derive steady state equations in machine variables, frequency conversion is needed. Multiplying the above equation by $e^{j(\omega_6-\omega_{rs})t}$ and also noting that

$$\dot{V}_{q6} = \sqrt{\frac{3}{2}}\ \dot{V}_A\ ,\ \dot{V}_{q2} = \sqrt{\frac{3}{2}}\ \dot{V}_a \tag{6-24}$$

$$\dot{I}_{q6} = \sqrt{\frac{3}{2}}\ \dot{I}_A\ ,\ \dot{I}_{q2} = \sqrt{\frac{3}{2}}\ \dot{I}_a \tag{6-25}$$

after the frequency conversion, we have

$$\begin{bmatrix} \dot{V}_A \\ \frac{\dot{V}_a}{s} \\ 0 \end{bmatrix} = \begin{bmatrix} r_6 + jX_{s6} & 0 & jX_{m6} \\ 0 & \frac{r_2}{s} + jX_{s2} & -jX_{m2} \\ jX_{m6} & -jX_{m2} & \frac{r_r}{s_1} + jX_r \end{bmatrix} \begin{bmatrix} \dot{I}_A \\ \dot{I}_a \\ \dot{I}_{ar} \end{bmatrix} \tag{6-26}$$

where $\dot{I}_{ar} = \sqrt{\frac{2}{3}}\ \dot{I}_{qr}$ is the "equivalent rotor a-phase" current resulting from a linear combination of physical rotor loop currents.

It is understood that in Eqn. (6-26) all the phasor quantities have the frequency of 60Hz and (6-26) represents a per phase equivalent circuit for the synchronous mode of operation of the BDFM. With proper

modifications, (6-26) is also valid for singly-fed induction mode of operation, i.e. $\dot{V}_a = 0$ for 2-pole terminals short circuited, and $\dot{I}_a = 0$ for 2-pole terminals open circuited.

6.3 The Torque Equation in Steady State Operational Conditions

Eqn. (4-81) in Chapter 4 is the torque equation expressed in the dq domain in which all the currents are instantaneous quantities. In steady state operational conditions, these currents can be obtained by solving the steady state equations developed above and represented by the following set of sinusoidal functions

$$i_{q6} = \sqrt{2}\, I_{q6} \cos[\, (\omega_6 - 3\omega_r)\, t - \phi_{q6}\,] \tag{6-27}$$

$$i_{d6} = -\sqrt{2}\, I_{d6} \sin[\, (\omega_6 - 3\omega_r)\, t - \phi_{q6}\,] \tag{6-28}$$

$$i_{q2} = \sqrt{2}\, I_{q2} \cos[\, (\omega_2 + \omega_r)\, t - \phi_{q2}\,] \tag{6-29}$$

$$i_{d2} = \sqrt{2}\, I_{d2} \sin[\, (\omega_2 + \omega_r)\, t - \phi_{q2}\,] \tag{6-30}$$

$$i_{qr} = \sqrt{2}\, I_{qr} \cos[\, (\omega_6 - 3\omega_r)\, t - \phi_{qr}\,] \tag{6-31}$$

$$i_{dr} = -\sqrt{2}\, I_{dr} \sin[\, (\omega_6 - 3\omega_r)\, t - \phi_{qr}\,] \tag{6-32}$$

with $I_{q6} = I_{d6}$, $I_{q2} = I_{d2}$ and $I_{qr} = I_{dr}$ are the rms values of the currents and ϕ_{q6}, ϕ_{q2}, ϕ_{qr} are the phase angles of the currents with respect to the reference voltage v_{q6}.

Upon substitution of equations (6-27) through (6-32) into (4-81), the following torque equation is derived

$$T_e = T_{e6} + T_{e2} = 6M_6\, I_{q6}\, I_{qr} \sin(\phi_{qr} - \phi_{q6}) + 2M_2\, I_{q2}\, I_{qr} \sin(\phi_{qr} - \phi_{q2}) \tag{6-33}$$

Eqn. (6-33) is valid for both synchronous mode and induction mode (with 2-pole side short circuited) of operation. For induction mode with 2-pole open circuited the second term vanishes, T_e simply has a form of that a conventional 6-pole induction motor. Torque expression (6-33) and BDFM voltage equations will be used to obtain the steady state solutions in the later sections.

6.4 Steady State Model Solutions

6.4.1 The Synchronous Mode of Operation

The solutions to the steady state equations, depending on voltage or current control, motoring or generating , may be different. This thesis discusses mainly the motoring operation of the system and as an example a solution method for the voltage control scheme is given, which can be modified easily to account for a current control scheme.

In motoring operation of the system, the load torque is usually given and it can be shown that although the 6 and 2-pole input voltages are given, the angle, β, between the reference voltage $\dot{V}_{q6}$ and $\dot{V}_{q2}$ is an unknown function of both the load torque and the 2-pole excitation voltage (or current). The solution of the steady state equations characterized by (6-23) thus requires that they be solved simultaneously with the torque equation (6-33). Before these equations are solved, complex equations must be changed into real algebraic equations.

Denote

$$\dot{V}_{q6} = V_{q6r} + jV_{q6i} = V_{q6r} + j0 \tag{6-34}$$

$$\dot{V}_{q2} = V_{q2r} + jV_{q2i} = V_{q2}\cos\beta - jV_{q2}\sin\beta \tag{6–35}$$

$$\dot{I} = I_r + jI_i \tag{6-36}$$

where subscripts r and i represent real and imaginary parts of the phasor quantities, respectively.

By substitution of the above relationships into the steady state equations (6-7), (6-10) and (6-11) and separating the real parts from the imaginary parts, the following set of nonlinear simultaneous equations are obtained

$$r_6 I_{q6r} - X_{s6} I_{q6i} - X_{m6} I_{qri} - V_{q6r} = 0 \tag{6-37}$$

$$r_6 I_{q6i} + X_{s6} I_{q6r} + X_{m6} I_{qrr} = 0 \tag{6-38}$$

$$\frac{r_2}{s} I_{q2r} - X_{s2} I_{q2i} + X_{m2} I_{qri} - \frac{1}{s} V_{q2} \cos\beta = 0 \tag{6-39}$$

$$\frac{r_2}{s} I_{q2ri} + X_{s2} I_{q2r} - X_{m2} I_{qrr} + \frac{1}{s} V_{q2} \sin\beta = 0 \tag{6-40}$$

$$- X_{m6} I_{q6i} + X_{m2} I_{q2r} + \frac{r_r}{s_1} I_{qrr} - X_r I_{qri} = 0 \tag{6-41}$$

$$X_{m6} I_{q6r} - X_{m2} I_{q2i} + \frac{r_r}{s_1} I_{qri} + X_r I_{qrr} = 0 \tag{6-42}$$

$$6M_6 I_{q6} I_{qr} \sin(tg^{-1} \frac{I_{qri}}{I_{qrr}} - tg^{-1} \frac{I_{q6i}}{I_{q6r}}) + 2M_2 I_{q2} I_{qr} \sin(tg^{-1} \frac{I_{q2i}}{I_{q2r}} - tg^{-1} \frac{I_{qri}}{I_{qrr}}) - T_L(\omega_r) = 0 \tag{6-43}$$

with $I_{q6} = \sqrt{I_{q6r}^2 + I_{q6i}^2}$, $I_{q2} = \sqrt{I_{q2r}^2 + I_{q2i}^2}$ and $I_{qr} = \sqrt{I_{qrr}^2 + I_{qri}^2}$

Eqns (6-37) through (6-43) can be represented by

$$\mathbf{F(Y) = 0} \tag{6-44}$$

where $Y = [\ I_{q6r}\ I_{q6i}\ I_{q2r}\ I_{q2i}\ I_{qrr}\ I_{qri}\ \beta\ ]^t$ is the unknown vector and

$F = [\ f_1(Y)\ f_2(Y)\ f_3(Y)\ f_4(Y)\ f_5(Y)\ f_6(Y)\ f_7(Y)\ ]^t$ is the function vector containing the seven scalar functions of (6-37) through (6-43).

Solution techniques for (6-44) are readily available and it was found that Newton-Raphson's algorithm is adequate in founding the solution. Let i be the iteration index,

$$\mathbf{Y}^{(i)} = \mathbf{Y}^{(i-1)} - \Delta\mathbf{Y}^{(i-1)} \tag{6-45}$$

then
$$\Delta\mathbf{Y}^{(i-1)} = \left[\frac{\partial \mathbf{F}}{\partial \mathbf{Y}}\right]^{-1} \mathbf{F}^{(i-1)} \qquad i=1,2,...,7 \tag{6-46}$$

The entries of the Jacobian matrix, $\left[\frac{\partial \mathbf{F}}{\partial \mathbf{Y}}\right] = \left\{\frac{\partial f_{mn}}{\partial y_{mn}}\right\}$, m, n = 1,2,...7. are computed as follows:

It is noticed that four out of seven equations in (6-37) through (6-43) are linear so that the Jacobian matrix entries for these equations are just the circuit parameters themselves. Other entries of the Jacobian matrix are given below without providing intermediate results

$$\frac{\partial f_3}{\partial \beta} = \frac{1}{s} V_{q2} \sin\beta\,, \quad \frac{\partial f_4}{\partial \beta} = \frac{1}{s} V_{q2} \cos\beta$$

$$\frac{\partial f_7}{\partial I_{q6r}} = -6M_6 I_{qri}\,, \quad \frac{\partial f_7}{\partial I_{q6i}} = 6M_6 I_{qrr}\,, \quad \frac{\partial f_7}{\partial I_{q2r}} = -2M_2 I_{qri}\,, \quad \frac{\partial f_7}{\partial I_{q2i}} = 2M_2 I_{qrr}\,,$$

$$\frac{\partial f_7}{\partial I_{qrr}} = 6M_6 I_{q6i} + 2M_2 I_{q2i}\,, \quad \frac{\partial f_7}{\partial I_{qri}} = -6M_6 I_{q6r} - 2M_2 I_{q2r}$$

The initial values for the solution vector $\mathbf{Y}^{(o)}$, which have to be reasonably close to the true solution, need to be given in order to start the algorithm. To ensure good convergence to an acceptable solution, the initial estimated values can be obtained by an appropriate initial guess for $\beta^{(o)}$, followed by solutions for the other unknowns using (6-23). So long as $\beta^{(o)}$ is chosen to be close to the true solution, other initial values are also

close to the solution. It was found that that for 230V 6-pole supply voltage and moderate level of 2-pole excitation voltage, it is appropriate to assign

$$\beta^{(o)} = 20^{\circ}, \qquad \text{for } 0.5 \leq T_L \leq 10 \text{ (Nm)}$$
$$\beta^{(o)} = 60^{\circ}, \qquad \text{for } 10 < T_L \leq 20 \text{ (Nm)}$$
$$\beta^{(o)} = 90^{\circ}, \qquad \text{for } 20 < T_L \leq 30 \text{ (Nm)}$$

Depending on different 2-pole excitation voltage, the $\beta^{(o)}$ values may be adjusted so that fast convergence can be obtained.

Fig. 6-2 shows typical computational results of β angle for different values of constant load torque operation of the BDFM drive system. A constant V/Hz ratio of 5 is maintained over the entire speed range. Rapid changes of β at low 2-pole frequencies or high speeds, which contribute to the changes of circuit impedances due to slips (both s_1 and s), can be observed. At low speeds, β can be seen remain fairly constant.

6.4.2 Singly-Fed Induction Mode of Operation

The synchronous mode of operation of the BDFM is a highly preferred operational mode for ASD and VSG applications of the system. However, as pointed out in Chapters 1 and 5, with the present state converter controls it can not be realized unless a successful synchronization process has been carried out from the induction mode. Two possible singly-fed induction modes of operation exists with 2-pole terminals open and short circuited. The former case is well known while the latter needs more discussion.

Solving for the steady state equations is a straightforward process. What is of interest is the torque speed characteristics in this mode of operation. A closed form solution to T_e, which can be obtained by first solving (6-13)-(6-16) for currents then substituting them into (6-33), is tedious and

complicated thus will not be given. Numerical computation results are presented and discussed below.

A typical torque speed characteristic is given in Fig. 6-3. It is clearly seen that for a given load torque/speed characteristic, such as a constant load, there might exist two possible stable operating points. There also exists a region between two stable regions in which the motor can not operate stablely. Conventional induction motors do not possess this feature. Experimental and computer simulation results reveal, however, that it is usually easier for the motor to be synchronized if the motor is running around 900 r/min in the induction mode before synchronization begins.

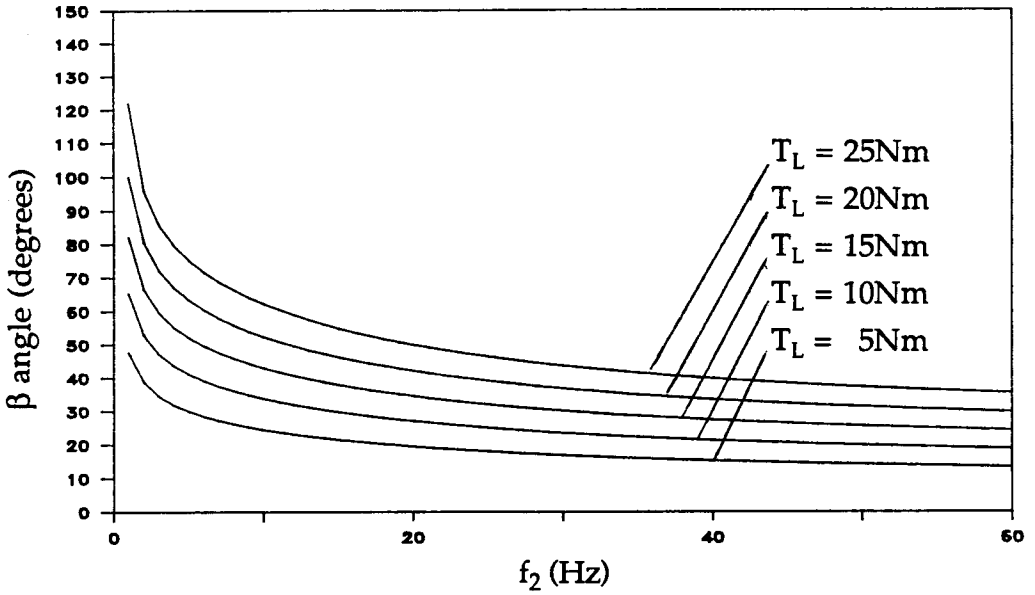

Fig. 6-2 β angle vs speed f_2 for T_L = constant and V/Hz = 5.0

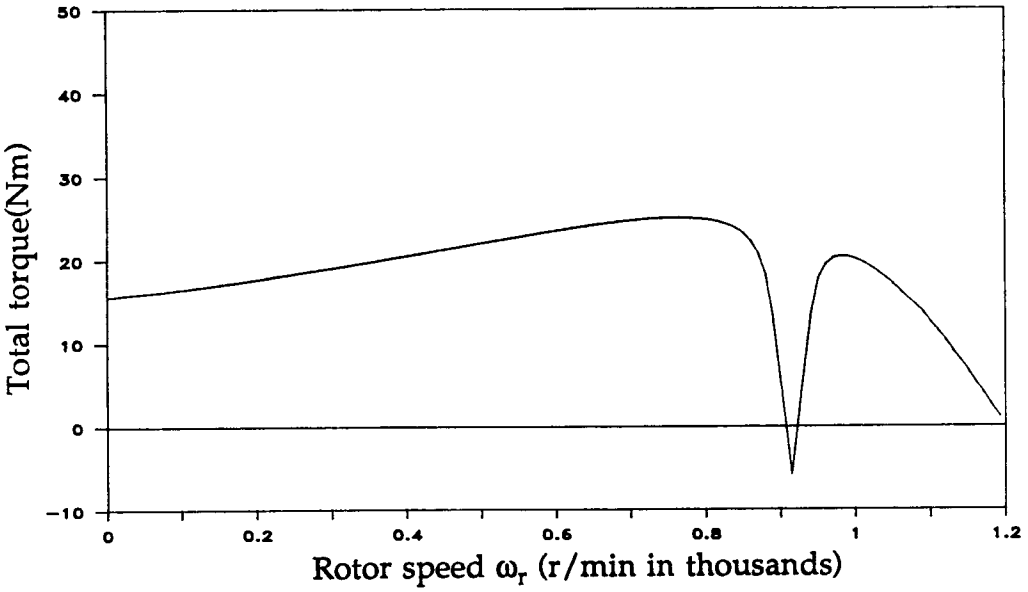

Fig. 6-3 Singly-fed induction mode torque speed characteristics

(2-pole stator system short-circuited)

7. STABILITY ANALYSIS OF THE BDFM

The primary purpose of developing a two-axis model is to analyze the dynamic behavior of the machine and to develop control strategies for specific applications of the BDFM system. In Chapter 2, the dynamic performance of the machine in synchronous mode of operation was investigated at a fixed 2-pole frequency. It was shown that for 230V 6-pole input voltage and 2Hz 2-pole excitation, although the response of the machine to sudden changes of inputs was oscillatory, stable operation could be maintained after transitions. It was found in the laboratory, however, that stability problems may arise when a wide range of speed control is required. It is hence important to investigate the stability of the machine on a wide speed range basis.

A search of appropriate literature indicates that the stability problems of this type of machine have been investigated using a two wound rotor induction machine model in cascade connection. This was necessary because of a lack of a truly representative model and its parameters for the **single-frame self-cascaded** machine. Previous studies have shown that over much of the potentially useful operating region the machine is either inherently unstable or its dynamic response is seriously underdamped. It is concluded from the studies that by appropriate design, certain areas of instability may be reduced or removed and the response improved, but that it is not possible, by design changes alone, to remove all such unstable areas. These results, however, do not seem to be in agreement with the test results found in the laboratory. Tests showed that for the 6 and 2-pole BDFM with a common stator winding and a "Broadway rotor", there existed an unstable region between roughly 630 r/min to 525 r/min (corres-

ponding to 18Hz to 25Hz for the 2-pole input frequency), which was not predicted correctly by [9,10]. For a newly designed BDFM with truly balanced stator windings [13,15] and a "Broadway rotor", open loop stability occurs over the entire speed range under proper 2-pole excitation.

In order to carry out stability and control studies in more depth in conjunction with machine and drive system design, a two-axis model derived in Chapter 4 is used to investigate the stability of the system in the synchronous mode of operation.

The stability characteristics of ASDs using either induction machines or synchronous machines have long been known [19,20]. Stability analyses of electric machines and drive systems commonly utilize Lyapunov's indirect method, in which the original nonlinear differential equations are linearized around an equilibrium point, at which the stability characteristics of the point are evaluated. The result is then applied to the original nonlinear system.

In order to use Lyapunov's indirect method, reference frames must be selected carefully so that the linearized machine or drive equations are as simple as possible. For example, the stability of an induction machine and its drive system is usually investigated in the synchronous reference frame in which all the steady state quantities (equilibrium points) are constants. This will, in turn, result in a linear time-invariant system after linearization has been carried out. For the synchronous machine and its drive system, since the rotor reference frame coincides with the synchronous reference frame in steady-state operations, the resulting linearized-machine and drive equations are also time-invariant. Unfortunately, this is not true for a BDFM system for which the two-axis model must be expressed exclusively in the rotor reference frame. In

steady state operation, all dq quantities are found to vary sinusoidally at a slip frequency, with the result that the linearized machine equations are time-varying. Consequently, commonly used eigenvalue analysis techniques cannot be applied to perform stability studies.

A closer examination of the linearized system of equations of the BDFM reveals that although the system matrix is time-varying, it is periodic. Thus, the generalized theory of Floquet can be utilized to transform the linear time-varying system of equations into an equivalent set of equations with a constant system matrix. Since the two systems are equivalent in the sense of Lyapunov, eigenvalue analysis can be performed on the Floquet transformed system to predict the stability characteristics of the original nonlinear system at a given equilibrium point.

7.1 Linerized Two-axis Model Equations

Linearized two-axis model equations are obtained using Taylor series expansion at a given equilibrium point. The results of the linearized equations are incorporated into one matrix equation as shown in (7-1).

$$\begin{bmatrix} \Delta \mathbf{v} \\ 0 \\ \Delta T_L \end{bmatrix} = [\, \mathbf{R}'(t) + \mathbf{L}p \,] \begin{bmatrix} \Delta \mathbf{i} \\ \Delta \theta_r \\ \Delta \omega_r \end{bmatrix} \tag{7-1}$$

where $\Delta \mathbf{v} = [\, \Delta v_{q6} \;\; \Delta v_{d6} \;\; \Delta v_{q2} \;\; \Delta v_{d2} \;\; 0 \;\; 0 \,]^t$

$\Delta \mathbf{i} = [\, \Delta i_{q6} \;\; \Delta i_{d6} \;\; \Delta i_{q2} \;\; \Delta i_{d2} \;\; \Delta i_{qr} \;\; \Delta i_{dr} \,]^t$

In doubly-fed operation, the two sets of applied three-phase voltages with opposite sequence, namely v_A, v_B, v_C from the 6-pole system and v_a, v_b, v_c from the 2-pole system can be transformed into two sets of orthogonal dq voltages plus the zero sequences through two

transformation matrices C_{s6} and C_{s2} . In particular, with balanced excitation,

$$v_{q6} = \sqrt{2}\, V_{q6} \cos(\omega_6 t - 3\theta_r + \phi_6) \tag{7-2}$$

$$v_{d6} = -\sqrt{2}\, V_{d6} \sin(\omega_6 t - 3\theta_r + \phi_6) \tag{7-3}$$

$$v_{q2} = \sqrt{2}\, V_{q2} \cos(\omega_2 t + \theta_r - \beta) \tag{7-4}$$

$$v_{d2} = \sqrt{2}\, V_{d2} \sin(\omega_2 t + \theta_r - \beta) \tag{7-5}$$

with $V_{q6} = V_{d6}$ and $V_{q2} = V_{d2}$ being the RMS phase voltages of the two sets of dq voltages. β is the phase angle between the reference voltage v_{q6} and v_{q2} in steady state operation.

Since the input voltages are functions of rotor angle θ_r, it follows from (7-2) to (7-5) that

$$\Delta v_{ij} = \frac{\partial v_{ij}}{\partial V_{ij}} \Delta V_{ij} + \frac{\partial v_{ij}}{\partial \omega_j} \Delta \omega_j + \frac{\partial v_{ij}}{\partial \theta_r} \Delta \theta_r$$

$$= \Delta v'_{ij} + \frac{\partial v_{ij}}{\partial \theta_r} \Delta \theta_r \qquad i = q, d \text{ and } j = 6, 2 \tag{7-6}$$

Eqn. (7-6) represents 4 equations and suggests that small increments of dq voltages are caused not only by the system inputs, V, ω, but also by the rotor angle θ_r. Moving the second term of (7-6) to the right hand side of Eqn. (7-1), and incorporating the four terms with the $\mathbf{R}'(t)$ matrix, we obtain the linearized BDFM equation as shown in (7-7), where a subscript o stands for an equilibrium point under steady state operating conditions.

In the state variable form, (7-7) becomes

$$\dot{\mathbf{X}} = \mathbf{A}(t)\mathbf{X} + \mathbf{B}\mathbf{U} \tag{7-8}$$

where $\mathbf{X} = [\, \Delta i_{q6} \;\; \Delta i_{d6} \;\; \Delta i_{q2} \;\; \Delta i_{d2} \;\; \Delta i_{qr} \;\; \Delta i_{dr} \;\; \Delta \theta_r \;\; \Delta \omega_r \,]^t$

$$
\begin{bmatrix} \Delta v'_{q6} \\ \Delta v'_{d6} \\ \Delta v'_{q2} \\ \Delta v'_{d2} \\ 0 \\ 0 \\ 0 \\ \Delta T_L \end{bmatrix} = \begin{bmatrix} r_6+L_{s6}p & 3L_{s6}\omega_{ro} & 0 & 0 & M_6p & 3M_6\omega_{ro} & -3V_{q6p}\sin[(\omega_6-3\omega_{ro})t+\phi_6] & 3(L_{s6}i_{d6o}+M_6i_{dro}) \\ -3L_{s6}\omega_{ro} & r_6+L_{s6}p & 0 & 0 & -3M_6\omega_{ro} & M_6p & -3V_{d6p}\cos[(\omega_6-3\omega_{ro})t+\phi_6] & -3(L_{s6}i_{q6o}+M_6i_{qro}) \\ 0 & 0 & r_2+L_{s2}p & L_{s2}\omega_{ro} & -M_2p & M_2\omega_{ro} & V_{q2p}\sin[(\omega_2+\omega_{ro})t-\beta_o] & (L_{s2}i_{d2o}+M_2i_{dro}) \\ 0 & 0 & -L_{s2}\omega_{ro} & r_2+L_{s2}p & M_2\omega_{ro} & M_2p & -V_{d2p}\cos[(\omega_2+\omega_{ro})t-\beta_o] & (-L_{s2}i_{q2o}+M_2i_{qro}) \\ M_6p & 0 & -M_2p & 0 & r_r+L_rp & 0 & 0 & 0 \\ 0 & M_6p & 0 & M_2p & 0 & r_r+L_rp & 0 & 0 \\ 0 & 0 & 0 & 0 & 0 & 0 & p & -1 \\ 3M_6i_{dro} & -3M_6i_{qro} & M_2i_{dro} & M_2i_{qro} & M_2i_{d2o}-3M_6i_{d6o} & M_2i_{q2o}+3M_6i_{q6o} & 0 & -Jp \end{bmatrix} \begin{bmatrix} \Delta i_{q6} \\ \Delta i_{d6} \\ \Delta i_{q2} \\ \Delta i_{d2} \\ \Delta i_{qr} \\ \Delta i_{dr} \\ \Delta\theta_r \\ \Delta\omega_r \end{bmatrix}
$$

(7-7)

$$\mathbf{U} = [\, \Delta v'_{q6} \;\; \Delta v'_{d6} \;\; \Delta v'_{q2} \;\; \Delta v'_{d2} \;\; 0 \;\; 0 \;\; 0 \;\; \Delta T_L \,]^t$$

$$\mathbf{A}(t) = -\mathbf{L}^{-1}\mathbf{R}(t), \quad \mathbf{B} = \mathbf{L}^{-1}$$

The **L** matrix contains the inductive parameters of the derivative terms of (7-7) while **R**(t) is composed of the rest of the entries of (7-7).

Eqn. (7-8) describes fully the small signal characteristics of the BDFM system at a given operating condition. It is an 8th order set of linear time-varying differential equations with periodic coefficients, i.e.

$$\mathbf{A}(t+T) = \mathbf{A}(t) \tag{7-9}$$

where T is the period of the sinusoidal quantities in matrix **R**(t).

7.2 Determination of Equilibrium Points

The equilibrium points used to linearize Eqn. (4-61) are obtained by solving the set of steady state equations which are developed in Chapter 6. In the synchronous mode steady state operation with ac excitation on the 2-pole terminals, the equilibrium points are found to vary sinusoidally with frequencies equal to the sum of, or the difference between, the supply frequencies f_2, f_6 and rotor frequency.

$$f_{rs} = f_2 + f_r = f_6 - 3f_r \tag{7-10}$$

Solution techniques for solving the steady state equations of the BDFM in motoring mode of operation have been presented in Chapter 6 and the results of the computation can be utilized directly in stability analysis.

7.3 . The Generalized Theory of Floquet and Computer Implementation

According to the generalized theory of Floquet [24,25], if

$$\dot{\mathbf{X}} = \mathbf{A}(t)\mathbf{X} + \mathbf{B}\mathbf{U} \qquad \text{with } \mathbf{A}(t+T) = \mathbf{A}(t) \tag{7-11}$$

then there exists a linear transformation matrix $\mathbf{P}(t)$ defined by

$$\mathbf{P}(t) = e^{\bar{\mathbf{A}}T}\,\psi^{-1}(t) \tag{7-12}$$

such that Eqn. (16) can be transformed into

$$\dot{\bar{\mathbf{X}}} = \bar{\mathbf{A}}\,\bar{\mathbf{X}} + \mathbf{P}(t)\mathbf{B}\mathbf{U} \tag{7-13}$$

and it is equivalent, in the sense of Lyapunov, to (7-11). In addition,

$$\psi(t+T) = \psi(t)\,\mathbf{Q} = \psi(t)\,e^{\bar{\mathbf{A}}T} \tag{7-14}$$

is true for all $0 \leq t < \infty$, where $\psi(t)$ is a fundamental matrix of (7-11) and $\bar{\mathbf{A}}$ is the corresponding equivalent constant system matrix.

In the above transformation, the new set of state variables, $\bar{\mathbf{X}}$, and the transformed set of state variables, $\mathbf{X}$, are related by

$$\bar{\mathbf{X}} = \mathbf{P}(t)\,\mathbf{X} \tag{7-15}$$

The significance of the Floquet theory lies in the fact that it relates a linear time-varying system with a periodic system matrix $\mathbf{A}(t)$ with another equivalent linear system with a constant system matrix $\bar{\mathbf{A}}$ in terms of stability. Since $\bar{\mathbf{A}}$ is constant, eigenvalue analysis can be performed to investigate the stability characteristics of the original system. In practice, the fundamental matrix $\psi(t)$ of (7-11) cannot, in general, be determined analytically, nor can the equivalent system. However, the problem can be solved numerically, which is explained as follows.

From (7-14), it follows that

$$\mathbf{Q} = \psi^{-1}(t)\,\psi(t+T) = e^{\bar{\mathbf{A}}T} \tag{7-16}$$

this operation is possible since $\psi(t)$ spans dimension of n, thus $\psi^{-1}(t)$ exists for all $0 \leq t < \infty$. Let t = T, thus

$$Q = \psi^{-1}(T)\,\psi(2T) \tag{7-17}$$

Computation of $\psi(t)$ can be performed in the following way;

Define $$\psi(t) = [\,\psi_{i1}(t)\ \psi_{i2}(t)\ \psi_{i3}(t) \ldots \psi_{in}(t)\,] \quad i=1, \ldots n \tag{7-18}$$

where $\psi_{i1}(t)$, $\psi_{i2}(t)$, $\psi_{i3}(t)$ and $\psi_{in}(t)$ represent each column of $\psi(t)$.

Thus, $\psi_{in}(t)$ can be obtained by numerically integrating the homogeneous part of Eqn. (7-16) for a set of given initial conditions. As long as n sets of initial conditions are selected to be linearly independent, the resultant n columns of $\psi(t)$ are also linearly independent. Consequently, $\psi(t)$ is qualified for being a fundamental matrix. It can be shown that other fundamental matrices are linear combinations of $\psi(t)$. The n sets of initial conditions can simply be taken as

$$E_i(0) = \begin{bmatrix} 0 \\ 0 \\ 0 \\ 0 \\ \cdot \\ \cdot \\ 0 \\ 1 \\ 0 \\ 0 \\ \cdot \\ \cdot \\ \cdot \\ 0 \\ 0 \end{bmatrix} \rightarrow \text{ith row, } i = 1, 2, \ldots n \tag{7-19}$$

After the **Q** matrix is found from (7-22), stability analysis can be performed. For the system characterized by Eqn. (7-18), there exists a similarity transformation matrix **K** such that

$$\Lambda = K \bar{A} K^{-1} \tag{7–20}$$

where Λ is a diagonal matrix whose elements are the eigenvalues of $\bar{A}$. Matrix **K** is composed of eigenvectors of $\bar{A}$.

The solution of the homogeneous part of Eqn. (7-12) is

$$\bar{X}(t) = K e^{\Lambda t} K^{-1} \bar{X}(0) = e^{\bar{A}t} \bar{X}(0) \tag{7-21}$$

therefore,

$$\bar{X}(T) = K^{-1} e^{\Lambda T} K \bar{X}(0) = e^{\bar{A}T} \bar{X}(0) = Q \bar{X}(0) \tag{7-22}$$

and $$e^{\Lambda T} = K^{-1} Q K = \text{diag}(\sigma_1, \sigma_2, \sigma_3, \ldots, \sigma_n) \tag{7–23}$$

where $\sigma_1, \sigma_2, \sigma_3, \ldots, \sigma_n$ are the eigenvalues of the **Q** matrix.

The above expression indicates that matrix **K** can also be used to diagonalize the **Q** matrix, in other words, eigenvectors of $\bar{A}$ and eigenvectors of **Q** are the same.

Define $$\Lambda = \text{diag}(\lambda_1, \lambda_2, \lambda_3, \ldots, \lambda_n) \tag{7-24}$$

from $$e^{\Lambda T} = \text{diag}(e^{\lambda_1 T}, e^{\lambda_2 T}, e^{\lambda_3 T}, \ldots, e^{\lambda_n T})$$

$$= \text{diag}(\sigma_1, \sigma_2, \sigma_3, \ldots, \sigma_n) \tag{7–25}$$

we obtain $$e^{\lambda_i T} = \sigma_i \qquad i = 1, 2, \ldots n \tag{7-26}$$

Eqn. (7-26) suggests a conformal mapping from one complex plane to another. If all the eigenvalues of $\bar{A}$ are on the left half of W plane, all the

eigenvalues of **Q** will fall into a unit circle on the Z plane, where $\lambda_i \in W$ and $\sigma_i \in Z$, i = 1, 2, . . . , n. After all the eigenvalues of **Q** have been computed, eigenvalues of the $\bar{\mathbf{A}}$ matrix can be obtained. From (7-26), it follows that

$$\lambda_i = \frac{1}{T}[\ln|\sigma_i| + j\,tg^{-1}(\sigma_i)] \qquad i = 1, 2, \ldots n \tag{7-27}$$

Computation of the $\bar{\mathbf{A}}$ matrix, if required, is performed using Eqn. (7-20)

$$\bar{\mathbf{A}} = \mathbf{K}^{-1}\Lambda\,\mathbf{K} \tag{7-28}$$

where the similarity transformation matrix **K** is composed of eigenvectors of the **Q** matrix (or the $\bar{\mathbf{A}}$ matrix).

The flow chart shown in Fig. 7-1 summarizes the computational algorithm for digital implementation of the theory of Floquet .

7. 4 Computation Results

Case studies are given in this section to show the effectiveness of the method. It is assumed that the drive system is running synchronously with or without load torque. The shaft speed of the drive in this mode of operation is determined by the following expression

$$\text{shaft speed(r/min)} = 60\,\frac{f_6 - f_2}{P_6 + P_2} \tag{7-29}$$

hence, when f_2 is changed from 1Hz to 60Hz, the shaft speed varies from 885 r/min to standstill. The rotor slip frequency, defined by (6-22), will, in turn, alter from 15.75Hz to 60Hz. This change of rotor slip frequency can be shown to cause substantial increase in the rotor resistance due to skin effect. In the computation process, this has been taken into consideration. The change of rotor resistance with rotor slip frequency is modeled as a

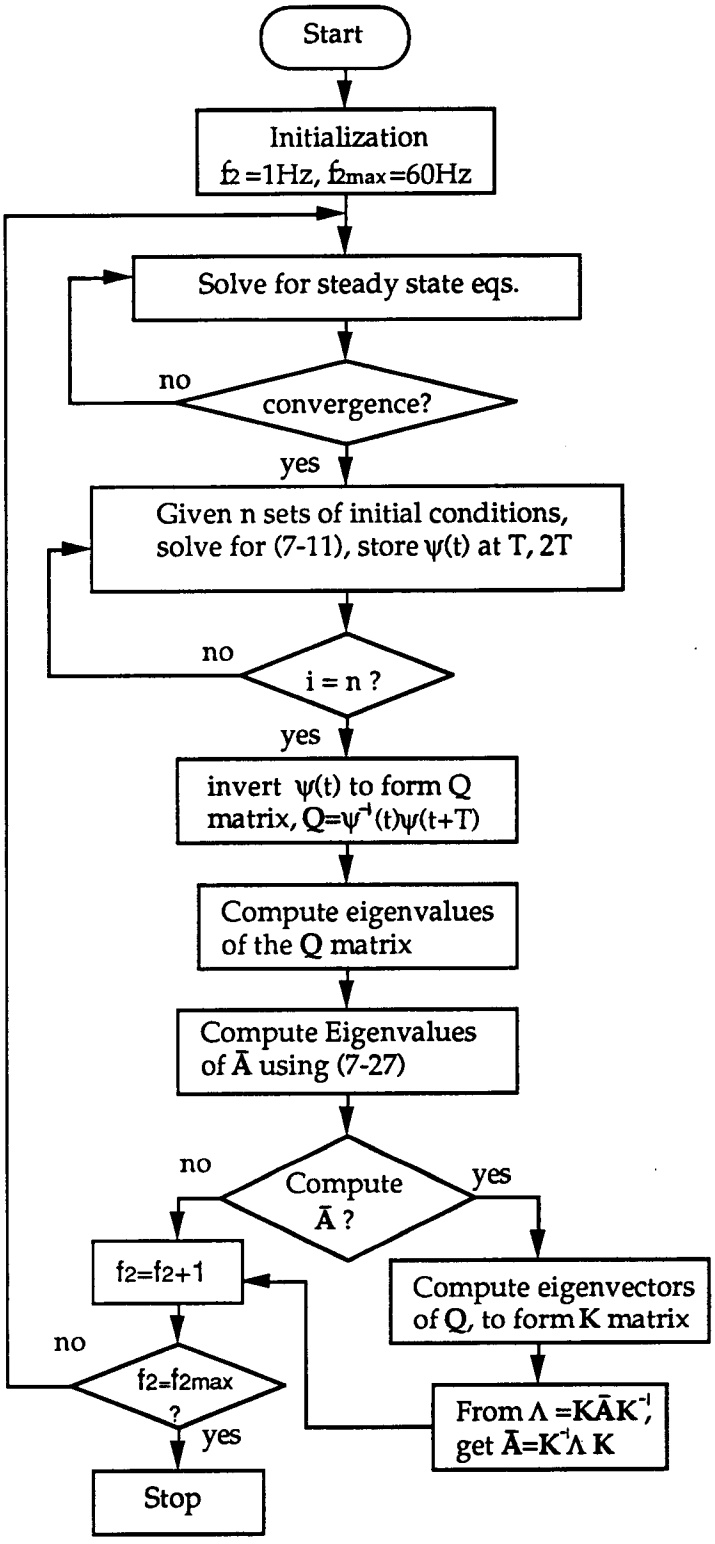

Fig. 7-1 Computer implementation of the theory of Floquet

linear function. The slope of the straight line is determined such that at 60Hz the rotor resistance is 2 to 3 times higher than that at dc at which the value of the rotor resistance is computed.

Stability characteristics of the BDFM system at any operating point are evaluated by examination of the eigenvalues of the $\bar{\mathbf{A}}$ matrix. In doing that, the power converter frequency, f_2 , is varied from 1Hz to 60Hz and the computed real parts of the dominant eigenvalues of the $\bar{\mathbf{A}}$ matrix are plotted as functions of the converter output frequency. The 2-pole voltage and frequency is increased in such a way that a constant V/Hz ratio is maintained. In addition, the load torque is kept constant.

Over most of the operating range, the eigenvalues comprise four complex conjugate pairs, each of which corresponds to a particular system (namely the 6-pole stator, 2-pole stator, the rotor and the mechanical systems). No repeated eigenvalues are expected from practical considerations. Fig. 2(a) and (b) show the typical computational results for no load conditions in which the real parts of the two critical eigenvalues are plotted. The third and the fourth ones are not shown since they are always large and negative. Similar eigenvalue characteristics have been obtained for different V/Hz ratios and loads. It should be pointed out that at high V/Hz ratios and loading conditions, eigenvalue analysis predicts that one eigenvalue approaches zero and becomes slightly positive at high 2-pole frequency (or low rotor speed). Tests show, however, that no unstable region exists at low speeds. The discrepancy is due to the difference between the calculated parameters and the actual parameters which change with operating conditions. Also, iron loss and other possible losses were not considered in the calculation.

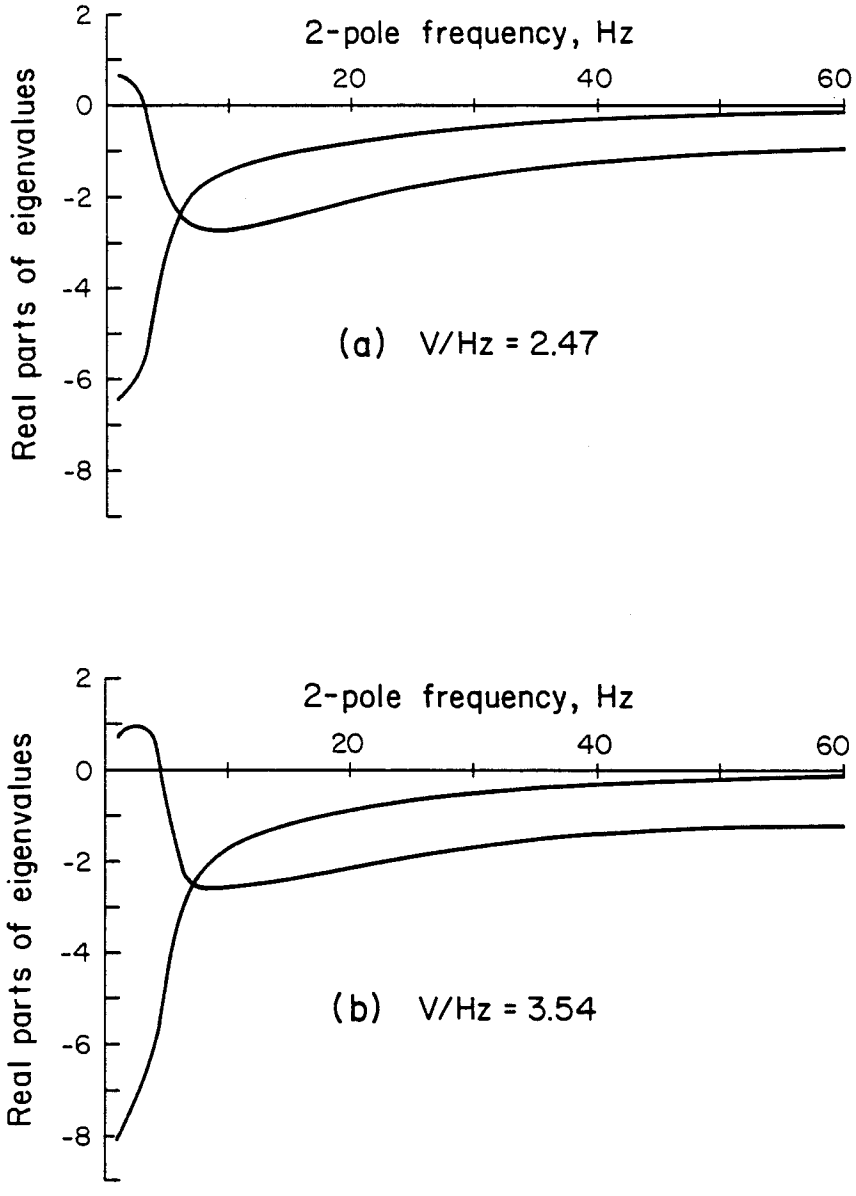

Fig. 7-2 Real parts of dominate eigenvalues vs 2-pole excitation frequency f_2

Fig. 7-3(a) shows the experimental data of 2-pole excitation currents vs f_2 for stable operation of the system for no load and 50% rated load torque. The corresponding V/Hz ratio vs f_2 is plotted in Fig. 7-3(b). As would be expected, the required 2-pole excitation current must be adjusted in order to maintain synchronous operation when load torque is increased. These

adjustments result in a decrease in the stable region. Compared with Fig. 7-2, it is seen that the eigenvalue analysis on the transformed linearized system gives good results in predicting stable operation of the BDFM. For frequencies greater than 5 Hz, a constant V/Hz control will ensure stability, and at low 2-pole frequencies, a dc offset needs to be incorporated to over-

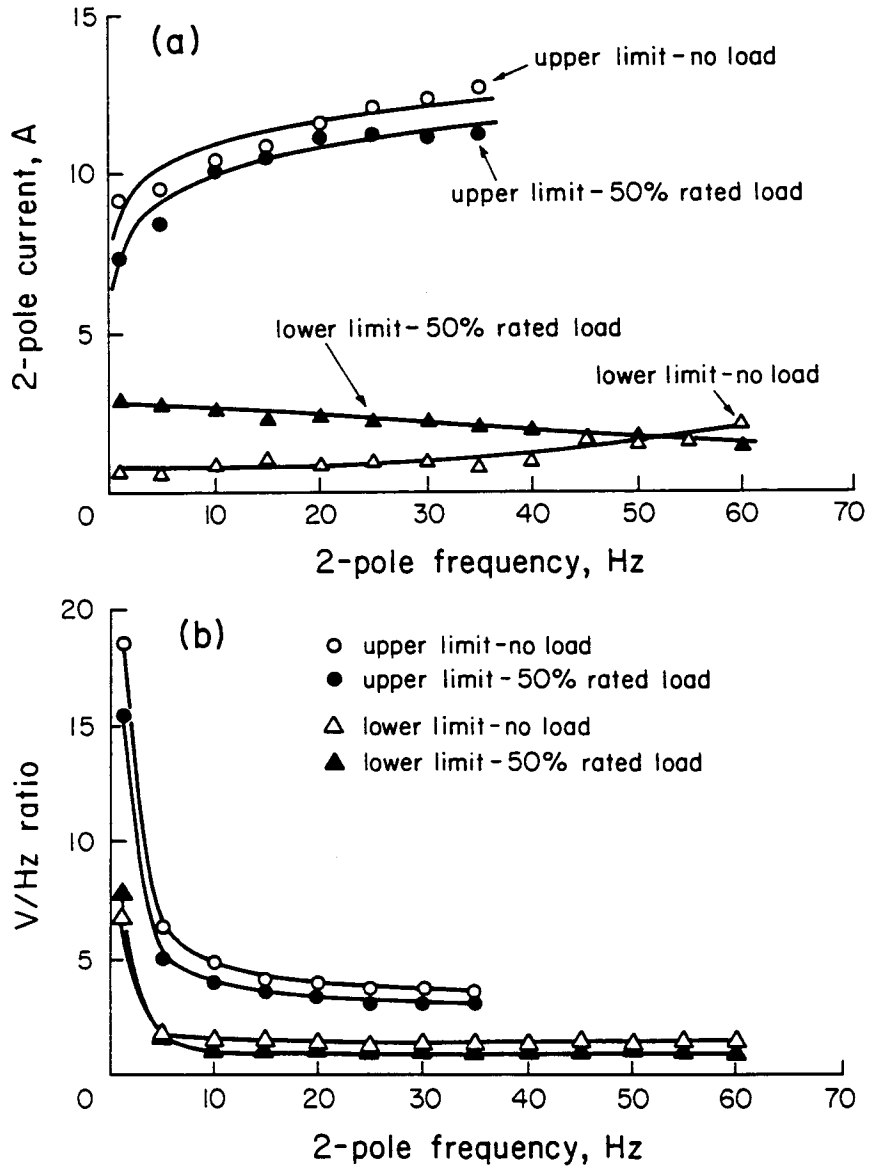

Fig. 7-3 Experimental stability envelopes

(a) Current control (b) Voltage control

come a resistive dominated low frequency impedance in order to push the eigenvalues into the left half of the complex plane and thus to provide open-loop stability. It is seen that these considerations are equivalent to scalar control of conventional induction motor drives. Thus, existing controllers can easily be adapted to interface with BDFM drives.

It should be noted that the eigenvalue analysis presented above considers only whether stable operation can be maintained for a given V/Hz ratio, or 2-pole excitation current. From a steady state operation point of view, efficiency, power factor and other aspects must also be taken into account. The converter control algorithms should be such that while maintaining stable operation of the drive system, at least one of the steady state performance parameters should be maximized. It was found in the laboratory and computer simulation that 2-pole excitation (voltage or current) has profound effects on power factor of the system. Fig. 7-4(a) and (b) show experimentally how 2-pole excitation voltage affects the 6-pole current and power factor of the drive for f_2=1Hz under no-load conditions. Similar plots can be drawn for other 2-pole frequencies and various loading conditions. It can be seen from Fig. 7-4 that control of power factor can be made by adjusting the 2-pole excitation voltage or current. Increasing excitation can result in a leading power factor operation. However, there exists a practical maximum beyond which the phase angle is seen to decrease. From the consideration of economic operation under a power factor control constraint, it is appropriate to keep the excitation voltage (or current) within a certain range. This is desirable since reducing the 2-pole voltage means reducing the converter KVA requirement and thus the cost of the system. In addition, the machine tends to be overexcited with high

2-pole current so that torques produced by the two systems (6 and 2-pole) can strongly oppose each other. In this way, the efficiency of the overall system becomes low.

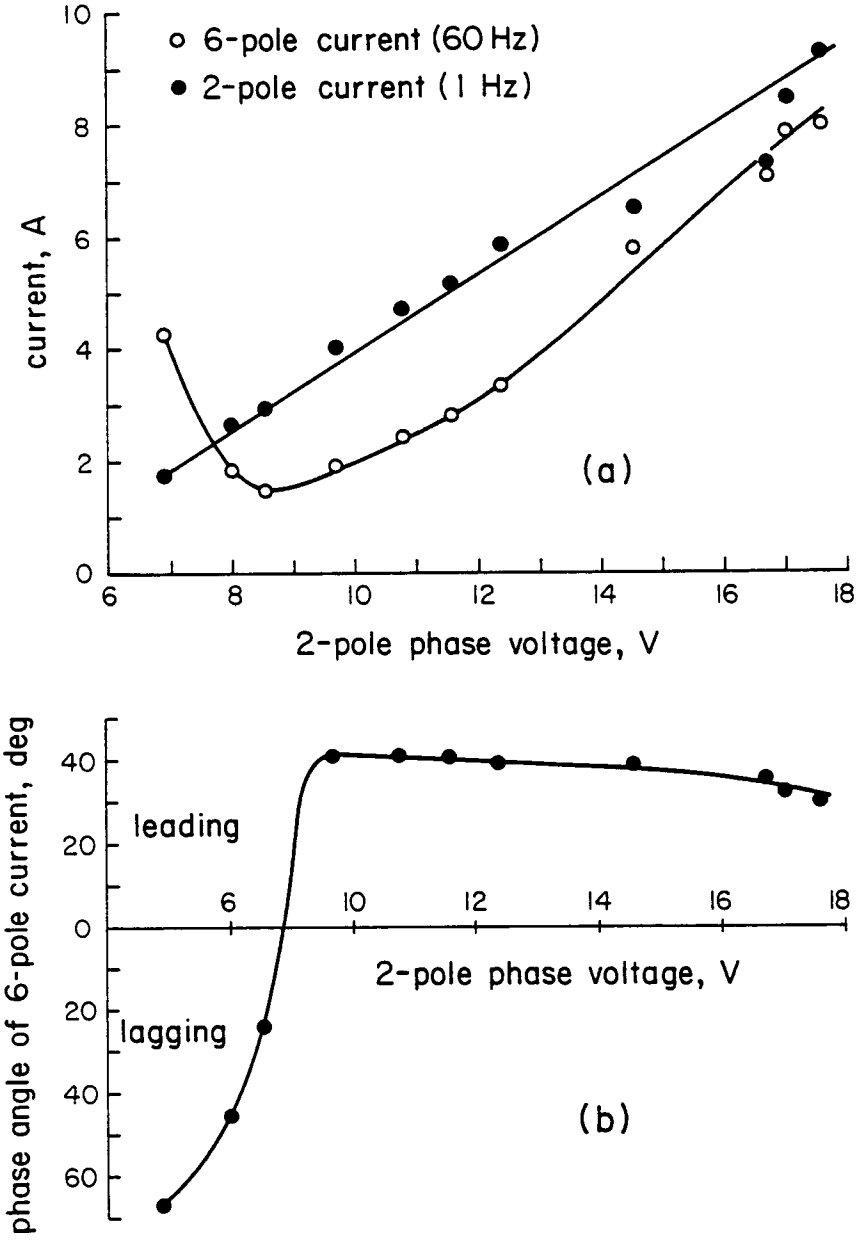

Fig. 7-4 Steady state operational characteristics

(a) 6-pole and 2-pole line currents vs 2-pole excitation voltage

(b) 6-pole phase angle vs 2-pole excitation voltage

8. SUMMARY, CONCLUSION AND FUTURE WORK

8.1 Summary and Conclusion

The primary objective of this research work was to develop a rigorous two-axis model and its parameters for dynamic simulation, stability and control studies. In summary, the following have been accomplished.

Starting from a detailed machine design model, which represents a 6- and 2-pole BDFM with a common stator winding and a castable rotor, we have developed a two-axis model. Methods for calculating the model parameters in both machine and dq domains are also developed.

Dynamic simulation for different modes of operation has been performed and correlated with available test data. Simulations include machine run-up, synchronization dynamics, synchronous behavior as well as fault tolerant behavior of the machine.

The constraints of specific operating conditions make necessary the rigorous development of steady state models from the d-q representation which have been utilized for steady state performance analysis of the machine. The models, although derived from simplified assumptions, strive to capture the essence of the operating characteristics of the machine while maintaining simple computational requirements and are found to be valuable for machine design and other analysis purposes as well.

A new method for analyzing the stability of the BDFM is developed by introduction of the theory of Floquet. This was found necessary because of the time-varying nature of the linearized two-axis model equations. Using the theory of Floquet allows the eigenvalue analysis technique to be applied to the stability studies of the BDFM.

It is concluded from the studies that the proposed two-axis model is a valid representation of the BDFM and possesses the following advantages

(1) The resistive and inductive parameters can be determined from the machine geometries and the rules of the transformations;

(2) No approximations, such as assumed equivalences to two interconnected machines, reduce the validity of the predictions obtained from the model;

(3) When compared with more detailed models, the reduced order of the two-axis model allows its application to general stability and control studies;

(4) The model is complete valid for all conceivable operating conditions including

   (a) Singly-fed induction mode dynamics

   (b) Singly-fed induction mode steady-state characteristics

   (c) Doubly-fed synchronous dynamics

   (d) Doubly-fed synchronous steady-state characteristics

   (e) Doubly-fed asynchronous dynamics

   (f) Doubly-fed asynchronous steady-state characteristics

   over complete ranges of speed and frequency (including dc excitation) and for all connection sequences.

Dynamic performance simulation illustrates the following characteristics of a BDFM in adjustable speed drives and variable speed generation systems

(1) Dynamic synchronization from induction mode;

(2) Synchronous operation without a speed feedback signal;

(3) Maintenance of synchronism for both positive and negative step changes of load torque;

(4) Continued operation after converter failure (reverting to induction mode).

These features can be realized while maintaining robust and inexpensive construction similar to induction motors whist utilizing a power converter whose rating is only a fraction of machine rating.

Stability study presented in this thesis shows that Lyapunov's indirect method can be applied to analyze the stability characteristics of the BDFM since a linear transformation matrix $\mathbf{P}(t)$ always exists such that the linearized time-varying system of equations of the BDFM can be transformed into an equivalent system of equations with a constant system matrix using the generalized theory of Floquet. Both theoretical and experimental results show that stable speed control of a BDFM system can be obtained by control algorithms similar to those for a conventional induction machine. Constant converter current or constant V/Hz ratio with an initial low frequency off-set results in open loop stability over the entire speed range. Within these stable ranges, the converter control algorithms can be developed in such a way as to produce desirable operational conditions for efficiency and power factor.

8.2 Recommended Future Work

The results reported in this thesis reflect the evolution of the two-axis model, model verification against experimental data and initial utilization of the model for stability studies as well as the exploration on converter

control algorithms for stable steady state operation of the system. It is recommended that future work include the following

(1) More accurate d-q modeling of the BDFM to account for saturation;
(2) More detailed investigation of the machine dynamics including the super-synchronous operation of the BDFM system;
(3) Detailed studies of the steady state performance of the machine using the steady state models and the solution techniques developed in this thesis. The investigation should take iron losses and possibly saturation into account in order to obtain high accuracy of prediction;
(4) Establishment of control strategies for both dynamic and steady state operation of the BDFM;
(5) Investigation of system controller design and implementation to improve both dynamic and steady state performances;
(6) Development of a generalized two-axis model to account for different pole number combinations of the BDFM.

The above activities can be accomplished using the existing simulation programs already developed for the purpose of this research. It should be emphasized that recent development of a simulation program with graphics capabilities will certainly help enhance investigation into the above areas that need to be addressed in the future.

NOMENCLATURE

VARIABLES:

v_{gi}, i_{gi}	Coil group voltage and current , i=1, 2, . . ., 9
v_{AN}, v_{BN}, v_{CN}	6- pole stator phase voltages
i_A, i_B, i_C	6-pole stator phase currents
$\mathbf{v}_{s6}$, $\mathbf{i}_{s6}$	6-pole stator phase voltage or current vectors
v_{an}, v_{bn}, v_{cn}	2-pole stator phase voltages
i_a, i_b, i_c	2 pole stator phase currents
$\mathbf{v}_{s2}$, $\mathbf{i}_{s2}$	2-pole stator phase voltage current vectors
$\mathbf{V}_r$, $\mathbf{i}_r$	Rotor loop voltage or current vector
$\mathbf{V}_{r6}, \mathbf{V}_{r2}$, $\mathbf{i}_{r6}$, $\mathbf{i}_{r2}$	6-pole or 2-pole rotor loop voltages or currents
$\xi_{q6}, \xi_{d6}, \xi_{o6}$	6-pole qdo variables such as voltages, currents, flux linkages
$\xi_{q2}, \xi_{d2}, \xi_{o2}$	2-pole qdo variables
ξ_{qr} , ξ_{dr}	Rotor qd variables
θ_r	Rotor angle displacement in mechanical degrees
ω_r	Rotor speed in mechanical rad/second
T_{e6}	6-pole electromagnetic torque
T_{e2}	2-pole electromagnetic torque
T_e , T_L	Total torque $T_e = T_{e6} + T_{e2}$ and load torque
f_2	2-pole source frequency
f_{r6}, f_{r2}	Rotor current frequencies due to 6- or 2-pole stator fields
f_{rs}	6-pole rotor slip frequency
ω_2	2-pole excitation source frequency
Δx	Small increment of a variable

V_2	2-pole peak phase voltage, a function of f_2
V_{q2p}, V_{d2p}	dq 2-pole peak phase voltage,
p	Differentiation operator $p = \frac{d}{dt}$
s_1	6-pole to rotor slip
s_2	2-pole to rotor slip
s	Total slip $s=s_1 s_2$
β	Phase angle between V_{q6} and V_{q2}

TRANSFORMATION MATRICES:

$\mathbf{C}_1$	Coil group connection matrix
$\mathbf{C}_g$	Generalized orthogonal transformation matrix
$\mathbf{C}_T$	Overall transformation matrix
$\mathbf{C}_{s6}$	6-pole stator transformation matrix
$\mathbf{C}_{s2}$	2-pole stator transformation matrix
$\mathbf{C}_s$	Stator transformation matrix, $\mathbf{C}_s = \text{diag}(\mathbf{C}_{s6} , \mathbf{C}_{s2})$
$\mathbf{C}_{r6}$	6-pole rotor transformation matrix
$\mathbf{C}_{r2}$	2-pole rotor transformation matrix
$\mathbf{C}_r$	Rotor transformation matrix, $\mathbf{C}_r = \text{diag}(\mathbf{C}_{r6} , \mathbf{C}_{r2})$
$\mathbf{C}_{r6i}$	Submatrices of C_{r6} , i=Z,Y,X,W,V,U
$\mathbf{C}_{r2i}$	Submatrices of C_{r2} , i=Z,Y,X,W,V,U

PARAMETER MATRICES (IN BOLD):

$\mathbf{Z}_s$	Stator impedance matrix $\mathbf{Z}_s=\text{diag}(\mathbf{Z}_{s6} , \mathbf{Z}_{s2})$
$\mathbf{Z}_{s6}=r_6+L_{s6}p$	6-pole stator impedance matrix
$\mathbf{Z}_{s2}=r_2+L_{s2}p$	2-pole stator impedance matrix
$\mathbf{Z}_{s6r}$	6-pole stator to rotor loop mutual impedance matrix
$\mathbf{Z}_{s2r}$	2-pole stator to rotor loop mutual impedance matrix

$\mathbf{Z_r}=r_r+L_rp$	24x24 rotor loop impedance matrix
$\mathbf{Z_{ij}}$	Submatrices of $\mathbf{Z_r}$
$\mathbf{L_{s6ri}}$	6-pole stator to rotor "ith" loop mutual inductance matrix, i=Z,Y,X,W,V,U
$\mathbf{L_{s2ri}}$	2-pole stator to rotor "ith" loop mutual inductance matrix, i=Z,Y,X,W,V,U

SCALAR PARAMETERS (NOT IN BOLD):

r_6	6-pole stator phase resistance
r_2	2-pole stator phase resistance
r_r	Rotor resistance in the dq domain
L_A	6-pole per phase inductance
L_a	2-pole per phase inductance
L_{6m}	6-pole dq domain magnetizing inductance
L_{2m}	2-pole dq domain magnetizing inductance
L_{rm}	Rotor dq domain magnetizing inductance
L_{l6}	6-pole phase leakage inductance
L_{l2}	2-pole phase leakage inductance
L_{lr}	Rotor phase leakage inductance
L_{s6}	dq domain phase inductance, $L_{s6}= L_{6m} + L_{l6}$
L_{s2}	dq domain phase inductance, $L_{s2}= L_{2m} + L_{l2}$
L_r	Rotor inductance $L_r = L_{rm} + L_{lr}$
M	6-pole mutual inductance among ABC phases
M'	2-pole mutual inductance among abc phases
M_6	dq domain 6-pole stator to rotor mutual inductance
M_2	dq domain 2-pole stator to rotor mutual inductance

M_{s6ri}	Peak value of the fundamental component of the 6-pole phase and rotor "ith" loop mutual inductance
$M_{cg}(\theta_r)$	Coil group rotor loop mutual inductance
M_{s2ri}	Peak value of the fundamental component of the 6-pole phase and rotor "ith" loop mutual inductance
$M_{A-i}(3\theta_r)$	Mutual inductance between 6-pole A-phase and rotor loop i, i=Z,Y,X,W,V,U
$M_{a-i}(\theta_r)$	Mutual inductance between 2-pole a-phase and rotor loop i, i=Z,Y,X,W,V,U
$M_{j-i}(\theta_r)$	Mutual inductance between coil group j and rotor loop i, j=1,2,...9, i=Z,Y,X,W,V,U
$r_g+L_g p$	Coil group impedance
M_{mn}	Mutual inductance between coil groups m and n, m, n=1,2,. . 9
r_{ii} , r_{ij}	Rotor loop or common end ring resistances, i, j = Z,Y,X,W,V,U
L_{ii}	Rotor loop self inductance , i = Z,Y,X,W,V,U
M_{ii}	Mutual inductance between similar rotor loops in other nests, i, j = Z,Y,X,W,V,U
M_{ij}	Mutual inductance between rotor loops in the same nests, i, j = Z,Y,X,W,V,U
M'_{ij}	Mutual inductance between different rotor loops of different nests, i, j = Z,Y,X,W,V,U
f_6	6-pole source frequency
P_6 , P_2	Pole pair numbers of the 6 and 2-pole stator systems
ϕ_6	initial angle of 6-pole reference voltage V_{q6}
V_6	6-pole peak phase voltage
V_{q6p} , V_{d6p}	dq domain 6-pole peak phase voltage

BIBLIOGRAPHY

[1] H. K. Lauw, "Characteristics and Analysis of the Brushless Doubly-Fed Machines," Report for the Bonneville Power Administration, Contract No, 79-85BP24332-Mod4, June 1989.

[2] A. K. Wallace, R. Spee and H. K. Lauw, "The Potential of Brushless Doubly-Fed Machines for Adjustable Speed Drives," Conf. Record, *IEEE IAS Pulp and Paper Induction Conference*, 1990, pp. 45-50.

[3] A. R. Broadway and L. Burbridge, "Self-Cascaded Machine: A Low Speed Motor or High-Frequency Brushless Alternator," *IEE Proc.*, 1970, 117(7), pp. 1277-1290.

[4] L. J. Hunt, "A New Type of Induction Motor," *J. IEE*, 1907, 39, pp. 648-667.

[5] F. Creedy "Some Development in Multi-Speed Cascade Induction Motors," ibid., 1921, 59, pp. 511-532.

[6] B. H. Smith, "Synchronous Behavior of Doubly-Fed Twin Stator Induction Machine," *IEEE Trans. PAS*, Vol. PAS-88, October 1967, pp. 1227-1236.

[7] A. Kusko and C. B. Somuah, "Speed Control of a Single Frame Cascade Induction Motor with Slip-Power Pump Back, "*IEEE Trans. on IAS*, Vol, IA-14, No. 2, pp. 97-105, May/April 1978.

[8] F. Shibata and K. Taka, "Speed Control System for Brushless Cascade Induction Motors in Control Range of $s_1>1$ and $s_2>1$,"*IEEE PES Winter Meeting 1986*, paper 86WM 226-5.

[9] C. D. Cook and B. H. Smith, "Stability and Stabilization of Doubly-Fed Single-Frame Induction Machines," *IEE Proc.*, 1979, 126(11), pp. 1168-1174.

[10] C. D. Cook and B. H. Smith, "Effects of Machine Parameter Values on Dynamic Response and Stability Regions of Doubly-Fed Cascade Induction Machines," *IEE Proc.*, March 1983, Vol. 130, Pt. B, No. 2, PP. 137-142.

[11] A. K. Wallace, R. Spee and H. K. Lauw, "Dynamic Modeling of Brushless Doubly-Fed Machines," *IEEE Industry Application Society Annual Meeting 1989*, San Diego.

[12] R. Spee, A. K. Wallace and H. K. Lauw, "Simulation of Brushless Doubly-Fed Adjustable Speed Drives," *IEEE Industry Application Society Annual Meeting 1989*, San Diego.

[13] P. Rochelle, R. Spee and A. K. Wallace, "The Effect of Stator Winding Configuration on the Performance of Brushless Doubly-Fed Machines Adjustable Speed Drives," *IEEE Industry Application Society Annual Meeting* , Seattle, WA, Oct. 8-11, 1990.

[14] A. K. Wallace, P. Rochelle and R. Spee,"Rotor Modeling and Development for Brushless Doubly-Fed Machines," *Int'l Conf. on Electric Machines*, Cambridge, Mass, Aug. 12-15, 1990.

[15] P. Rochelle, "Design and Analysis of the Brushless Doubly-Fed Machine," M.S. Thesis, Oregon State University, 1990.

[16] G. C. Alexander, "Characterization of the Brushless Doubly-Fed Machines by Magnetic Field Analysis," *IEEE Industry Application Society Annual Meeting* , Seattle, WA, Oct. 8-11, 1990.

[17] R. Li, A. K.Wallace, R. Spee and Y. Wang,"Two-axis Model Development of Cage-Rotor Brushless Doubly-Fed Machines," *IEEE PES winter Meeting 1991*, New York, paper 91WM061-2EC, also to appear on *IEEE Trans. on Energy Conversion*, 1991.

[18] R. Li, A.K. Wallace and R. Spee, "Dynamic Simulation of Brushless Doubly-Fed Machines," *IEEE PES Winter Meeting 1991*, New York, paper 91WM060-4EC, also to appear on *IEEE Trans. on Energy Conversion*, 1991.

[19] R. Li, A.K.Wallace and R. Spee,"Determination of Converter Control Algorithms for Stable Brushless Doubly-Fed Drives Using Floquet and Lyapunov Techniques," *Power Electronics Specialists Conf.* , MIT, Boston, June 24-28, 1991.

[20] A. K. Wallace and A. Wright, "Novel Simulation of Cage Windings Based on Mesh Circuit Model," *IEEE PES Summer Meeting and EHV/UHV Conf.* , Vancouver, Canada, July 15-20, 1973.

[21] T. A. Lipo and P. Krause, "Stability Analysis of a Rectifier Inverter Induction Motor Drive,"*IEEE Trans. PAS* , Vol. PAS-88, Jan. 1968, pp. 55-66.

[22] P. Krause, *Analysis of Electric Machinery*, McGraw-Hill, 1986.

[23] R. Hoft, "Lyapunov Stability Analysis of Reluctance Motors," *IEEE Trans. PAS*, Vol. PAS-87, June 1968, pp. 1485-1491.

[24] C. T. Chen, *Linear System Theory and Design*, Second Edition, Holt, Rinehart and Winston, 1984.

[25] Henry D'Angelo,*Linear Time-Varying Systems:Analysis and Synthesis*, Allyn and Bacon, Boston, 1970.